TECHNICAL MEMORANDUM

452

Moist physical processes in the IFS: Progress and Plans

A. M. Tompkins, P. Bechtold,
A. C. M. Beljaars, A. Benedetti,
S. Cheinet, M. Janisková, M. Köhler,
P. Lopez, and J.-J. Morcrette

Research Department

Paper presented to the SAC, 33rd Session, September 2004

December 2004

European Centre for Medium-Range Weather Forecasts
Europäisches Zentrum für mittelfristige Wettervorhersage
Centre européen pour les prévisions météorologiques à moyen terme

Series: ECMWF Technical Memoranda

A full list of ECMWF Publications can be found on our web site under:
http://www.ecmwf.int/publications/

Contact: library@ecmwf.int

European Centre for Medium-Range Weather Forecasts
Shinfield Park, Reading, RG2 9AX, England

Abstract

This paper summarizes the moist physics parametrizations, namely for clouds, convection and vertical diffusion, used in both the forecast model and the 4DVAR assimilation system. Model cycle 23r4 is used as a starting point of the discussion because the ERA-40 reanalysis is based on this model version and it also forms the atmospheric component of the system-2 seasonal forecasting suite.

The developments made during the intervening period up to the current cycle 28r3 are documented for both the convection and cloud parametrizations. The net effect of these and other enhancements on the long term model climate is investigated, and it is shown that a number of model fields, such as liquid water path and top of the atmosphere radiation budgets, are significantly improved. Some systematic deficiencies, such as a lack of both deep convection over the tropical continents and of stratocumulus in the eastern Pacific and Atlantic Oceans, are still present. Apart from the improvements that have been achieved, the model development work has also provided information about remaining deficiencies, uncertainties and sensitivities, which can be used to guide future work.

The changes in the convection scheme were mainly aimed at making the scheme more active, resulting in a reduction in the occurrence of grid-scale convection and contributing directly to a reduction of tropical wind errors. The enhanced activation of convection at night led to a reduction of analysis increments over North America with the consequence of improved Northern Hemispheric height errors in the medium range. This model change also improved the phase of the diurnal cycle over land although precipitation still starts too early compared to observations. The convection work has clearly demonstrated the importance of a good balance between parametrized convection and ”resolved” convection. This partition is very subtle and will certainly require attention with future resolution changes. The entrainment parametrization is identified as an uncertain area which might benefit from further optimization. Additionally, convective momentum transfer shows some deficiencies and will require further work. CRM simulations performed by external partners will be valuable in this context.

The cloud scheme has been rationalized and its numerics has been improved. This work has demonstrated the importance of the numerical aspects and the sensitivity of the ice processes. Since the time scales of cloud processes tend to be short, numerical time integration errors can overwhelm the parametrization uncertainties. Implicit schemes are necessary and it is important to use formulations that guarantee a proper balance between cloud generation and destruction processes. Further weaknesses of the cloud scheme are the ice processes and the difficulty in keeping consistency between the cloud cover and cloud condensate variables. It is therefore proposed to introduce a separate ice variable, to use the subgrid variance of total water as a new variable and to link cloud water/ice and cover to this variable using statistical distribution assumptions. It will also facilitate the coupling with the new moist boundary layer mixing scheme.

To address the systematic underestimation of stratocumulus in the eastern Pacific and Atlantic Oceans, a new boundary layer scheme has been developed. The scheme combines turbulent diffusion and mass flux transport in moist conserved variables. Results show that the scheme indeed produces stratocumulus in the correct regions. A crucial ingredient is a switching algorithm that decides between the shallow convection scheme and the moist mixing that leads to stratocumulus. After implementation, further research will be oriented towards improved switching algorithms and unification of the shallow convection and moist boundary layer schemes.

The representation of moist physics in the 4D-Var data assimilation system is also important for forecast skill, and therefore one section is devoted to describing two completely new convection and cloud schemes for which the tangent linear and adjoint codes are available. The superior approximation to the full nonlinear model and the improved linear characteristics are demonstrated, along with an example of their use in a 1D-Var framework to assimilate rainfall information. These schemes are crucial for the precipitation assimilation work, are being

tested for the singular vector computations and will be further evaluated in the context of 4DVAR.

Finally, a strategy for future development of the moist physics is presented. To continue the improvement of representing the physics of the atmosphere and further the associated success in improving IFS forecast skill, it is proposed that greater coherency between model components is needed. One way to accomplish this would be to introduce a core parametrization for subgrid-scale variability of thermodynamical and dynamical quantities. Such a parametrization would provide cloud cover, but additionally this information could be used to remove biases or improve closure assumptions in microphysics, radiation and convection. It is suggested that by removing each model component's requirement for separate assumptions concerning subgrid variability, the number of tuning parameters is reduced, and the successful implementation of future enhancements will be facilitated.

Contents

1 Introduction

The physics of the ECMWF integrated forecast system (IFS) model is, and has always been, under continual development to better represent the physical processes of the atmosphere in order to reduce systematic biases and improve forecast skill in both the medium and longer range.

A number of these processes involve moisture in the atmosphere, such as cloud and precipitation formulation, and are collectively termed 'moist physics'. The representation of moist physics is not just crucial for the quality of the model's dynamical fields in the Tropics and midlatitudes, upon which traditional model metrics such a 500 hPa geopotential heights scores are based. Moist physical processes also directly affect the prediction of central weather parameters such as cloudiness and surface precipitation by which the general public judge and assess the forecast quality. This paper aims to review the model moist physics and the developments that have occurred over recent years, and then outlines the vision of the future direction in which the IFS physics package will evolve.

1.1 Moist physics

The term 'moist physics' encompasses a wide range of processes, ranging from fair-weather cumulus, organized or isolated deep convective events, through stratiform cloud processes involving a complexity of ice and warm rain microphysical processes. The interrelationships of these processes are such that any attempt to group them into broad (or less broad) categories is fraught with difficulty and approximation. The concept of a "unified" physics treatment has been central to the development of the Centre's physics package for some years, nevertheless for a number of practical reasons it is usual to group them into broad parameterizations with further sub processes. The IFS considers moist processes in three parametrization schemes representing: (i) the subgrid turbulence that mostly (but not exclusively) occurs in the planetary boundary layer (PBL), (ii) convection, which incorporates both shallow and tropospheric-deep motions in addition to mid-level convection and (iii) stratiform cloud processes, which includes all cloud generation, destruction and microphysical processes not directly addressed by the prior two categories. These three categories are often named the vertical diffusion, convection and cloud schemes, respectively. It is stressed however, that the coupling of these is an integral and crucial component of the model physics. The cloud scheme plays a central role in this coupling as further discussed in sections 4 and 7.

In additional to the complex nonlinear schemes used for forecast integrations, the representation of moist processes in the linear physics of the 4D-VAR analysis system also plays a critical role for forecast accuracy (Rabier et al., 1998; Janisková et al., 1999; Mahfouf, 1999). The IFS thus also has a parallel set of simplified parametrizations for use in the assimilation for which tangent linear (TL) and adjoint (AJ) versions exist.

1.1.1 Scheme nomenclature

To describe these components with clarity, it is necessary to introduce a clear nomenclature. Each scheme is given a label comprising of three components. The first describes the purpose of the parametrization: CNV/CLD/VDF referring to the convection, cloud and vertical diffusion schemes respectively. The second provides the scheme's principal use: FC referring to the complex nonlinear scheme used in the forecasts, and AN for the simplified physics parametrization used in 4DVAR. Finally the model cycle at which the scheme was operational is appended. Thus CNV.FC.23r4 refers to the version of the complex convection parametrization, originally described by Tiedtke (1989), that was operational in the ERA-40 cycle 23r4. CLD.AN.28r1 refers to the Slingo (1987) scheme currently used in the 4DVAR system. The different approximations of the simplified schemes are identified by appending -NL (nonlinear), -TL (tangent linear) and -AJ (adjoint) as appropriate (thus

CLD.AN.28r1-TL)[1].

1.2 Document scope

As the starting point of the model history description model cycle 23r4 is selected, which became operational in June 2001. This cycle is one of the major releases of recent years, since it is the version that was used to conduct the ERA-40 reanalysis project, and also forms the atmospheric component of the operational coupled seasonal forecasting system, which is updated less frequently than the medium range system.

All generalized model descriptions[2] contained in this document refer to the system as it stood at cycle 23r4. All references to recent modifications refer to changes made between this cycle and the current one: 28r3. However, during this three year period there have been a total of six intermediate cycles with physics modifications (in addition to a considerable number of intermediate cycles incorporating technical changes), namely: 24r3, 25r1, 25r4, 26r3, 28r1, and 28r3. In order to provide the reader with an overview of the model development time-line, the major changes incorporated into each of the cycles is summarized in table 1.

For reasons of brevity Table 1 neglects numerous developments that affect the humidity in the analysis system, such as the recently implemented new humidity control variable. That said, in order to provide a reasonable overview of the forecast system, it does include some modifications, such as upgraded radiation schemes, which are not directly related to moist physics and are consequently not discussed further in this document. Table 1[3] shows that there are two cycles which implemented major changes to moist physics, namely cycle 25r4 and 28r3. Of these, the upgrade in moist physics in cycle 25r4 were the most beneficial for the medium range forecast scores.

1.3 Document outline

It is impossible to assess the impact of moist physics parametrization alterations without a comprehensive scheme of metrics for evaluating model performance. Therefore, before the details of the moist physics are presented, section 2 describes some of the diagnostics used to judge the IFS model, and briefly illustrates the model simulation of some basic moist process-related model quantities, such as total cloud cover or total column liquid water, and the improvement attained between cycle 23r4 and 28r3.

From table 1, it is apparent that a significant proportion of the changes made in terms of *moist physical processes* consisted of modifications to the cloud and convection schemes. These schemes, and the enhancements made for the two major cycle releases of 25r4 and 28r3 are documented in the relevant convection and cloud sections, (sections 3 and 4, respectively).

After the convection and clouds are described, section 5 focusses attention on the model planetary boundary layer (PBL) scheme. While successful, certain systematic inadequacies with the current scheme exist and are illustrated. Some possible reasons for these are highlighted. Over recent years, considerable effort has been expended to develop a completely new moist PBL scheme, which will be implemented in the near future, and is outlined in some detail in section 5.

[1] Note that this nomenclature can still contain ambiguities. For example, the 4D-Var system prior to cycle 28r3 contained two different vertical diffusion approximations, with an extremely simple version used in the outer loops, and a more complex (but nevertheless simple relative to the forecast model scheme) one used in the inner loops! However, in order to keep the scheme identifier to a manageable length we choose to neglect these complications, and identify these finer points in the text.

[2] These descriptions are usually in the form of a brief overview. For further details the reader should refer to the online documentation of this model cycle located at: http://www.ecmwf.int/research/ifsdocs/CY23r4/

[3] Date given for cycle 28r3 is for the planned implementation

Table 1: dates and content of model cycle releases involving updates to physical process parametrization since 23r4

Cycle	Date	Revisions
24r3	22/01/02	convective precipitation generation allowed throughout column
25r1	9/04/02	revised shortwave radiation scheme (increase from 4 to 6 solar spectral bands and new spectral coefficients improved adjustment for supersaturation
25r4	14/01/03	revised cloud numerics revised cloud physics - cloud top entrainment, subsidence and ice sedimentation revised convection - triggering and entrainment functions, cloud base properties
26r3	07/10/03	new radiation scheme in tangent linear of 4DVAR radiation scheme on separate low resolution grid instead of sub-sampled gridpoints relaxed mass flux limiter for shallow convection for timesteps $>$ 15mins new aerosol climatology
28r1	09/03/04	corrected evaporation/melting of precipitation fluxes
28r3	Sept 04	change to numerics of moist physics (first guess cloud tendencies applied to convection) new convection and cloud schemes for 4DVAR linear physics - not operational

In cycle 28r3, two major new parametrizations were introduced for the linear physics of clouds and convection, which will be described in section 6. These new schemes are not currently active in the operational model, but the intention is to start taking advantage of their superior approximation to the full model and improved linear characteristics in the near future.

The final section summarizes the modifications made to date, and exposes the future directions that the enhancement of the ECMWF moist physics will take. Part of the aim is to introduce greater coherency between the various model components. This can to some extent be achieved by replacing the current various (and often conflicting) assumptions concerning subgrid-scale fluctuations of thermodynamic and dynamics quantities with a centralized scheme for providing these, which could also form the core of a statistically based cloud scheme. This final section justifies this long-term development plan, outlines a strategy for its implementation, and discusses other moist physics parametrization enhancements that will be introduced in tandem.

2 Validation

2.1 Overview

The increase in complexity of the forecast model physics must occur concurrently with a commensurate expansion of the metrics used to judge the model. In addition to the standard evaluation of medium range mean biases and anomaly correlations, an effective and encompassing system for forecast verification is required for both the medium and longer range.

In acknowledgment of this, development of model diagnostics is awarded high priority, and a number of new diagnostic packages have recently been completed. Some of these are specifically aimed at certain model characteristics. For example, the Atmospheric Radiation Experiment program (ARM, Ackerman and Stokes, 2003), provides a plethora of ground based observations that are processed and utilized to judge the performance of the forecast model boundary layer scheme. These metrics are illustrated in section 5 which discusses that scheme. Further effort has been expended to evaluate the model precipitation in the tropics using remotely

Table 2: The observational datasets used for validation purposes in cycle 28r3. The datasets marked with 'X' are earmarked for inclusion in future cycles but are not available in 28r3

Field	Dataset	Reference	Period Available
Surface Precipitation	GPCP V2	Huffman et al. (1997)	Jan 1979-Oct 2002
	Xie-Arking	Arking and Xie (1994)	Jan 1979-Dec 1999
	SSM/I	Wentz (1997)	Jul 1987-Oct 2003
	TRMM/TMI	Shin et al. (2001)	Jan 1998-Sept 2003
Cloud Cover	ISCCP (D2)	Rossow and Schiffer (1991)	Jul 1983-Sept 2001
	Modis (X)	King et al. (1996)	Sept 2000 -
TOA OLR fluxes	CERES	Wielicki et al. (1996)	Mar 2000 - Jun 2003
	ERBE (X)	Barkstrom (1984)	Jan 1986 - Dec 1988
	NOAA (X)	Liebmann and Smith (1996)	Jan 1974 - Feb 2004
TOA solar fluxes	CERES		Mar 2000 - Jun 2003
	ERBE (X)		Jan 1986 - Dec 1988
TOA cloud rad'ye forcing	CERES		Mar 2000 - Jun 2003
Total column water vapour	SSM/I		Jul 1987-Oct 2003
	TRMM/TMI		Jan 1998-Sept 2003
Total column liquid water	SSM/I		Jul 1987-Oct 2003
	TRMM/TMI		Jan 1998-Sept 2003
Total column ice water	NOAA (X)	Rädel et al. (2003)	1987-1991 climate
10m wind speed	SSM/I		Jul 1987-Oct 2003
	Quikscat (X)		Aug 2000 - Sept 2001
Surface net fluxes	Dasilva	da Silva et al. (1994)	1979-1989 climate

sensed observations. Since this pertains directly to the convection scheme, this remote sensing validation exercise is described in section 3.

In addition to these specific diagnostics which are utilized in the relevant sections of the paper, here a brief overview of the model performance is presented.

2.2 Model climate

In addition to the specific focused diagnostics that will be introduced later, an automated system has been developed that facilitates the identification of systematic model errors. The IFS model, as any other forecast or climate model, has a number of systematic (asymptotic) errors that develop during a model integration. These are identifiable by integrating the model for a period of many months to allow it to attain its "climate", and comparing the model quasi-equilibrium state to other sources such as reanalysis or satellite observations. A recent attempt to document these was made by Jung and Tompkins (2003). By relating these systematic climate features to specific moist physical processes, and consequently addressing these with improved parametrisations, advances will also be attained for the medium-range forecast quality, together with the obvious benefits for the coupled seasonal forecast system. The success of such an approach depends on the ability to associate specific model climate features, such as a lack of stratocumulus cloud off the coast of the Americas, with short-comings in the model physics, such as an inadequate representation of boundary layer turbulence for example.

A new climate diagnostics package has thus been implemented into model cycle CY28r3. Specifically the package produces:

(i) Maps of model surface parameters compared to observations (see below)

(ii) Vector maps of winds at various heights compared to ERA-40 reanalysis

(iii) Z500 NH errors maps compared to ERA-40 reanalysis

(iv) Zonal mean maps of all data available on pressure or model levels compared to control experiment and ERA-40 reanalysis

It is clear from the above list that the new package represents a major enhancement on the previous diagnostic systems used at the Centre. Additionally, to aid model developers, maps of model surface parameters compared to a specified control experiment are provided. Table 2 below provides the datasets used for comparison and their respective availability.

While some of these diagnostics will also be shown in relevant sections (for example, cloud cover in section 4) the advances made in the model climate between cycle 23r4 and 28r3 are illustrated briefly, to summarize the overall impact of *all* moist physics modifications made between these cycles. Naturally it is not feasible to isolate only the moist physics modifications, and some of the improvements in the model cycle 28r3 are also due to other aspects, in particular the improved radiation schemes and a modified aerosol climatology. Nevertheless, some improvements, particularly in cloud and precipitation characteristics are directly identifiable with moist physics modifications. An attempt is made to illustrate where progress has been made with respect to reduction of systematic biases, and where problems remain.

Although the package's flexibility allows plotting for any chosen period, it is useful to specify a simulation "default", so that a comparable history of model performance can be constructed over time, and also to allow intercomparison between various model parametrisation developments. Some of the observational datasets span a considerable period, exceeding two decades in some cases, but Table 2 indicates that the years 2000 and 2001 maximize the available data sources, since newer observational platforms such as MODIS become available after this point. A three ensemble member default experiment is thus defined, with each forecast lasting for 13 months initialized on the first three days of August 2000, respectively. This default experiment will be conducted for all future major model cycles to allow their intercomparison, and will serve as a central tool in future parametrization development. With this experimental framework, comparisons can be made for the four principal seasons of JJA, SON, DJF and MAM, in addition to the annual mean. It is likely that this default scenario will be supplemented by others in the future, covering a major El-Nino period for example.

2.2.1 Surface precipitation

The surface precipitation is compared to GPCP V2 products in Fig. 2.1. It is apparent that the main features have not drastically changed; the model tends to produce too much precipitation over deep convective regions over the tropical oceans, while the rainfall is deficient over the tropical continents of Africa, the Americas and the Asian Maritime continent. However, the maps of total precipitation obscure a dramatic shift in the division between the rainfall produced by the large scale cloud scheme and the parametrized proportion. Although part of the large-scale rainfall in the tropics is produced by anvils generated by deep convective detrainment, a significant proportion in the earlier cycles was the result of convective motions occurring on the grid scale. Considerable effort has been expended in the convection scheme to tackle this, and are discussed in detail in section 3 later. The cumulative effect of these is to shift the balance towards parametrized rainfall, as witnessed by Fig. 2.2. This shift was associated with a significant improvement in forecast scores and is discussed in much greater detail in section 3 of this document.

Concerning the deficiencies of the precipitation climatology, the lack of precipitation over the continents indicates that the local boundary forcing is in some way deficient. One possibility could be a drift in the land surface soil moisture, which would affect surface heat fluxes and ultimately the low level relative humidity and CAPE. However, comparison to ERA-40 reanalysis data reveals this not to be the case (not shown) with no significant drift in boundary layer relative humidity apparent. The lack of precipitation could also indicate that the convective scheme is ignorant of some feature in the underlying surface. Indeed, section 7 of this document indicates that an adjustment to the triggering function over land masses can improve the rainfall climatology over Africa and S. America.

The second precipitation bias occurred over the maritime continent, western Pacific warm pool region. This region is typically a low wind region where the boundary layer thermodynamic conditions are critically sensitive to the parametrization of unresolved gustiness. Indeed, prior to the implementation of such a scheme the model suffered from far stronger cold and dry biases in the boundary layer of the Western Pacific, associated with a substantial underestimate of precipitation there (Miller et al., 1992). If the model cycle 23r4 and 28r3 are compared however, it is clear that the 10m wind speed is substantially lower in the latter cycle, with reductions of up to 3 m s^{-1} (Fig. 2.3). Moreover, it is clear that the reduction occurs precisely in the locations which undergo deep convection. This indicates that the increase in rainfall produced by the deep convective parametrization is accompanied by a reduction in low level winds.

The above finding also suggests that the parametrization for subgrid-scale gustiness is even more crucial in

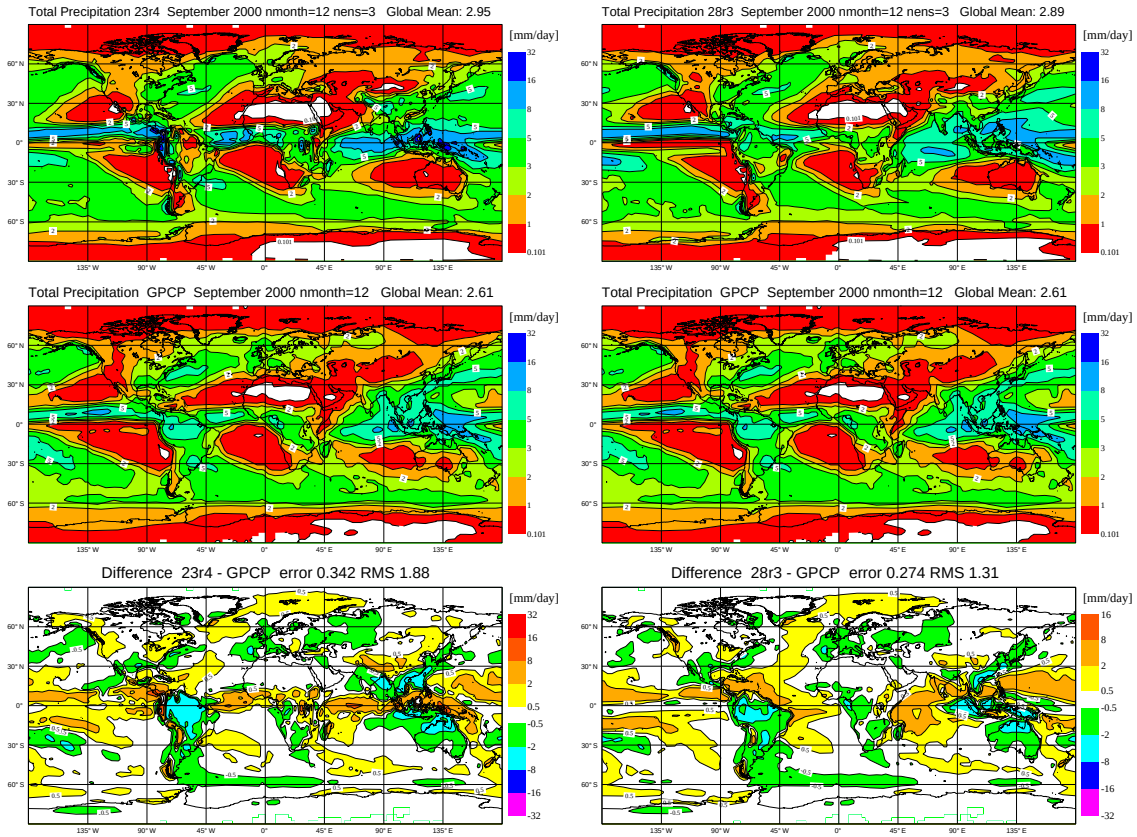

Figure 2.1: Top panels: the annual mean surface precipitation of model ensembles (3 members) initialized at the start of August 2000 with the first month discarded. Middle panels: GPCP V2 observations for corresponding period, lower panels: model-observations differences. The left column is for 23r4 while the right column is the latest model cycle 28r3.

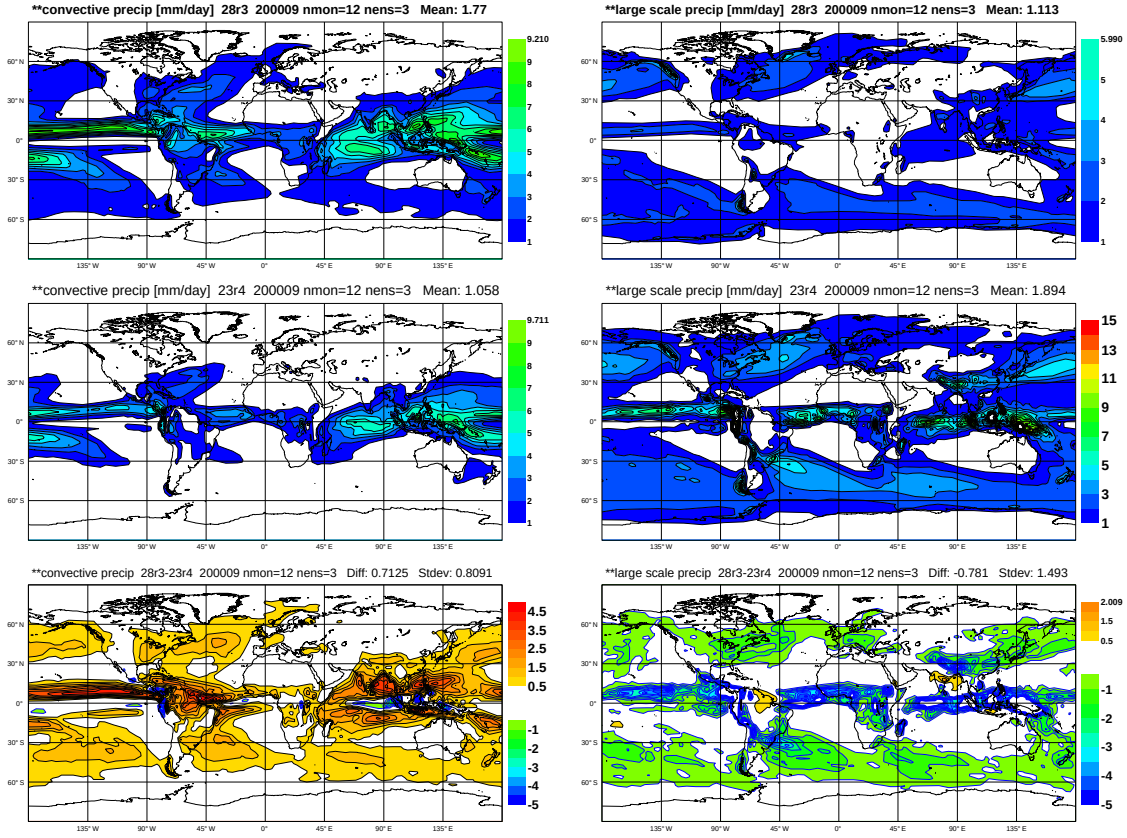

Figure 2.2: Left (right) column shows the annual mean surface convective (large-scale) precipitation of model ensembles initialized at the start of August 2000. Top row shows cycle 28r3, middle row is cycle 23r4, while the bottom row is the model difference.

the latter cycle. Sensitivity tests conducted at cycle 28r3 do confirm that further enhancing the gustiness in convectively active boundary layers increases the precipitation in this region (not shown). Further investigations show that implementing a prognostic form of the mesoscale gustiness enhancement by convectively driven downdraughts, presented by Redelsperger et al. (2000), contribute a further minor but positive impact. This will be investigated further.

2.2.2 Cloud quantities

The basic cloud quantities of total cloud cover and total column liquid water are compared to ISCCP and SSM/I retrievals in Figures 2.4, and 2.5, respectively. The total cloud cover reveals that, as for the precipitation fields, certain systematic biases remain. These include an overestimation of cloud cover in the Indian Ocean and Pacific warm pool regions, and an underestimation of cloud cover over the Amazon, although the latter shortcoming is somewhat improved in the latest cycle.

One systematic bias that clearly stands out is the lack of cloud cover in the stratocumulus regions off the west coast of the the American and African continents. In fact, this error appears to have worsened between the ERA-40 (23r4) and most recent model cycle (28r3), which along with the slight reduction in cloud cover over the southern oceans, contributes significantly to the increase in RMS error in cloud cover, compared to the retrieved product. This features is discussed is much more detail in chapter 5.

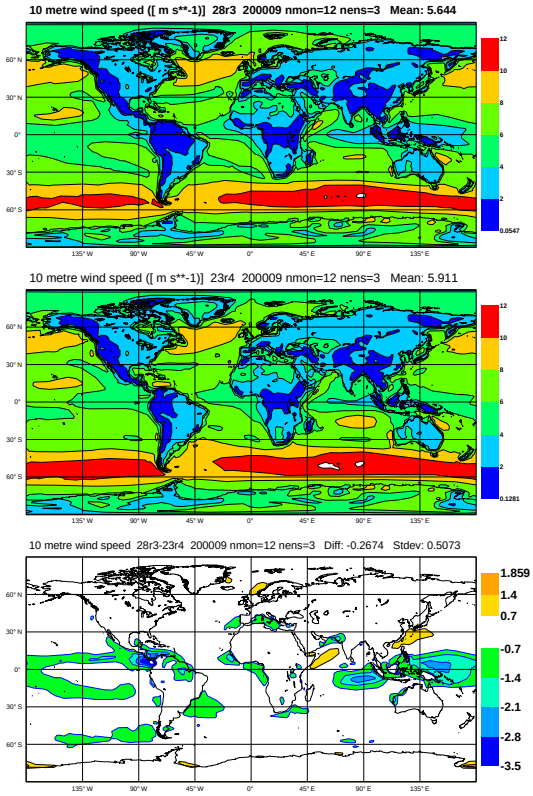

Figure 2.3: 10 m wind speed for 28r3 (upper), 23r4 (middle) and difference (lower).

The total column liquid water, on the other hand, shows a dramatic improvement due to a number of reasons. The earlier cycle strongly overestimated the column integrated liquid water almost globally (over oceans, since SSM/I retrievals are not available over land). This error was gradually improved by the revisions in the convective precipitation treatment and the convective scheme closure, the new cloud numerics and finally also the modified numerics for the physics introduced in cycle 28r3, leading to a total reduction in RMS error from over 65 g kg^{-1} to less than 25 g kg^{-1}. The main regions where cloud liquid water now appears to be underestimated are the stratocumulus regions, in agreement with the cloud cover comparison, and the Western Pacific. However, the latter should be treated with caution, since comparison to the Remote Sensing Systems (RSS) product of TRMM/TMI instead shows almost perfect agreement in the Western Pacific, while confirming the lack of cloud water in the stratocumulus regions (Fig. 2.6).

Naturally, it would be highly desirable to conduct equivalent comparisons to observations for ice water path. However, the sole dataset currently available for comparison is the retrieval of cloud ice properties from NOAA described by Rädel et al. (2003). The severe criteria applied to restrict these retrievals (single layer, ice-only clouds with low to medium optical depth ranges) renders comparison to the model output difficult, and further research will be required before reliable comparisons can be conducted. There remains a critical requirement for more accurate ice information from observation in order to facilitate the future development in ice microphysics described in section 4. The potential of the future missions EarthCARE and CloudSat to fill the information vacuum concern ice cloud climatology is significant, and they are awaited with anticipation.

The shortcomings in convection and cloud discussed above have associated problems in the large-scale dynamical fields. Figure 2.7 examines this by comparing the annual mean of the two forecast ensembles to the ERA-40 reanalysis, with plots centred over the Pacific ocean to concentrate on the Walker circulation and the

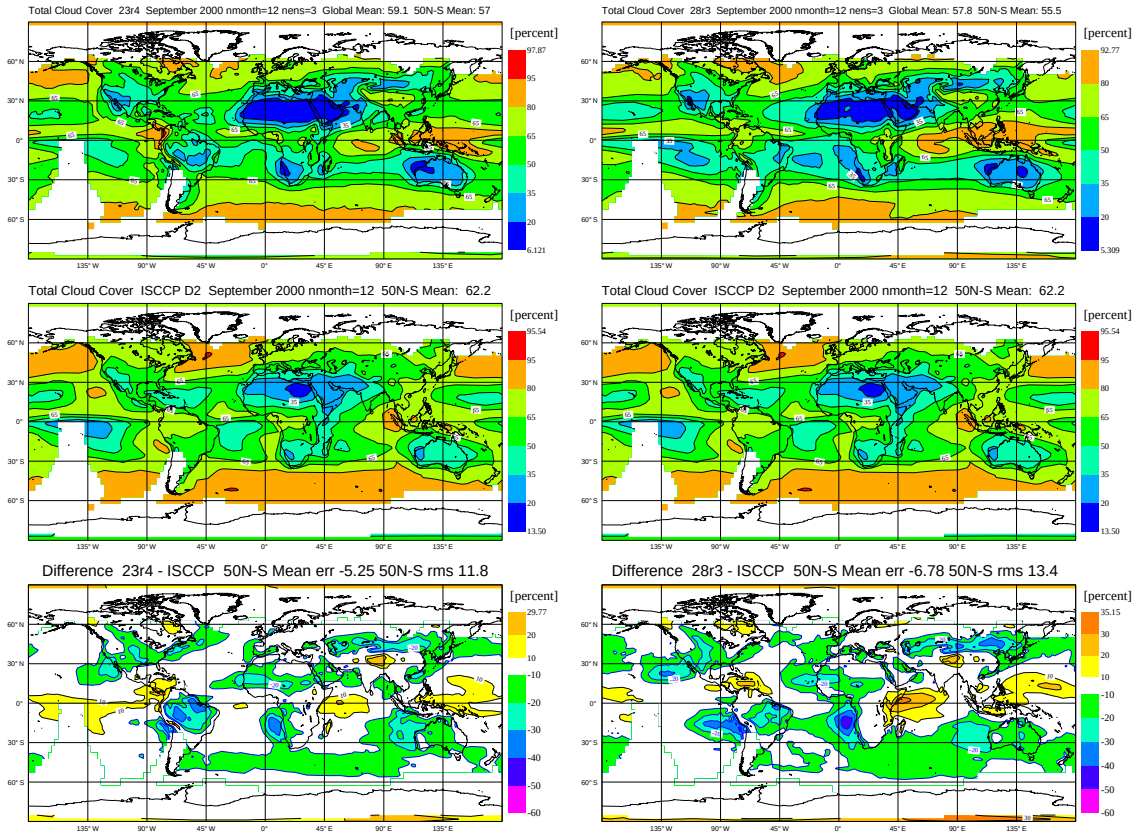

Figure 2.4: Top panels: the annual mean total cloud cover of model ensembles initialized at the start of August 2000 with the first month discarded to neglect model spin up. Middle panels: ISCCP D2 observations for corresponding period, lower panels: model-observations differences. The left column is for 23r4 while the right column is the latest model cycle 28r3

stratocumulus regions.

In the Western Pacific both model versions have a lack of deep convection, agreeing with the precipitation diagnostics. However, the nature of the problem seems to have evolved somewhat. In the earlier model version, deep convective activity appeared to be confined to a smaller geographical area close to the maritime continent, with convective activity apparently 'locked in' at these positions. This could be linked to the tendency of this model version to produce a higher proportion of its tropical rainfall in the form of grid-scale convective events, witnessed by the vastly different balance between convective scale and grid scale precipitation. Meanwhile, the later model cycle produces better agreement with regard to the geographical extent of the deep convecting region, but convection is too weak. In both cases the Walker circulation is less strong than the reanalysis suggests it to be, although one should bear in mind that the reanalysis itself is particularly influenced by the moist physics parametrisations in these regions.

On the east side of the Pacific, the obvious feature of the reanalysis is the large region of subsidence, which is drastically underestimated in both model versions, again pointing to a weakened Walker circulation. It is likely that the lack of subsidence leads to a weakened inversion and thus contributes to the missing stratocumulus regions that were identified in the total column liquid water analysis conducted above. Instead, a large part of the compensating subsidence appears to occur artifically over the adjacent American continent, again agreeing with the lack of deep convection that occurs there, as documented by the TOA IR budgets and the precipitation analysis. In agreement with other statistics this problem appears to have ameliorated slightly in the latest cycle.

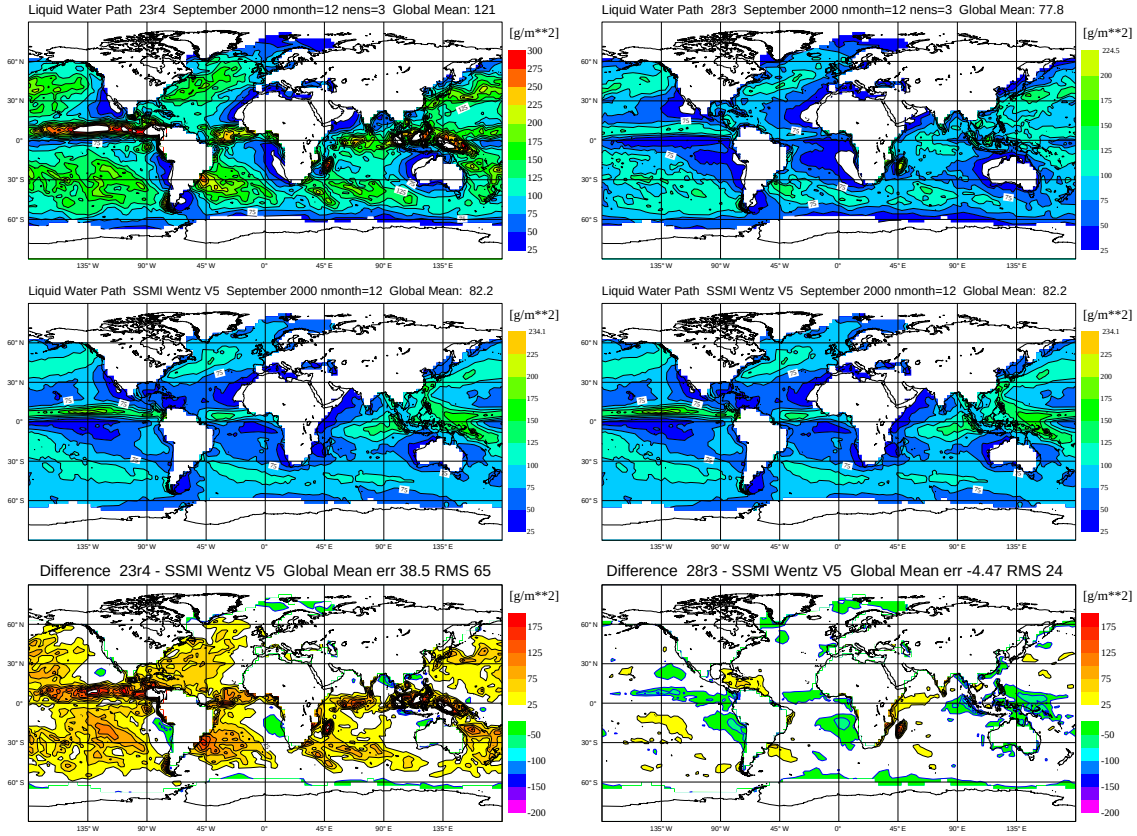

Figure 2.5: Top panels: the annual mean total column liquid water of model ensembles initialized at the start of August 2000 with the first month discarded. Middle panels: SSM/I observations for corresponding period, lower panels: model-observations differences. The left column is for 23r4 while the right column is the latest model cycle 28r3

2.2.3 TOA radiative fluxes

Analysis of the top-of-atmosphere (TOA) net fluxes reinforces the conclusions drawn from the other cloud retrievals products (Fig. 2.8). The overestimate of liquid water in the tropics and particularly the trades produces a significant shortwave (SW) TOA net flux bias in the earlier cycle, which was partly offset by the low albedo in stratocumulus regions. In agreement with the ISCCP and SSM/I data the former error is reduced and the latter increased in the most recent model cycle. Alterations to the SW scheme, such as increased spectral resolution, will have also impacted these changes. Note that the error over the Sahara has improved, despite the significant reduction in aerosol optical depth that occurred over this region at cycle CY26r3, which would have the effect of decreasing albedo.

In contrast to the RMS error reduction of 6 W m^{-1}, the TOA outgoing longwave (OLR or infra-red, IR) radiation RMS error increases slightly by just over 1 W m^{-1} (Fig. 2.8, lower panels). The main problematic areas are the tropical continents. The error point to either a lack of clouds in these regions, or to the clouds being too warm (ie. cloud tops too low). Since the shortwave errors are small in these regions, and the cloud cover compares reasonably well in later cycles, it is likely that too low cloud top heights are contributing the most to this bias. The future addition of cloud top pressure statistics from ISCCP and MODIS data will confirm or refute this hypothesis. Part of the increase in error derives from the midlatitudes, in particular the southern oceans. The revised cloud scheme numerics at cycle 25r4 improved this aspect by increasing ice water contents in these mid latitude clouds. However, changes to other aspects of the model such as the numerics and convection have

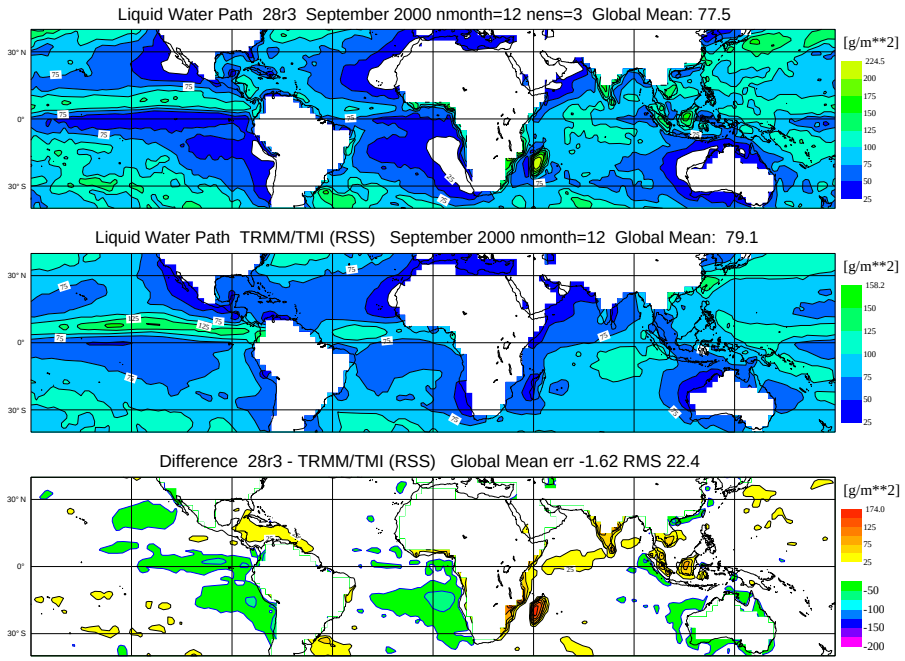

Figure 2.6: Top panel: the annual mean total column liquid water of model ensembles (cycle 28r3) initialized at the start of August 2000. Middle panel: TRMM/TMI observations for corresponding period, lower panel: model-observations differences

offset these gains by reducing total column ice water.

2.2.4 Zonal mean thermodynamical fields

Although some aspects of the model climate have notably improved, fig. 2.9 is included to show that this is accompanied by a small but nevertheless significant deterioration in the basic mean thermodynamic fields when compared to ERA-40 reanalysis for the same period. The figure indicates a cooling of up to 1.5 K in the zonal mean temperature fields with respect to ERA-40 in the tropics; a bias that was absent from the earlier cycle. This bias developed on the introduction of cycle 26r3 and was compounded by the alterations involved in 28r3. Both of these cycles introduced significant benefits for the forecasts scores in the medium range, highlighting the difficulties of introducing changes that target model deficiencies without impacting other areas of model performance.

Likewise a considerably moist bias appears to have developed in the upper troposphere, although for humidity, the ERA-40 reanalysis has to be treated with more caution, especially in the upper troposphere above 300 hPa, where radiosonde humidity information is not utilized.

As pointed out earlier, the reanalysis necessarily is sensitive to model parametrisations, particularly in data-sparse tropical regions. The reported deterioration in the thermodynamical qualities in the tropics should therefore carry the strong caveat that the ERA-40 reanalysis was conducted using the 23r4 cycle.

2.2.5 Conclusions

To summarize the statistics above, it is apparent that the model has a number of systematic biases, some of which have considerably improved between model cycles 23r4 and 28r3, while others have remained unchanged

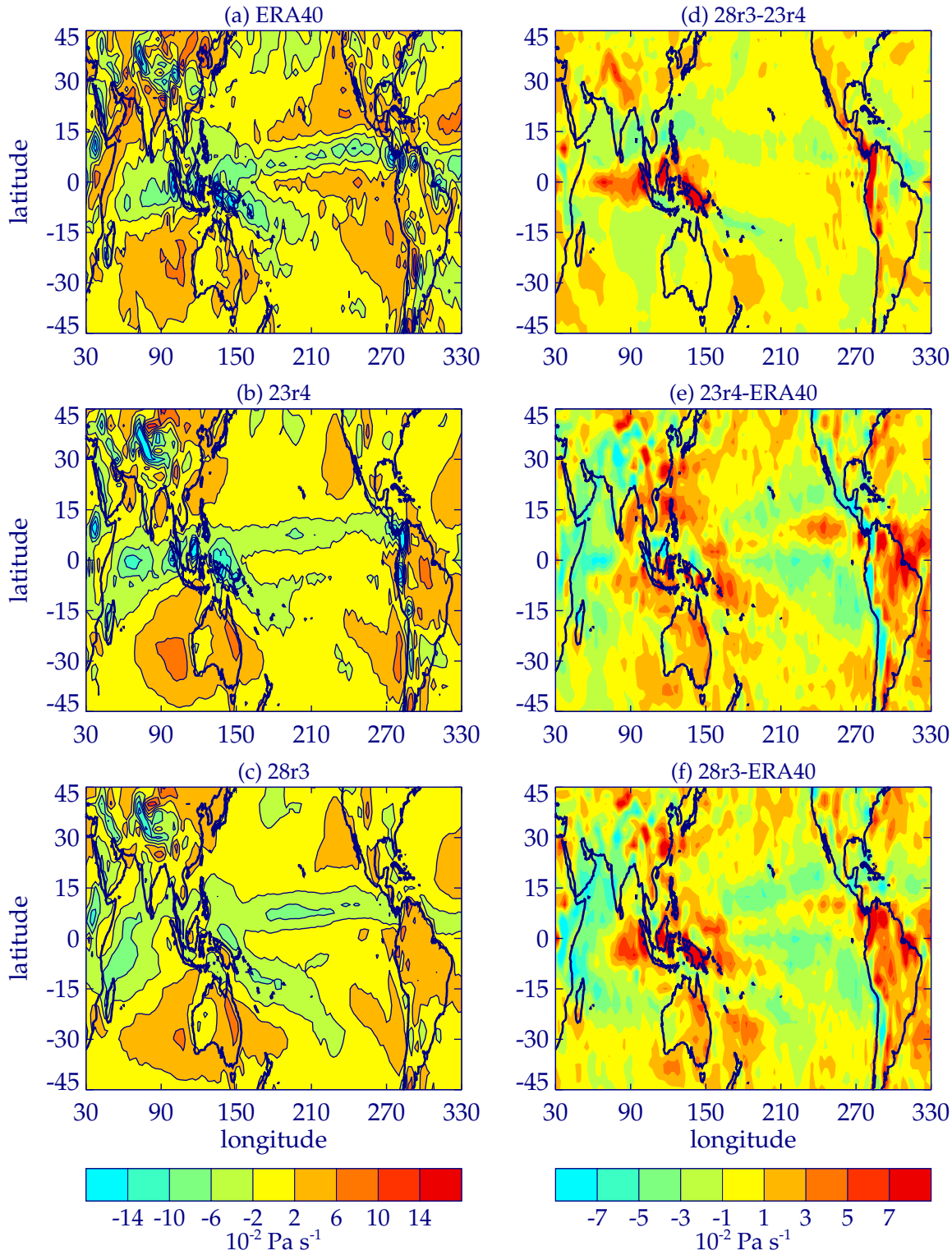

Figure 2.7: annual mean 500hPa vertical velocity (10^{-2} Pa s^{-1}) for (a) ERA40 reanalysis (b) 23r4 (c) 28r3 (d) 28r3-23r4 (e) 23r4-ERA40 (f) 28r3-ERA40

or even deteriorated slightly. Many of these biases are discussed in further detail later. To guide the reader, Table 3 briefly summarizes these results.

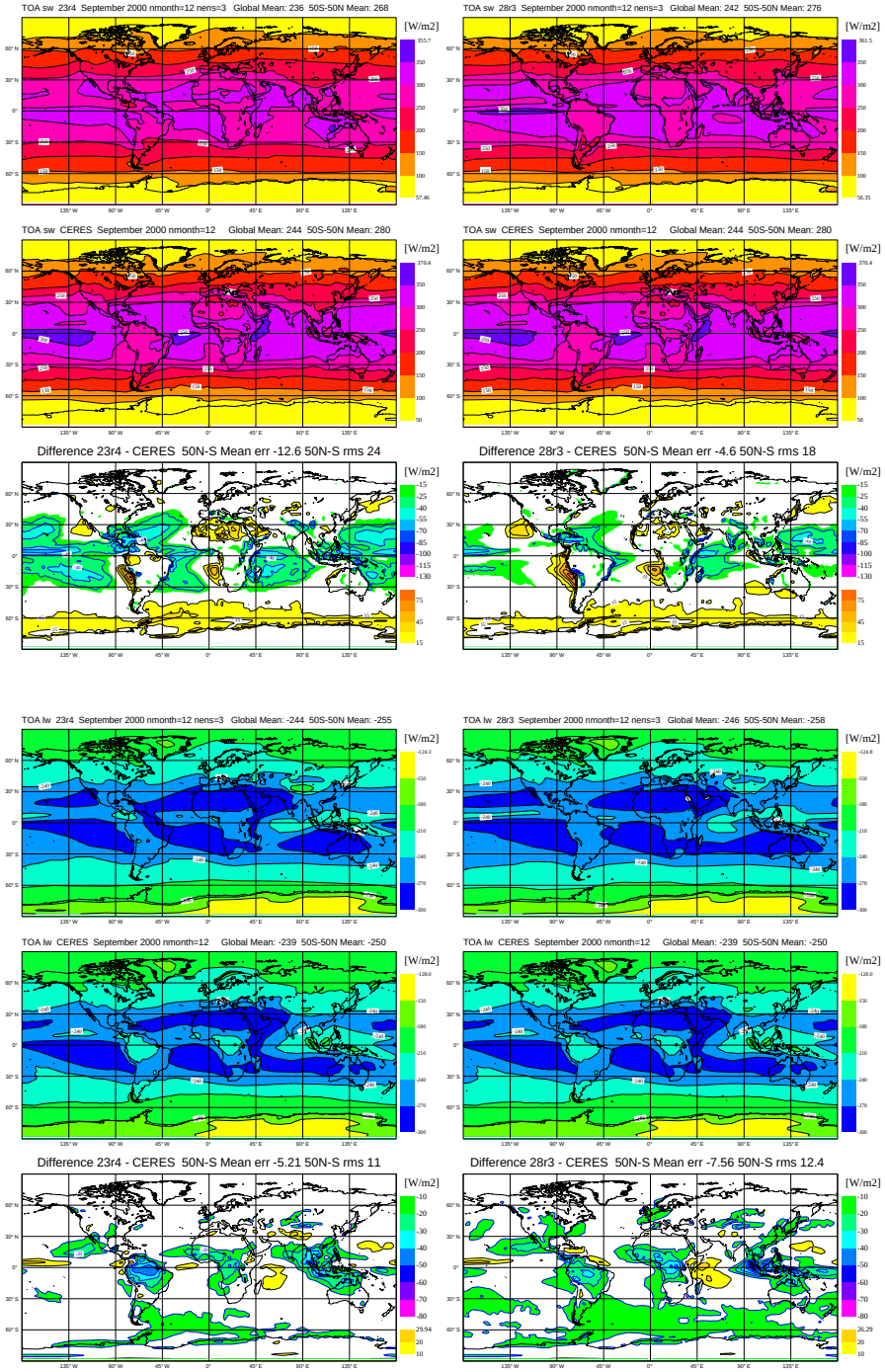

Figure 2.8: As Fig. 2.1 with upper three panels comparing model to CERES TOA SW net fluxes, and lower three panels comparison models to CERES TOA LW net fluxes.

3 Convection: CNV.FC

The ECMWF convection scheme represents the vertical mixing and microphysical processes in shallow, deep and elevated (mid-level) convective clouds. The main purpose of the scheme is to provide a moist adjustment of initially conditionally unstable grid columns and to compute subgrid-scale convective precipitation. The

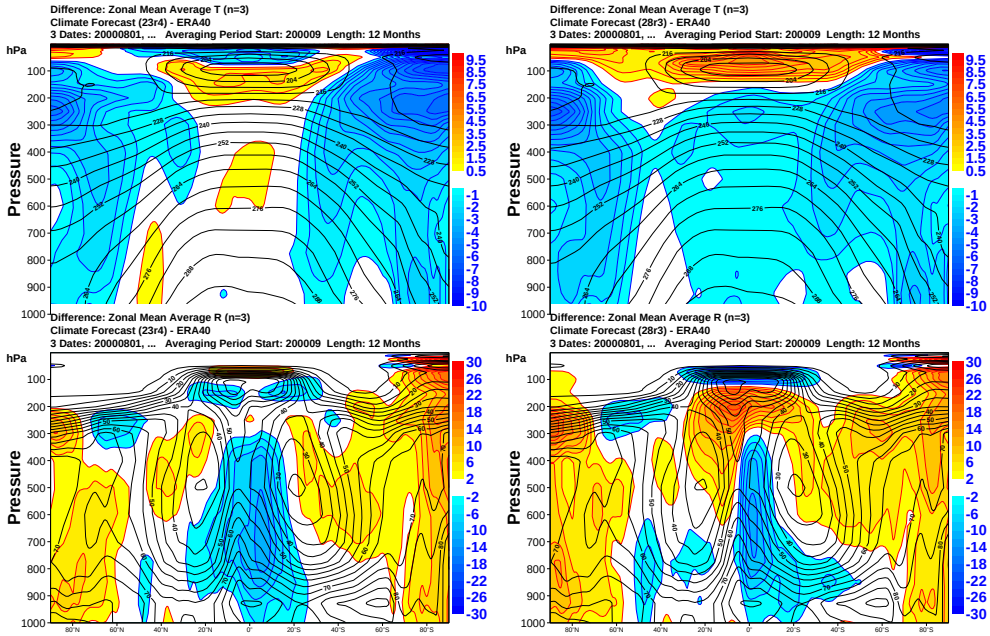

Figure 2.9: Zonal mean of temperature (top) and humidity (bottom) compared to ERA-40 reanalysis for model cycles 23r4 (left) and 28r3 (right)

scheme has been originally developed by Tiedtke (1989), and is based on a bulk mass flux formulation with one characteristic convective updraught and one characteristic convective downdraught. Since then, the scheme has undergone numerous modifications that concern the specification of entrainment/detrainment rates (mixing rates for cloudy air with the environment), the formulation of the convective downdraughts, the convective closure, the momentum transport, and the numerical stability of the scheme. The modifications up to cycles 23r4 and their consequences on model performance have been documented in Gregory et al. (2000).

Since 2002 the formulations of the convection initiation and the numerics have been thoroughly reformulated, and the convective transport of passive tracers has been included. All these modifications have been successively included in model cycles 25r4 to 28r3, and led to an important improvement in forecast performance. In the following these modifications and their overall impact on forecasts are summarized, before more specific topics like the diurnal cycle of convection, and the transport of momentum and passive tracers are addressed. Finally, the remaining problems/limitations with the current convection formulation are discussed, and some lines for further improvement and possible alternatives are given.

Table 3: Systematic biases in the IFS model, their tendency between cycles 23r4 and 28r3

Bias	Tendency 23r4-28r3	Further reference
Lack of stratocumulus cloud	slightly deteriorated	section 5
Lack of deep convection over tropical continents	slightly improved	sections 3 and 7
Frequent occurrence of grid scale convection	significantly improved	section 3
Lack of deep convection over W. Pacific warm pool	unchanged	section 7
Too much liquid water in tropics and midlatitudes	strongly improved	sections 3 and 4
Too little ice in mid latitudes	unchanged	sections 3 and 4

3.1 Convection initiation

The scheme first determines the occurrence of convection in a model grid column (i.e. identifies conditionally unstable model columns) and the type of convection on the basis of a simplified first-guess updraught computation. Then the entrainment/detrainment rates are specified as a function of cloud height, and a first full updraught/downdraught computation is performed including the complete mass flux equations and microphysical processes. This is followed by the convective closure, where the mass fluxes are scaled as a function of the CAPE (Convective Available Potential Energy) for deep convection, by the large scale vertical velocity for midlevel convection, and as a function of the moist static energy convergence integrated over the subcloud layer for shallow convection; the latter being equivalent to a closure as a function of the surface fluxes. After this procedure a second, final updraught computation is performed, followed by the computation of the precipitation fluxes and the environmental (grid-scale) tendencies .

In model cycles prior to 25r4 convection is initiated by computing the condensation level of a parcel originating at the lowest model layer, and testing for the parcel buoyancy at the condensation level. With a parcel buoyancy in excess of -0.2 K convection is activated, and the type of convection is specified as a function of the cloud thickness. If the cloud is thicker than 200 hPa then deep convection is active, and shallow convection otherwise. The cloud top is simply defined as the level where the moist static energy of the surface parcel becomes smaller than the environmental moist static energy at saturation. However, it turned out that this convection initiation procedure suffers from two main problems, i) it underestimates convective activity in the presence of a stable surface layer, or more generally when convection originates from elevated unstable layers, and ii) it results in the occurrence of convection too early in the morning over land when the surface layer quickly heats.

In cycle 25r4 the convection procedure has been revised with the objective to improve these deficiencies on the basis of a first-guess updraught computation that is more physically-based, and as close as possible to the full updraught computation, while remaining numerically efficient. The revised procedure can be summarized as follows. Shallow convection is tested first by computing the ascent of a strongly entraining non-precipitating parcel originating at the surface that has been given an initial temperature and moisture perturbation proportional to the surface fluxes (Jakob and Siebesma, 2003). If the vertical velocity at cloud base is positive and the cloud thickness is smaller than 200 hPa, the grid column is identified as shallow convective. The cloud top is now defined as the level where the updraught vertical velocity vanishes. Next, deep convection is tested for by computing the ascent of a weakly entraining precipitating parcel originating from the next higher model layer (or a mixed-layer if the parcel originates in the boundary-layer). If the resulting cloud thickness is larger than 200 hPa a grid column is identified as deep convective and the results for the shallow test parcel are ignored. If no deep convective cloud is found for the given departure layer, the procedure is repeated starting from the adjacent model layer above and so on until the test parcel is more than 350 hPa above the surface. Mid-level convection (instability in a shallow elevated layer) is only activated if the relative humidity of the environment at the condensation levels exceeds 80% and neither deep nor shallow convection is active. Finally, adjustments were made to the entrainment rate and the precipitation conversion rate in order to minimize forecast temperature biases in the tropical tropopause region.

The resulting global distribution of the different convection types as obtained from a one year climate simulation for 2000 with cycle 28r1 is illustrated in Fig. 3.1. Deep convection occurs mainly in the tropical belt with a frequency of about 40%, but also with a frequency of roughly 20% in the storm tracks over warm ocean currents. In contrast, shallow convection is present over the entire oceans with maximum frequencies of over 90% in the subtropics. Mid-level convection mainly occurs over the Arctic regions and during winter in mid-latitude regions. However, the convective mass fluxes (or equivalently the convective tendencies) associated with mid-level convection are very weak, whereas the convective mass fluxes associated with shallow convection are particularly strong in wintertime over the North-West Atlantic and North-West Pacific, where they can

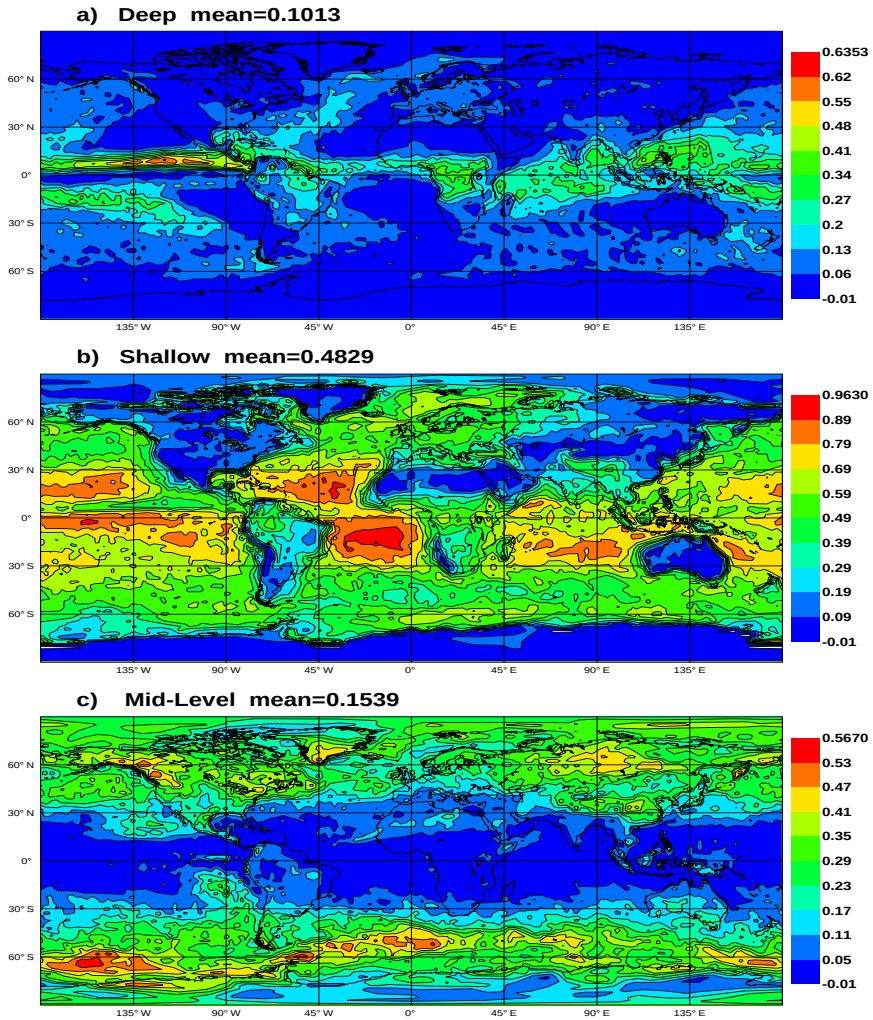

Figure 3.1: Annual mean distribution of the occurrence of deep (a), shallow (b), and mid-level (c) convective clouds as obtained from a 12 months climate integration for 2000 with cycle 28r1 at resolution T95.

substantially exceed typical values for deep convection that are of order 0.03 $kgm^{-2}s^{-1}$.

3.2 General evaluation

In order to illustrate the general impact of the recent convection changes to the operational suite, diagnostics of the precipitation and wind fields are shown that are additional to the routine evaluation of the forecast system that is performed by the Operations Department. In Fig. 3.2 is shown a time series from June 2001 to April 2004 of convective and stratiform precipitation rates averaged over the Globe and the Tropics, as obtained from the operational 12-72 h forecasts. In cycle 24r3 (from June 2001 to January 2002) the global total precipitation rate of 3.3 mm day^{-1} (corresponding roughly to a 100 W m^{-2} energy flux) is mainly of the stratiform type, with only 43% of the total precipitation being of the convective type. In cycle 25r1 a supersaturation check has been introduced after calling the individual physical routines, with the result that the convection and cloud scheme equally contribute to the total precipitation. Finally, with the introduction of the revised convection in cycle 25r4 the convective precipitation now roughly represents 57% of the globally averaged precipitation rate

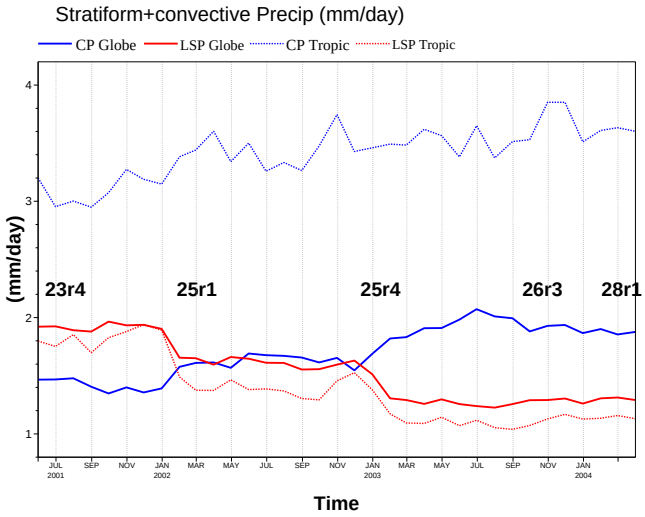

Figure 3.2: Time series of monthly mean convective (blue) and stratiform (red) precipitation rates averaged over the Globe (solid lines) and the Tropics (dotted lines) as obtained from operational 12-72 h forecasts. The implementation date of the different model cycles is also indicated by the position of the corresponding cycle name.

or 75% of the rainfall rate in the Tropics.

As a simple diagnostic of the evolution of the wind errors, an RMS difference between the monthly mean values of the 700 hPa wind vectors at 00 and 12 UTC from ERA40, and the archived monthly mean values from the 60 and 72h operational forecasts, has been computed for the Globe and the Tropics. The comparison of the evolution of the wind errors in Fig. 3.3 with the precipitation time series (Fig. 3.2) shows that with the introduction of cycle 25r4, and an increase in convective activity, a significant reduction in both global and tropical wind errors is obtained, and the tropical wind errors are now of the same order of magnitude as the globally averaged errors. Indeed, the increase in convective activity with cycle 25r4, and later the new humidity analysis in cycle 26r3, resulted in a reduction in the number and intensity of intense local precipitation events

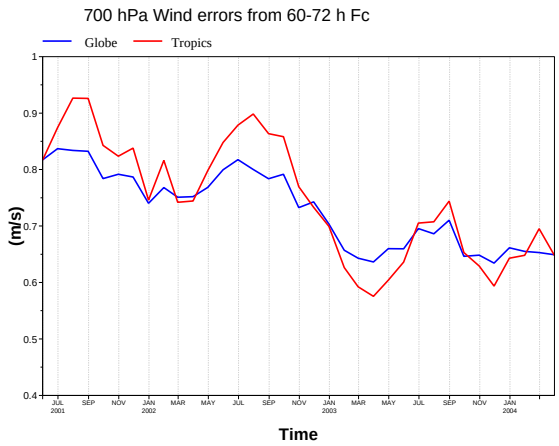

Figure 3.3: Time series of root mean square differences between monthly mean wind vectors from the operational 60-72 h forecasts and the analysis averaged over the Globe (blue lines) and the Tropics (red lines). Note that the absolute values are small since only the monthly mean field and not daily data has been used to compute a spatial mean error.

and associated local low-level convergent and upper-level divergent flow.

The impact of convective adjustment on forecast errors is particularly important during the Spring convective season over North America, where intense synoptic activity and the advection of moist and warm air from the Mexican Gulf can lead to large instabilities with CAPE values of up to 4000 J kg^{-1}. Figure 3.4 depicts the 200hPa RMS errors during May and June 2002 for height and horizontal wind, as obtained from differences between daily 12 h forecasts from 00 UTC, run either with cycle 25r1 or cycle 25r4, and the corresponding analyses. Cycle 25r1, operational at that time, produced large height and wind errors over the Great Plains of the United States and in the regions of the Great Lakes, but also over Argentina, where in the region around Buenos Aires intense mesoscale convective systems are frequently observed. With cycle 25r4, run in experimental mode, these errors are everywhere reduced (e.g. maximum RMS wind errors are reduced by about 30%), and also the tropical upper-level winds are improved. As model errors tend to propagate downstream, the improved forecasts over North America, particularly the improved forecasts of the upper-level subtropical and polar Jets, resulted also in better forecasts for Europe in the medium-range.

As a final example, the precipitation forecasts are evaluated in Fig. 3.5 using observations from the Tropical Rainfall Measuring Mission (TRMM) Precipitation Radar (PR). The evaluation is done using the instantaneous three-dimensional liquid and solid stratiform plus convective precipitation fluxes from short-range ($<$ 12h) forecasts, converting them to an equivalent radar reflectivity (Bauer et al., 2001), and comparing the results to the observations available at the closest observation time. The resulting biases (model minus observations) are presented as functions of vertical model levels and reflectivity categories based on the model reflectivity. At each point along the orbit the value of model reflectivity is checked and the difference between model and observations is ascribed to the corresponding reflectivity bin. The number of points for the average varies according to the reflectivity bin and the vertical level. To ensure robustness of the results, only bins with at least 50 points are considered. The use of instantaneous fluxes constitutes a very difficult forecast test, and the present procedure is also consistent with the algorithm applied by the assimilation group for the assimilation of rain rates during a 1D-Var/4D-Var 12 h assimilation cycle.

Figure 3.5 shows the reflectivity biases with cycle 26r3 using two different versions of the convection scheme: the version operational in cycle 25r1 (a), and that operational in cycle 26r3 (b). The forecasts correspond to 5 days in September 2003 during which the radar sampled medium to medium-heavy precipitation associated to tropical cyclones. Comparing the two forecast ensembles, one notes indeed a slight improvement with the most recent version of the convection with respect to the 25r1 version. This applies to most model levels and reflectivity bins, and in particular the high-reflectivity bins where the previous version produces too intense precipitation that is mainly of the stratiform type.

3.3 Numerics and time stepping

Routine monitoring of the EPS system (running at resolution T255 L40) with a timestep of 2700s identified a tendency to overdevelop mid-latitude and tropical cyclones, and also to overestimate the frequency and intensity of heavy precipitation events with respect to observations and the T511 deterministic forecast. Further experimentation showed that these problems largely disappeared when a short time step of 900 s was used. A time step dependency of the model physics was identified due to i) a limit (numerical stability criterion) applied to the convective tendencies , and ii) the way the individual physics processes (radiation, diffusion, convection, and the cloud scheme) are updated during a semi-Lagrangian time step.

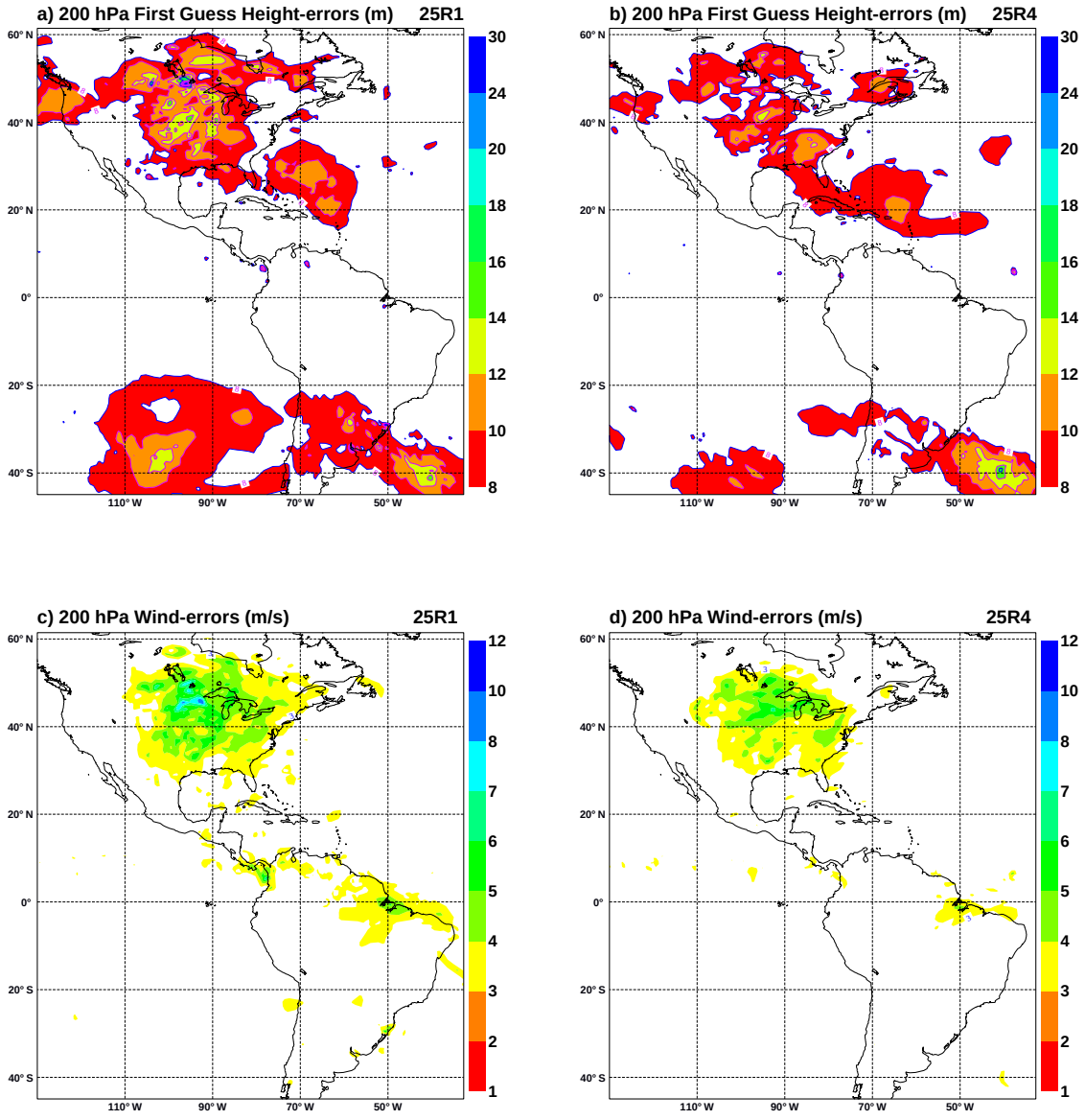

Figure 3.4: "First guess" root mean square height and wind errors for May-June 2002, as obtained with cycle 25r1 (a) and (c), and cycle 25r4 (b) and (d). The errors are computed from differences between daily 12 h forecasts starting at 00 UTC and the corresponding analysis of each experiment.

3.3.1 Mass flux advection

The time step dependency of the convection can be understood by examining the tendency (advection) equation that is written in flux form and solved for a large-scale conserved field Ψ (either momentum or a passive tracer)

$$\frac{\partial \overline{\Psi}}{\partial t} = g \frac{\partial}{\partial p} \left[M_u (\Psi_u - \overline{\Psi}) \right], \tag{3.1}$$

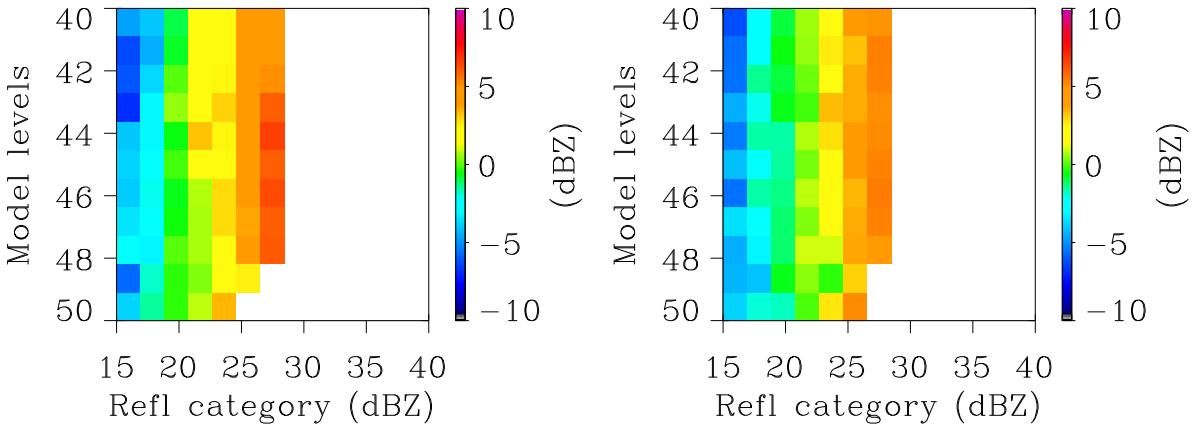

Figure 3.5: Bias of model-equivalent reflectivity (dbZ) with respect to radar observations from the TRMM/PR (Iguchi et al., 2000). Instantaneous fields from 12 h T511 forecasts for 5 days in September 2003, during which the PR sampled tropical cyclones are compared to observations. The forecasts are for cycle 26r3 using two different operational versions of the convection scheme: cycle 25r1 (left) and 26r3 (right).

where t is time, p is pressure, g the gravity constant, and M is the convective mass flux (kg s^{-1} m^{-2}), bars denote grid-mean values, and subscripts u denote updraught values. For simplicity no downdraughts are considered here. This equation is solved explicitly using the discretization

$$\frac{\overline{\Psi}_k^{n+1} - \overline{\Psi}_k^n}{\Delta t} = \frac{g}{\Delta p}\left[M^u(\Psi_u - \overline{\Psi}^n)\right]_{k+1/2}^{k-1/2}, \tag{3.2}$$

with $\Delta t = t^{n+1} - t^n$, $\Delta p = p_{k+1/2} - p_{k-1/2}$. Note that with the present vertical discretization Ψ is conserved by definition. The mass flux must be limited to a value of $\Delta p/(g\Delta t)$ given by the Courant-Friedrich-Levy (CFL) criterion, in order for the solution to be stable. This mass flux is exceeded when long model time steps are used and particularly for shallow convection, as shallow convective mass fluxes are typically a factor of two larger than deep convective mass fluxes. From cycle 26r3 onward, the mass flux limit for shallow convection has been increased by a factor of 3 for temperature and moisture, but not for momentum, for model time steps greater than 1800 s (horizontal resolutions $\leq$ T255). No numerical instability has been identified with this change.

Although the mass flux limiter is not very active with the relaxed mass flux limit (in $< 5\%$ of the shallow convective columns and $< 1\%$ of the deep convective columns), it is desirable to have a formulation that is not limited by any stability criterion. Therefore, an implicit form of (3.2) has been coded for momentum and tracers, leading to a linear bi-diagonal equation system. However, this method is rather complicated to formulate for temperature and humidity due to the additional tendencies that need to be taken into account in the RHS of (3.2), where the half-level environmental values are computed as an interpolation of the full-level values. Also a semi-Lagrangian formulation of (3.1) has been tested using

$$\frac{d\overline{\Psi}}{dt} = \frac{\partial\overline{\Psi}}{\partial t} + M_u g\frac{\partial\overline{\Psi}}{\partial p} = D_u(\Psi_u - \overline{\Psi}), \tag{3.3}$$

where D_u is the detrainment rate (s^{-1}), and $M_u g$ the vertical advection velocity (Pa s^{-1}). Unfortunately, this form of the equation is no longer mass/energy conserving (although it is possible to apply a posteriori a mass/energy correction). This together with the additional numerical cost of the method and the difficulty to develop the adjoint, made it less attractive to pursue this methodology further.

Both numerical methods have an implication for the parametrization, because they do not allow for an explicit specification of a flux profile below cloud base as is done in the operational scheme with equation (3.2). In the

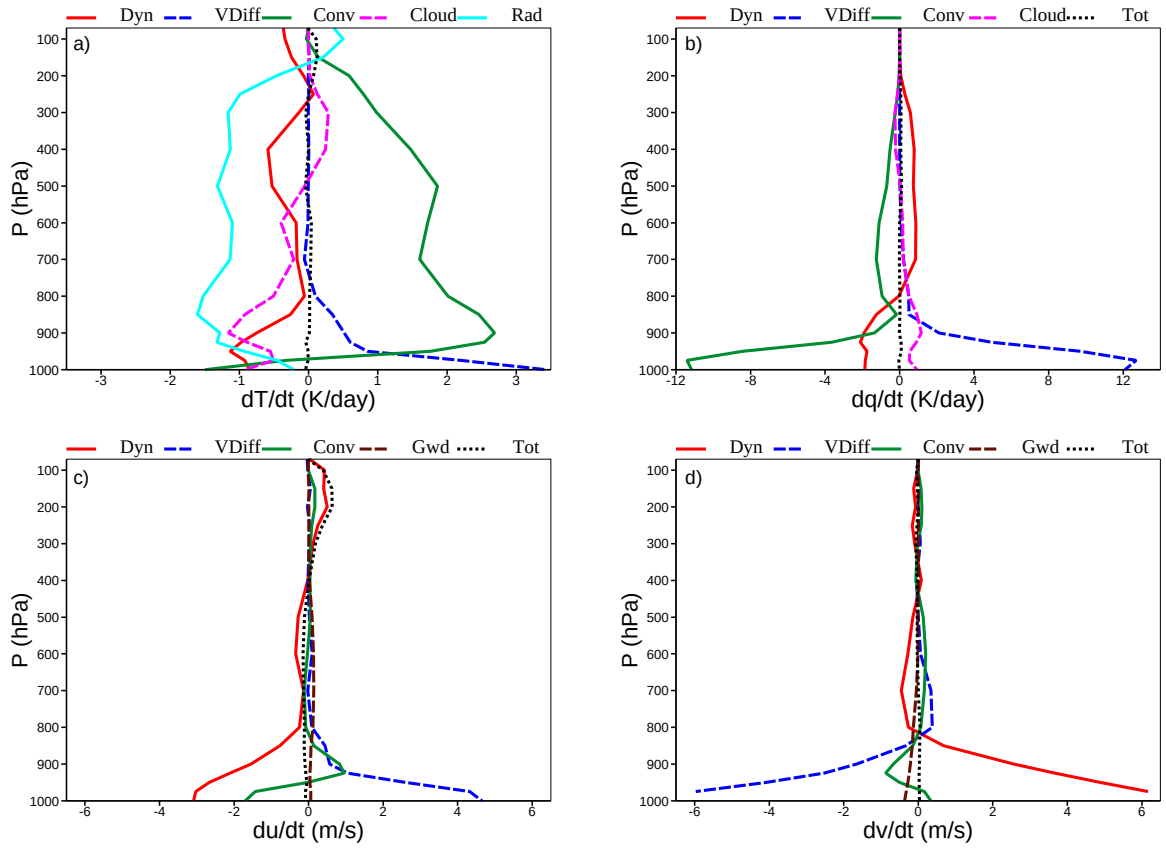

Figure 3.6: Budgets of temperature (a), specific humidity (b), and zonal (c) and meridional (d) wind components for the Tropics as obtained from 10-day forecasts at T159 with cycle 26r3. The individual tendencies correspond to the dynamics (red), the vertical diffusion (blue), the convection (green), the cloud scheme (pink), the radiation (sky blue) and the gravity wave drag (brown). The total tendency or model imbalance is denoted by the black dotted lines.

operational scheme, the fluxes below cloud base are defined to be linear implying vertically constant tendencies in the boundary-layer. This is not possible with either the implicit or the semi-Lagrangian formulation, where it is first necessary to solve for $\overline{\Psi}^{n+1}$ and then compute the tendency. This is believed to be the reason that both numerical schemes have a rather negative impact on the performance of the system.

3.3.2 Physics time stepping

The relaxed mass flux limiter that was introduced in cycle 26r3 was able to substantially alleviate the EPS problem of too deep and too slowly propagating wintertime cyclones in the northern hemisphere. However, the time step sensitivity in the Tropics and during northern hemisphere summer remained. This was solved by a revision of the time stepping procedure applied to the physics routines during one semi-Lagrangian time step. In the revised version of the time stepping procedure intermediate profiles are consistently computed after each call of the physics routines, and serve as input for the following routine.

As shown by Dubal et al. (2004) a 'sequential' numerical implementation is generally superior to a 'parallel' implementation. However, the model solution will be sensitive to the order in which the processes are con-

sidered. In particular the amount of convective activity will depend on the instability generated by the other processes preceeding the convective parametrization. The overall contribution of each physical process is best illustrated with the aid of the budgets of the prognostic quantities temperature, specific humidity, and zonal and meridional wind components. These budgets are shown in Fig. 3.6 for the tropical belt between 20°S and 20°N, including the model tendencies due to the dynamics (horizontal+vertical advection), the vertical diffusion, the convection, the cloud scheme (stratiform condensation/evaporation), the radiation, and the gravity wave drag. For temperature (humidity), negative tendencies above the boundary layer correspond to a destabilization (stabilization) of the atmospheric column. Inside the boundary-layer diffusive transport either offsets convective drying, or for momentum offsets the dynamical tendencies. Above the boundary-layer the radiative cooling rate of 1-2 K day^{-1} of the troposphere is mainly offset by convection, but the tendencies from the cloud scheme and the dynamics are important near the top of the boundary-layer and in the upper-troposphere. In particular, the cloud scheme produces a cooling in the lower troposphere due to the evaporation of stratiform rain and due to the evaporation of cloud water detrained from the convection. The model drift (the residual) is limited in magnitude except at the upper troposphere where a small warming tendency is observed as well as an acceleration of the zonal wind (corresponding actually to a deceleration of the upper-level easterlies).

In the above analysis, it is noted that in the Tropics the cloud scheme tends to destabilize the atmosphere, but since the cloud scheme is the last process to be considered, this destabilization is not appreciated by the convective scheme until the following timestep. A further modification to the 28r3 numerical framework was thus implemented, in which the cloud scheme is called twice. The first call occurs before the convection scheme in order to provide a first guess profiles. In this way, the convection can counteract the potentially destabilizing effect of the cloud scheme. The second call to the cloud scheme occurs after the convection scheme, with the convective detrainment taken into account, and with this final calculation providing the tendencies for the model's prognostic equations.

The new time stepping has been extensively tested with model cycle 26r3 in T255 L40 forecasts (using a model time step of 2700 s), and compared to the EPS control forecasts and forecasts using a 900 s time step. In Fig. 3.7 a comparison of 500 hPa geopotential height scores for Europe and tropical 850 hPa wind scores from an ensemble of 34 forecast at T255 L40 for June 2003 is shown. For both the mid-latitudes and in particular the Tropics, the results with the revised physics time stepping are better than the EPS control forecasts, and close to the short time step forecasts. Also, a comparison of the histograms of precipitation rates obtained from these runs and averaged over the tropical band from 20S/20N gives a similar picture (Fig. 3.8), namely that the precipitation rate histograms of the runs with the revised physics and 2700 s time step are close to those obtained from forecasts using a 900 s time step. Furthermore, with the revised physics the frequency of high precipitation events (mostly resolved-scale precipitation) is significantly reduced with respect to the EPS control runs. As stated previously, a reduction in high tropical resolved-scale precipitation events in the forecast is generally associated with an improvement in tropical wind scores.

The revised time stepping also improves (reduces) the liquid water path in the Tropics (see section 2), slightly improves the tropical wind scores in the T511 analysis cycle, and will be used operationally in model cycle 28r3.

3.4 Diurnal cycle

An accurate representation of the diurnal cycle of convection over land is of major importance for many aspects of the forecast and assimilation system, in particular via its strong modulation of the radiative budget by convective clouds, its resulting precipitation, and its control on surface temperature. Over land, most observational studies show that precipitation tends to occur in the afternoon or evening. The diurnal cycle of continental convection involves many coupled processes between the surface, the boundary layer, and the free troposphere

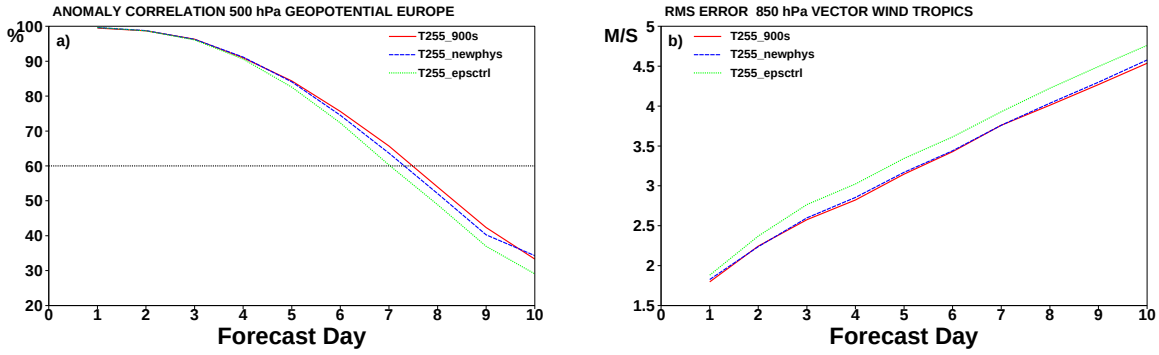

Figure 3.7: 500 hPa anomaly correlations for Europe (a) and root mean square errors of 850 hPa tropical winds (b) from an ensemble of 34 forecasts with model cycle 26r3 at truncation T255 L40 for June 2003: with a 900 s time step (red), with revised time stepping and a 2700 s time step (blue), and EPS control (green).

such as surface exchange, turbulence, and convection and cloud-radiation interactions. Although most of the current general circulation models (GCMs) predict reasonable mean rainfall rates, they tend to predict a too early onset of precipitation after sunrise, and fail to capture the broad pattern of the diurnal cycle of precipitation, with overestimated precipitation frequency and underestimated precipitation intensity (Slingo et al., 1992; Yang and Slingo, 2001).

Betts and Jakob (2002) studied in detail the representation of the diurnal cycle of convection in the ECMWF model, and pointed out that the model produces a strong early morning peak in convective precipitation that is not supported by observations. They suggested that the formulation of the initiation of convection could be responsible for these errors. Recently, the diurnal cycle of convection over land has been extensively studied in

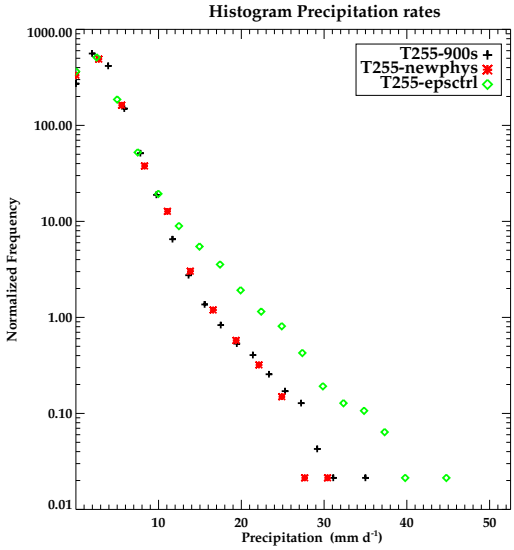

Figure 3.8: Histograms of precipitation rates averaged over the latitude band 20S/20N for June 2003 as obtained from 15 T255 L40 forecasts with cycle 26r3: with a 900 s time step (black), with revised time stepping and a 2700 s time step (red), and EPS control (green). The total number of data points used for each curve is (number of forecast ensembles × number of latitude bands × number of 12h time intervals in 10-day forecast) 13.5×10^4.

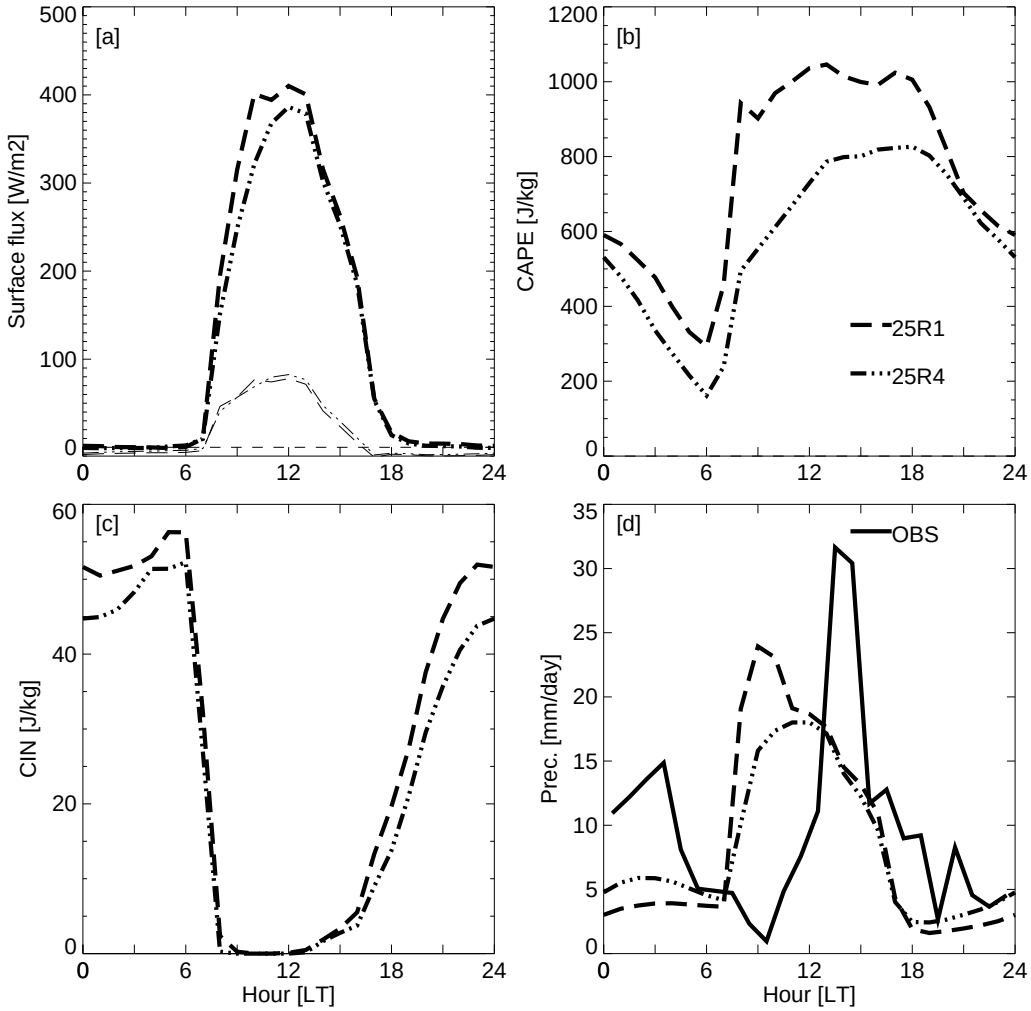

Figure 3.9: Diurnal cycle of (a) surface latent (sensible) heat flux with thick (thin) lines, (b) the convective available potential energy CAPE, (c) the cloud base convective inhibition CIN, and (d) the surface precipitation rate from daily T511 24-72 hour forecasts for February 2002 with model cycles 25r1 and 25r4. The surface rainfall observations for February 1999, collected during the TRMM-LBA campaign are denoted by the solid line in (d).

the context of the EUROCS (EURopean Cloud System) project by comparing idealized single column model simulations with cloud resolving model (CRM) simulations, and by comparing global forecasts with available satellite and surface observations. The results of this project are reported in Bechtold et al. (2004), and the results obtained from daily 24-72 h T511 forecasts with cycles 25r1 and 25r4 for February 2002 are summarized here.

During February the diurnal cycle of convection over land is most prominent over the Amazon basin. Figure 3.9 shows the mean diurnal cycle of the surface sensible and latent heat fluxes for the central Amazon basin, together with the CAPE, the convective inhibition (CIN) and the surface precipitation rate. The forecasts produce maximum latent and sensible heat fluxes around local noon, and vanishing CIN, therefore atmospheric conditions that are favorable for the development of convection between 9 and 15 LST. The differences between the forecasts become clearly evident concerning the CAPE and the surface precipitation. Indeed, cycle 25r4 produces a slower increase of CAPE and precipitation during the morning, and corrects the spurious 9 LST

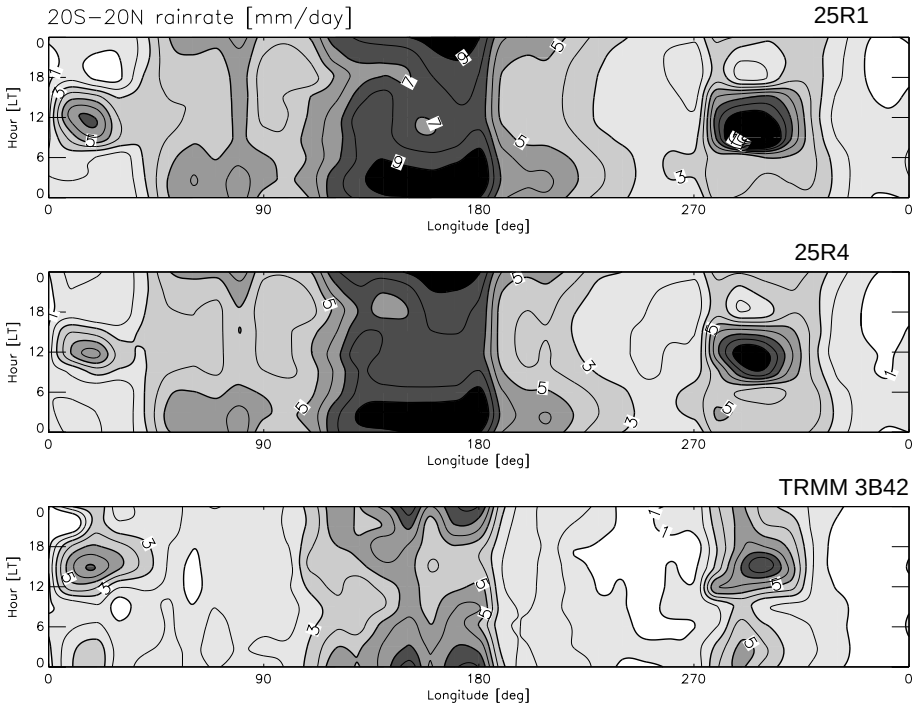

Figure 3.10: Global Hovmöller diagrams of the diurnal cycle of precipitation (mm day^{-1}) for February 2002, as obtained from 24-72 hour forecasts at horizontal resolution T511 with model versions 25r1 (a) and 25r4 (b), and as derived from TRMM measurements (c). Fields are averaged between 20°S and 20°N, and the time resolution of the data is 3 hours.

precipitation peak that is present in cycle 25r1, but not supported by the surface observations (Fig. 3.9d). The differences between cycle 25r1 and 25r4 can be mainly explained by the fact that the convection initiation procedure in cycle 25r4 uses mixed-layer values for the ascending parcel and not simply the values at the lowest model level; slightly higher entrainment rates in cycle 25r4 also contribute to a slower deepening of the cloud layer.

A global picture of the diurnal cycle is given in Fig. 3.10 with the aid of Hovmöller plots comparing the forecasts with satellite derived precipitation rates from the TRMM radar. The results are consistent with the results obtained for the Amazon basin, as cycle 25r4 produces over the African (0-45° longitude band) and South American (270-320° longitude band) continents a daily precipitation maximum at 12 LST that is three hours later than in cycle 25r1, but still 3 hours too early compared to observed maxima at 15 LST. However, for the West Pacific region (110-190° longitude band) the forecasts correctly produce a nighttime precipitation maximum, but tend to overestimate the precipitation totals. The overestimation of precipitation over the West Pacific in the short-range forecasts is at first glance at odds with the lack of precipitation observed in (Fig. 2.1), but the systematic underestimation of precipitation in this region is only present in long integrations.

It is yet not entirely clear if the remaining 3 hour difference in the diurnal cycle of convection between the forecast and the observations can be entirely corrected as the diagnostic mass flux convection scheme assumes an immediate (during one time step) growth of the cloud, whereas CRM simulations show that the convective clouds grow gradually from a cumulus congestus state around noon to the deep precipitating state at 15 LST. However, it is thought that the diurnal cycle can still be improved with the present scheme. Indeed, it has been found by Derbyshire et al. (2004) in an intercomparison study with CRMs that the current scheme underestimates the sensitivity of convection with respect to environmental humidity, producing too many deep clouds where shallow or cumulus congestus clouds are observed. Therefore, an improved entrainment formulation or some prognostic formulation of the scheme (e.g. a memory for humidity) might allow further improvements in

the diurnal cycle.

3.5 Tracer transport

Convection plays also an important role in the fast vertical transport of atmospheric trace gases and aerosols. In particular, the assimilation of tropospheric tracers like CO, CO_2, and possibly O_3, and the replacement of the existent aerosol climatology by a prognostic distribution, require a representation of vertical convective and diffusive mass transport. There is also a growing demand through the GEMS (Global Environmental Monitoring System) project, and by the user community of ECMWF products running chemical transport models forced with ECMWF analysis, to obtain a source code of convective tracer transport. Also, some users have either reported problems with the quality of the mass fluxes provided in the ERA 40-year reanalysis or reported technical problems and inconsistencies in recomputing the mass fluxes from the large-scale fields.

Therefore, a convective transport scheme and its adjoint have been developed that are consistent with the basic equations of the convection scheme. The scheme satisfies the following three constraints: i) mass conservation, ii) linearity, and iii) monotonicity. The linearity of the scheme is important for efficient adjoint applications, or more generally, backward integrations where one wishes, for instance, to determine the emission source of a tracer knowing the measurement at time t and location x,z. However, the linearity constraint only allows for advection schemes of first-order accuracy. Finally, the monotonicity constraint is important to avoid the formation of spurious local concentration maxima and minima.

The convective transport is best illustrated by the mixing matrix, where the contribution of each model source layer to a given target layer can be evaluated. An example obtained for a tropical deep convective profile is given in Fig. 3.11. Each column vector represents a convectively mixed tracer profile that initially had a concentration of unity at one single level (along the main diagonal). The matrix is inverted relative to the usual matrix notation, with the model source layer denoted by column number i, and the target layers denoted by row numbers j. The yellow-green coloured area above the main diagonal denotes air that has been transported upward by the updraughts. Transport by downdraughts is effective in the left part of the matrix below the diagonal, and transport in the environment by subsidence is characterized by the color shaded areas just below the main diagonal. Numerous tests have been performed with the scheme in forward and backward mode,

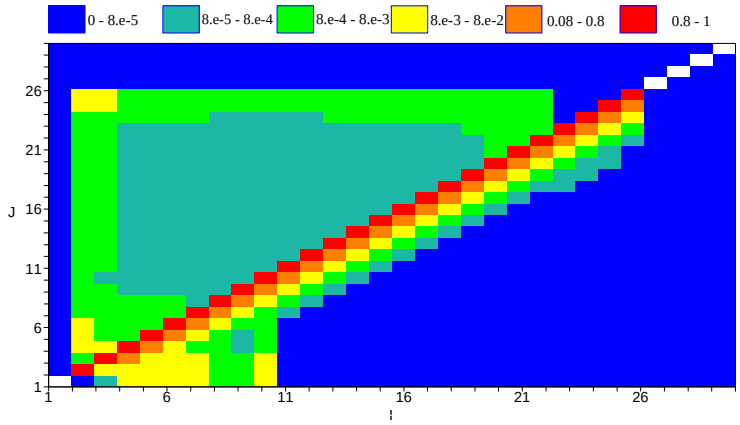

Figure 3.11: Convective mixing matrix characteristic for tropical deep convection that is valid locally for one grid column for a given model time step. An implicit solver is used, and the first model layer above the surface is denoted by 1. Deviations from the main diagonal (white) and background (blue) illustrate convective transport from model layer i to model layer j.

where for the backward integrations either the adjoint of the forward model or the transpose of the mixing matrix (corresponding actually to a local adjoint) has been used. Results show that in spite of the diffusive character of convection, useful backward integrations (recovering partly the initial information/sensitivity) can be made if the integration interval does not exceed 12-24 h. Evaluation of the transport using CRM data is in progress, and global tests are conducted using idealized aerosol distributions. However, for fully realistic applications some removal of tracers either by rain or surface deposition will have to be included.

3.6 Momentum transport

Some very recent results on the convective transport of momentum are presented. The connection between typical model wind errors in the tropics and the transport of convective momentum has been established. As a testbed, forecasts initialized with the ERA 40-year reanalysis have been rerun daily with cycle 28r3 for a period during the Tropical Ocean and Global Atmosphere Coupled Ocean-Atmosphere Response Experiment (TOGA-COARE) (Webster and Lukas, 1992). The results have been averaged over a domain ($152.5-157.5°\mathrm{E}, 5°\mathrm{S}-0°$) corresponding to the Intensive Flux Array (IFA), and compared to ERA-40. The reanalysis data is assumed to be of good quality for the IFA as 6-hourly soundings from 12 ships have been assimilated.

Fig. 3.12 shows a time series from 6 December 1992 to 13 January 1993 of averaged u and v wind components at the 850 hPa and the 150 hPa levels as obtained from 12-48 h forecasts, and the corresponding analysed values. Remarkably, the forecasted u-components deviate significantly from the analysis during the period from 20 December to 5 January, with an underestimation of both the low-level westerlies and the upper-level easterlies. In contrast, the forecasted meridional winds closely follow the analysis, except around 22nd December and the beginning of January at the 150 hPa level. Interestingly, as discussed by Tung and Yanai (2002a,b) the period from 20 December to 5 January corresponds to a major low-level westerly wind burst associated with the Madden-Julian oscillation (Madden and Julian, 1971, MJO), therefore the main meridional wind errors correspond to the northerly/southerly inflow/outflow before and after the easterly burst in the upper troposphere (very similar results are obtained at resolution T511, and are therefore not shown) .

The origin of the model errors can be explained with the aid of the momentum budgets including all physical

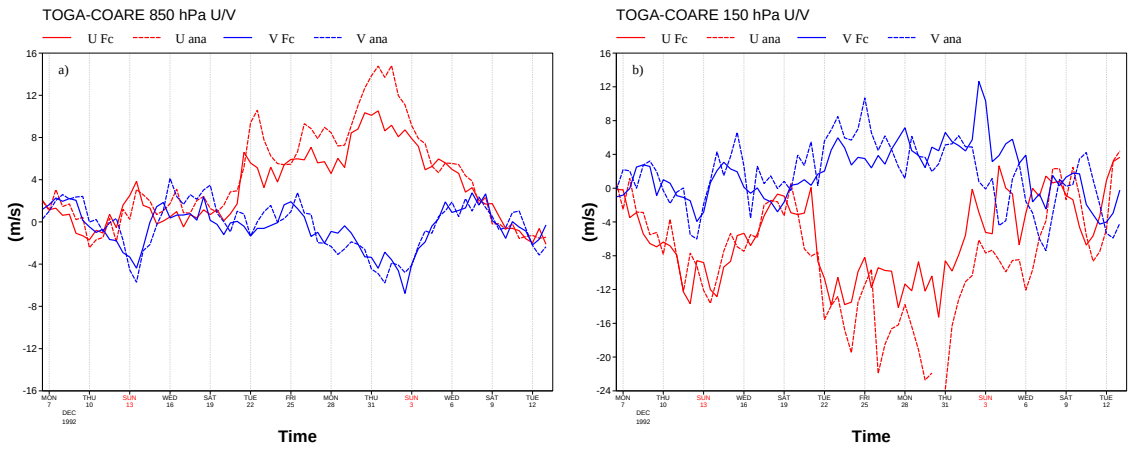

Figure 3.12: Time series of daily forecasted (solid) and analysed (dashed) zonal (red) and meridional (blue) wind speeds averaged over the TOGA-COARE IFA domain at the 850 hPa (a) and 150 hPa (b) level. The forecasts are run at resolution T159, and the plotted values are averages of two lagged forecasts (00UTC values are from d-1 +36h and d +12h, and 12 UTC values are from d-2 +48h and d-1 +24h).

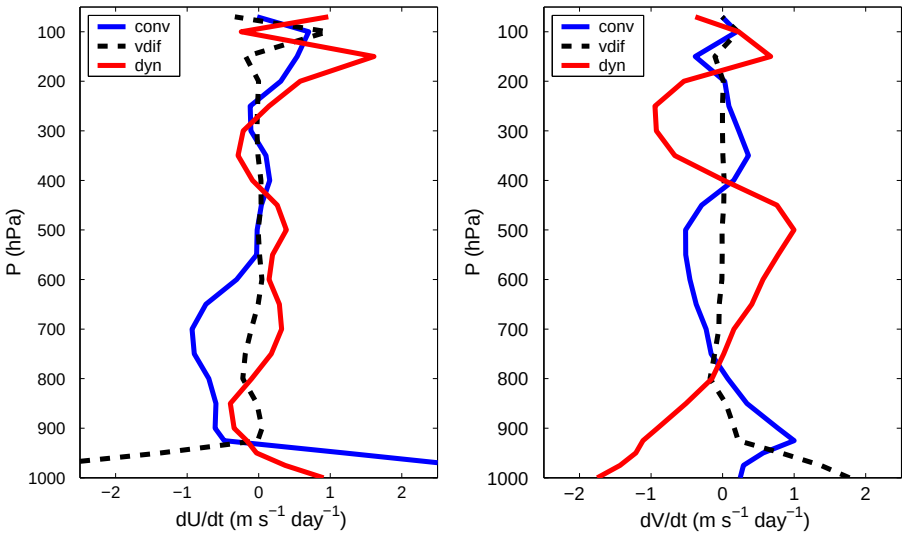

Figure 3.13: Momentum budgets of the zonal and meridional wind components averaged spatially over the IFA and averaged in time over the period from 6 December 1992 to 13 January 1993.

processes, i.e. convection, dynamics (horizontal+vertical advection) and vertical diffusion. From the time averaged tendencies of these physical processes plotted in Fig.3.13 it becomes clear that the U momentum budget is not balanced, as between 600 and 850 hPa the deceleration of the westerly flow by convection is important, whereas between 200 and 100 hPa all physical processes lead to a positive tendency in the zonal wind, i.e. deceleration of the upper-level easterlies. The v-momentum budget, however is well-balanced which is consistent with the relatively small forecast errors. U-momentum budget residuals (i.e. the sum of convective and diffusive tendencies) have also been computed from the radiosonde observations by Tung and Yanai (2002a)

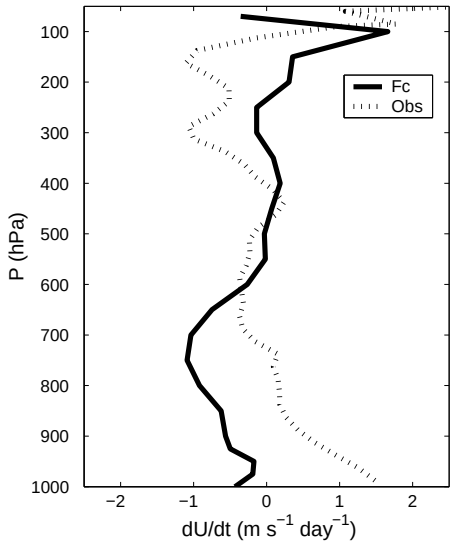

Figure 3.14: Momentum budget residual (sum of convective and diffusive tendencies) averaged over the IFA and the total period considered as computed by Tung and Yanai (2002a) from radiosonde data (dashed) and from T159 12-48 h forecasts (solid).

and have been kindly made available. The comparison of the mean observed and forecasted budget residuals for the zonal wind are shown in Fig. 3.14. Again, the comparison is consistent with the previous results in that the model produces a too strong deceleration of westerly winds at lower levels and a too strong acceleration (=deceleration of the easterlies) at upper-levels. Therefore, improvements in tropical wind forecasts seem to be possible by reducing the momentum friction during strongly sheared events. However, the problem at the upper-levels is more complicated as the dynamical tendencies are strongly coupled to the convective tendencies through the thermal wind balance. Preliminary results indicate that a reasonable fit to the observed upper-level winds can be obtained by an appropriate choice of the entrainment, determining the level of divergent outflow. However, the inclusion of an upgradient momentum transport that maintains the wind-shear instead of a down-gradient transport that reduces the shear might also be necessary, together with a reduction of the diffusive tendencies. This study on the TOGA-CARE period is ongoing, it is part of a collaboration with the UK Met Office, and will also serve as the next case study for the GCSS (GEWEX Cloud System Studies) working group on convection.

3.7 Conclusions

The recent changes in the convection parametrization increased the contribution of the convective rainfall to the total rainfall rate to about 57%, quasi-independently of the model resolution considered. As a result, the forecasts became more ”stable” and the wind and height errors are reduced, as spurious local low-level convergence patterns and associated upper-level divergent outflow due to intense resolved-scale precipitation/vertical motions are reduced. Overall, the precipitation scores and the PDF of rain events were also improved.

It is important to keep in mind that convection is primarily a ”slave” of the large-scale dynamics (instability) and also that every convection parametrization tends to introduce its own biases in a forecast system. Concerning the first point, it has been observed that the new humidity analysis introduced in cycle 26r3 not only had a very positive impact on the overall forecast scores, but also on the spin down and in particular the convective precipitation fields during the first 24 h of the integrations (not shown). Concerning the basic remaining forecast errors that can be attributed to the convection, there is a 3 h shift in the diurnal cycle of convection (maximum rainfall occurs at 12 LST in the forecast compared to 15 LST in the observations), and an underestimation of low and upper-level tropical winds in the presence of strong vertical wind shear. Another deficiency of the ECMWF convection scheme is the lack of sensitivity to environment moisture as documented with CRM studies by Derbyshire et al. (2004).

All these model errors suggest inadequate parametrization of the plume entrainment. However, the entrainment parametrization is very sensitive and improvements on some aspect may result in deterioration on other aspects. The mass entrainment rate is currently formulated as the sum of a constant ’turbulent’ entrainment and an ’organized’ entrainment rate that is proportional to the large-scale moisture convergence. This closure might be difficult to justify from a physical point of view, however it is crucial to assure a first-order balance of the deep convective mass fluxes with the large-scale lifting. Schemes that do not impose such a balance might produce the right radiative/convective equilibrium solution on a time scale of several days, but there is numerically no guarantee that on the scale of the individual synoptic system the ’right’ balance (small residual) between the large-scale lifting and the convection is achieved. As for a convectively unstable atmosphere there is no analytical solution of the ’right’ balanced state or the ’right’ amount of convection. Observables like the fit of short range forecasts of moisture, temperature and wind profiles to radiosonde observations might be used to optimize the convection scheme and its entrainment formulation in the context of the given forecast system. Future work will focus on such an optimization, preferably using a variational method.

Another possibility of revising the entraining plume model would be to use multiple plumes in order to construct a PDF of mass fluxes (for every model grid-column and time step) that is in theory exponential

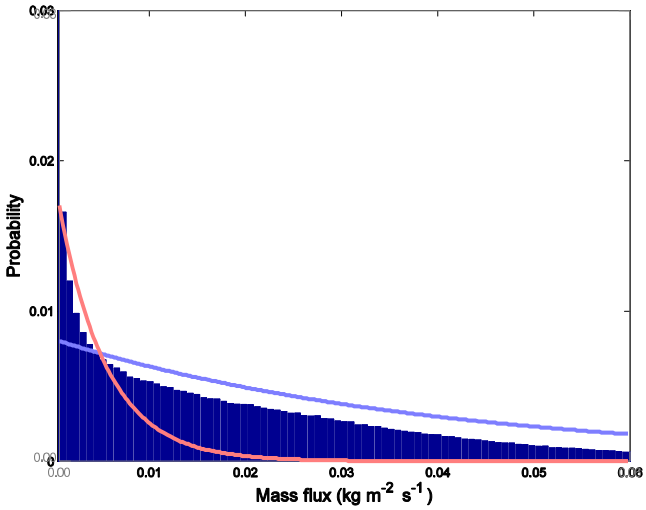

Figure 3.15: PDF of convective mass flux in the Tropics at 1.2 km height from T511 forecasts. The total number of data points used is of order 2×10^6. For comparison, the pink and blue thick lines describe exponential curves with inverse decay constants of 0.008 and 0.04 $kgm^{-2}s^{-1}$, respectively

(Craig and Cohen, 2004). When sampled over the tropical belt and over several model time steps the current scheme already produces a decaying PDF of mass flux (3.15), whose tail is approximately exponential. It is therefore not obvious that a multiple plume formulation would improve the forecasts in this respect, and it would also require the specification of optimal weights for the individual plumes (using a priori fixed weights, or once more, weights based on some notion of balance). That said, in theory a multiple plume model has the capability to concurrently predict both the cloud height and the mass flux profiles at each individual gridpoint (Emanuel, 1991). Moreover, a multi-plume model can include effects such as convective elements developing in the moist remnants of previous convection, (as observed during GATE by Esbensen, 1978; Johnson, 1978; Nicholls and Lemone, 1980). A parametrization for subgrid fluctuations of humidity, as discussed in section 7 would be a useful and probably necessary complement for such an approach.

Thinking towards a long term strategy and beyond the current simple and efficient bulk formulation of convection, the three main approaches considered by the community that are based on some explicit representation of convection should be mentioned: i) a multi-model approach, i) a multi-resolution approach, and iii) a neural network approach. The multi-model approach has been proposed by (Grabowski, 2003; Randall et al., 2003) and essentially consists of nesting a 2D or 3D cloud resolving model in each grid-cell of the global model. This approach includes the ability to comprehensively simulate the cloud-radiation interactions, and is technically relatively simple, but numerically very expensive (at least a factor of $O(10^2)$ compared to current simulations), and has not yet proven its superiority in climate forecasts. The multi-resolution approach consists in representing the meteorological fields by a set of flexible basis functions, e.g. wavelets, to consistently represent a meteorological field with a minimum number of modes. This approach has been applied to 2D turbulence by Schneider et al. (1997) and to date mainly diagnostically to atmospheric fields by Fournier (2002) and Yano et al. (2004). However, this approach is difficult as all basic dynamical model equations must be written in wavelet space with the physics remaining in grid point space, and a criterion has to be continously applied that decides whether new modes (higher resolution) should be introduced and unimportant modes neglected. Finally, the neural network approach (Hsieh and Tang, 1998) can be considered as an empirical method to fit uncertain convection parameters (entrainment, cloud/updraught properties), or even the entire convective tendencies or moist physics tendencies to CRM data. The method is appealing as it would allow a very efficient representation of convection in a dynamical model once an appropriate set of input/output parameters

is defined. However, the method has not yet been applied for this purpose in actual forecast models and also requires a global CRM data set. In the future, groups following the multi-model approach might provide the appropriate data.

4 Clouds: CLD.FC

4.1 23r4 cloud scheme

The ECMWF cloud scheme adds two prognostic equations for the large-scale cloud cover and the mass mixing ratio of total cloud water (the sum of ice and liquid). The scheme, described in detail by Tiedtke (1993) and Gregory et al. (2000), attempts to represent all the significant sources and sinks of these two quantities, and is thus highly coupled to the radiation, vertical diffusion and convection schemes, as well as to the large-scale dynamics (see schematic in fig. 4.1). These can be summarized as followed:

(i) Detrainment from deep and shallow convection

(ii) Horizontal sub-grid mixing of cloud and environmental air

(iii) Adiabatic or diabatic warming or cooling

(iv) Precipitation processes

(v) Subgrid fluxes in a turbulent boundary layer

(vi) Cloud-top entrainment

Note that process (iii) only takes cloud sources and sinks due to temperature changes into account and not total water. The justification is that the latter processes are accounted for separately; for example the source of cloud due to deep convection. Moreover, even if the large-scale flow causes a Eulerian net convergence of moisture at a grid point, any associated increase in cloud will be accounted for by the large scale advection of cloud quantities.

The dominant contributions are the detrainment of cloud water from convective updraughts, condensation/evaporation due to cooling/warming, conversion of cloud water to precipitation and finally dissipative processes (processes i-iv, Teixeira, 2001; Fillion and Mahfouf, 2003). The dominance of these four processes also resulted in their adoption as the basis for a new linearized scheme for data assimilation purposes, described by Tompkins and Janisková (2004) and in section 6 of the present document. Furthermore, processes (v) and (vi) concerning stratocumulus clouds will no longer be required with the implementation of the new boundary layer scheme described in section 5, since the new scheme will account for these processes separately.

In terms of the precipitation processes, ice in clouds can settle, which is an important process for determining the tropical high cloud structure and consequent radiative forcing (Jakob, 2002), while liquid water droplets are held in suspension. Currently the ice settling process acts as a proxy for snow creation processes, since settling into non cloudy regions is converted immediately into snow and falls out of the model column within one timestep. Some consequences of this simplification are addressed in the following section. For warm rain autoconversion a simple Sundqvist et al. (1989) formulation is used, which nevertheless compares reasonably well to observations of precipitating shallow clouds (Guan et al., 2002; Tisler and Savijarvi, 2002). Adjustments are made to the precipitation formation timescale and critical threshold for efficient production to crudely account for accretion and Bergeron-Findeisen processes. The scheme allows precipitation to evaporate (sublimate) during its descent and also includes the melting of snow.

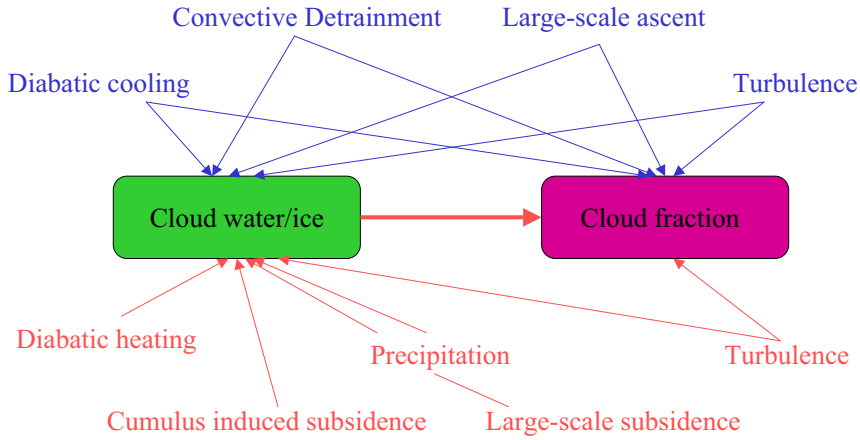

Figure 4.1: Schematic illustrating how the cloud scheme is linked to the other model components

4.2 25r4 modifications

A substantial package of changes was introduced into the cloud scheme at cycle 25r4, which had an impact on the climatology of clouds.

4.2.1 Numerics

As cloud processes are rapidly varying in time, care must be taken when the equations governing the evolution of cloud water and cover are integrated over the relatively large model time steps (for example, the standard timestep for the T_L95 model resolution is one hour). The approach of Tiedtke (1993) was to divide the equations governing cloud cover and water into two categories. The first category consisted of all the terms that were treated explicitly. Thus if a process is deemed to increase cloud cover by 30% in an hour then a increase of exactly 15% would occur after one timestep of 30 minutes. Thus for rapidly varying processes it is possible for cloud variables to exceed physically reasonable bounds and numerically unstable solutions can result if they are treated explicitly. Tiedtke approached this potential hazard by handling some processes implicitly; the second category. An equation for each generic cloud variable ϕ was thus introduced, which considers the n explicitly and m implicitly treated processes:

$$\frac{d\phi}{dt} = \sum_{i=1}^{n} C_i + \sum_{j=1}^{m} D_j \phi, \tag{4.1}$$

where C_i and $D_j\phi$ give the rate of change of ϕ due to the i^{th} explicit and j^{th} implicit terms, respectively. Any term that is treated implicitly is incorporated into the first order term D_j. For example, autoconversion is parametrized by the Sundqvist et al. (1989) form:

$$\frac{dq_l}{dt} = -Kq_l \left(1 - e^{-\frac{q_l}{q_{l\,crit}}^2}\right) \tag{4.2}$$

where q_l is the liquid water mass mixing ratio and q_{lcrit} is a critical value of q_l at which the process becomes efficient and K is a constant inverse timescale. This is incorporated into the numerical framework by setting

$$D_{j=precip} = -K\left(1 - e^{-\frac{q_l^0}{q_{lcrit}}^2}\right) \tag{4.3}$$

for this term, where the q_l^0 refers to the beginning of timestep value for q_l. For the cloud cover the following processes are treated in this way: convective detrainment, generation/destruction by cooling or warming, generation at the top of stratocumulus layers, destruction by turbulent mixing. On the other hand, for cloud water the implicit processes are: advection by convective subsidence, generation/destruction by cooling/warming, cloud top entrainment, sedimentation of ice and warm and mixed phase precipitation generation.

The above list of processes was modified slightly to treat convective subsidence and cloud top entrainment implicitly, but the major alteration to the numerics of the scheme in 25r4 involved the time level at which processes were treated. Originally, the processes of the cloud scheme were treated sequentially, with each (group of) process(es) modifying the initial profiles of temperature, humidity and cloud quantities that are used by the subsequent processes. Thus, for example, precipitation generation, given the lowest priority, would not operate if the higher priority dissipation term removes all cloud water over a timestep.

A revised philosophy was adopted for cycle 25r4, such that all cloud processes, whether explicit or implicit, were considered to operate in parallel in a stationary equilibrium state. All processes therefore use identical thermodynamical and dynamical input profiles. However, it should be noted that this treatment is only true at the level of the cloud scheme, and these are still ”first-guess” profiles: beginning of timestep values that have been subsequently modified to take into account the tendencies due to physics parametrizations such as deep and shallow convection, radiation and vertical diffusion processes.

As well as eradicating 'cloud processism'[4], an additional cosmetic benefit is that this approach allows a far greater modulization of the code, significantly facilitating its legibility and ease of understanding. A significant motivation for this is that it enables future development to be carried out with ease, with the possibility or adding or disabling individual cloud processes without the necessity of modifying the numerical implementation or having to decide which 'priority' should be allocated to the new process.

Despite all these apparent advantages and a clear motivation for the new approach, any numerical approach must be pragmatic and no perfect solution exists for a model such as the IFS using high vertical resolution with relatively long timesteps. For example, since a first order linear approach is used for implicit terms, rather than an exact solution, then the new approach can lead to time truncation errors. For the example of deep convection detraining into a cloud free grid box, then the linear approximation of Sundqvist et al. (1989) precipitation generation term will remain zero, since the zero value for q_l^0 in the initially cloud-free state will imply $D_{j=precip} = 0$ in eqn. 4.3. Thus the detrained water will increase over one timestep without producing precipitation, which will only begin to form at the subsequent timestep. This was not the case for the previous implementation which instead used a mid-timestep “first guess” value for q_l^0 in eqn. 4.3, such that detrained water from convection could produce precipitation during the same timestep. This timestep truncation would of course be avoided if eqn. 4.1 used an exact solution for each term.

Since some terms are treated explicitly, there is nothing to prevent values of cloud water or cloud cover from overshooting during one timestep, in other words that unphysical values may result. In earlier cycles, these were handled by simply clipping the final tendencies for each layer to maintain the cloud variables within physically reasonable limits. However, this approach can lead to significant conservation errors. For example, if ice sedimentation combined with other linear sink terms reduces the cloud mass below zero over a time step, and

[4]prejudice or discrimination based on the belief that certain cloud processes have traits that render superiority over others, and therefore deserve priority treatment

the final combined tendency is subsequently clipped to correct this, the ice sedimentation source term for layer below has to take this into account to prevent an artificial net creation of total water. The post-25r4 treatment therefore calculates the precise point during the timestep at which the cloud water or cover reaches zero (or additionally one in the case of cloud cover) and then limits the source and sink terms to equal precisely the advect transport terms for the remainder of the timestep. This approach ensures conservation of total water, and gives an effective balance between linear and nonlinear terms (i.e. once again no processes are given priority).

4.2.2 Ice microphysics

One of the major changes made to the 25r4 physics of the cloud scheme concerned the treatment of ice sedimentation. This has been shown by Jakob (2002) (among others) to be a crucial aspect of the ECMWF model (in common with other models); a result of its strong influence on TOA fluxes in the tropics. While the alterations of cycle 25r4 are referred to as changes to the physics of the scheme, they are in fact addressing model shortcomings due to the *numerics* of the scheme's implementation. This serves once again as a reminder of the importance of the numerical implementation of any aspect of a scheme, and that the physics and numerics are often inextricably bound.

The description of the pre-25r4 ice sedimentation scheme appears reasonable in its assumptions: The ice variable is diagnostically divided into two categories of large and small ice particle sizes. The mass mixing ratio of small ice particles, defined as having a dimension less than the threshold of 100 microns ($q_{i<100}$), is given in equation 5 of McFarquhar and Heymsfield (1997), and repeated here for clarity:

$$q_{i<100} = 81.7(\rho q_i)^{0.837} \tag{4.4}$$

The mass is not allowed to exceed q_i of course, and the modified constant 81.7 is simply due to the fact that McFarquhar and Heymsfield (1997) use units of gm^{-3}. The large particles are assumed to fall out of a column as snow within one timestep, while the smaller ones are converted to snow if they fall into a clear region or are allowed to sediment to the next layer if it is cloudy (using the maximum-random overlap rules for cloud cover to determine this). The sedimentation fallspeeds for small ice particles are specified according to mass mixing ratio and are given by Heymsfield and Donner (1990).

Although these 'rules' governing the sedimentation of ice appear reasonable, closer examination of their original numerical implementation as it stood at cycle 25r4 reveals that the scheme did not function as intended. The reason is as follows. Although sedimentation of ice was treated implicitly, an additional limit was placed on the large ice fall speed to prevent it from exceeding the speed specified by the CFL stability criterion. However, due to the high vertical resolution used by the model (currently 60 vertical levels), and the relatively long timesteps, this produces 'effective' sedimentation rates that are a fraction of a metre per second for the large ice particles. For example, for the T95 model, which uses a one hour timestep, the effective fall speed for large-ice in the upper troposphere is roughly 0.2 m s^{-1}. It is immediately clear why this is unreasonable, since the fallspeeds observed by Heymsfield and Donner (1990) exceed this level even for small ice mass mixing ratios. In other words, in the numerical implementation, small ice particles actually fall significantly faster than their large-diameter compatriots! The problem is compounded by the fact that the ratio of larger to small ice increases as a function of mean ice mass mixing ratio (McFarquhar and Heymsfield, 1997), which results in the mean ice fall speed (and thus indirectly the conversion from ice to snow) being almost completely independent of ice mass mixing ratio, in complete contrast to observations. This is illustrated in Fig. 4.2, which shows that for appreciable ice mass mixing ratios the mean fall speed is a constant for the T95 model resolution. The figure also shows that the same is true for the T511 version of the model despite the shorter timesteps; for $q_i > 0.1 gkg^{-1}$ the fall speed is almost a constant.

The solution adopted in cycle 25r4 was to allocate sedimentation rates (accordingly autoconversion rates) for

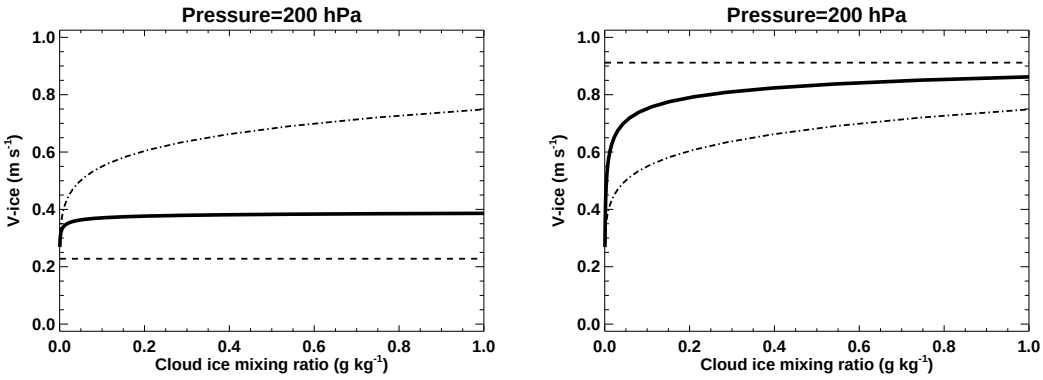

Figure 4.2: The pre-25r4 model cycle fall speed adopted for small (dot-dash), large (dashed) and mean (solid) diameter ice particles at a pressure level of 200 hPa. The left figure is for a 3600s timestep used by the T_L95 model, while the right panel is for the 900s timestep used by the T_L511 model, in both cases for the 60 level vertical grid.

the large ice particles according to their mass mixing ratios after McFarquhar and Heymsfield (1997), while small ice diameters particles are assumed to fall with a fixed and small sedimentation rate of 0.15 m s^{-1}. This gives a mean sedimentation rate (autoconversion to snow) that increases with mass mixing ratio. Note that while this form is resolution independent, this correction increases significantly the rate of ice to snow autoconversion, especially for longer timesteps, adversely affecting radiative fluxes in the tropics. As a short-term remedy to this problem, the constant in the Heymsfield and Donner (1990) relationship for ice fall speeds was reduced from 3.29 to 2.3, which is the solution shown in Fig. 4.3. This form gives fall speeds for large ice mass mixing ratios that lie someway between the earlier T95 and T511 solutions, while preserving at the same time the relationship between fall speeds and ice mass observed in measurements.

It should also be noted that one reason why observed fall speeds can not be adopted directly in the model is that the present approach crudely assumes ice falling into clear sky regions is converted automatically to snow which falls out of the column. The result of this is that a relationship which is intended to govern one particle process, sedimentation, is also applied to a completely different cloud process, namely the autoconversion of ice to snow. While both of these processes can be crudely approximated by a power law, i.e. $\frac{dq_i}{dt} \propto -q_i^K$, the value of the exponent according to observations is drastically different, taking a value of 0.16 for ice sedimentation according to Heymsfield and Donner (1990), while usually it is around unity for the ice to snow conversion process (e.g. Lin et al., 1983; Lohmann and Roeckner, 1996). This will be addressed in future when a separate prognostic variable for ice mass is introduced into the model.

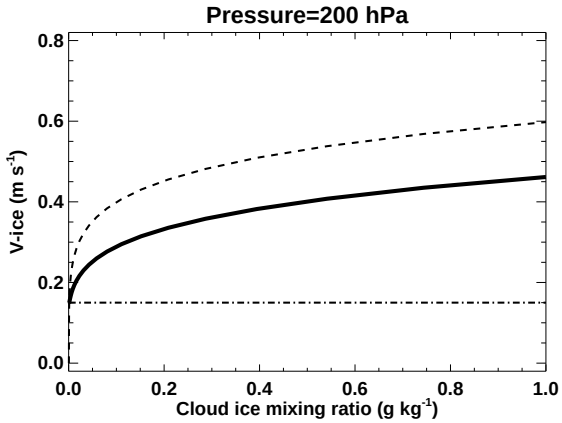

Figure 4.3: The post-25r4 model cycle fall speed adopted for small (dot-dash), large (dashed) and mean (solid) diameter ice particles at a pressure level of 200 hPa.

4.2.3 Cloud top entrainment

The pre-25r4 cloud scheme separately handled the mixing of prognostic variables through an inversion at cloud top. The numerical implementation often resulted in inconsistent mixing, and non-conservation of total water. The post-25r4 model version uses an implicit solution to mix the conserved variables through cloud top, ensuring conservation of total water. Care is taken to ensure that the mass flux implied by the mixing of cloud variables is used for the mixing of other thermodynamic and dynamical quantities.

4.2.4 Convectively-induced subsidence

The cloud water transport by convectively induced subsidence was previously treated separately from other quantities. The transport was handled as a simple flux between vertically adjacent levels. The evaporation of liquid water (or sublimation of ice) if the vertical transport resulted in subsaturated air parcels at the arrival point was neglected. This had the potential to falsely transport cloud water (and associated cloud cover) below the correct cloud base.

The new implementation addressed this problem by transporting total water, and calculating the evaporation of liquid water or ice that would occur at the arrival point, assuming no subsaturation is allowed to persist in the presence of clouds (which is of course a poor assumption for ice clouds, but one that can not be presently addressed until the implementation of a separate ice variable). Conservation of total water was ensured.

4.3 Impact on cloud climatology

As indicated in the introduction to this section, the main aim of the 25r4 cloud scheme update was to improve the numerics and organisation of the cloud scheme code without changing the physics substantially, to produce a scheme that was easy to maintain and develop in the future. However, during the development a number of physics changes were necessary, (as described above) and these, in combination with a number of error corrections and the modification of the numerical method used to implement the physical processes had a significant impact on the model climatology. In order to maintain the performance of the previous scheme, a number of parameters required 'tuning'. The main re-adjustment was the reduction in the constant in the Heymsfield and Donner (1990) relationship for ice fall speeds that was reduced from 3.29 to 2.3 (see section 4.2.2 above). However, it was also necessary to halve the diffusion coefficient for cloud mixing from 11.6 to 5.8 days, which is roughly equivalent to the mean timescale resulting from the (simple first order) horizontal shear driven turbulent mixing closure of Tompkins (2002).

The direct effect of the cloud scheme package on the cloud cover climatology of cycle 25r1 is shown in figure 4.4. This comparison is for one forecast only, lasting just four months, as used in the study of Jung and Tompkins (2003). While the fields are reasonably noisy due to the small temporal sample, certain robust features can be seen in the comparison. It is clear that the majority of the systematic errors in the cloud climatology were not significantly altered by the numerical update. For example, the lack of cloud over the summertime Eurasian continent is evident in both model experiments, and the lack of stratocumulus clouds has, if anything, slightly deteriorated. However, the package does have some benefits, in that the overestimate of cloud in tropics was improved slightly, while the significant underestimate in the southern hemisphere mid latitudes was significantly improved. A result of the revised ice formulation, this reduction in SH cloud cover bias also slightly improved biases in the infra-red TOA radiative budget in this region (not shown).

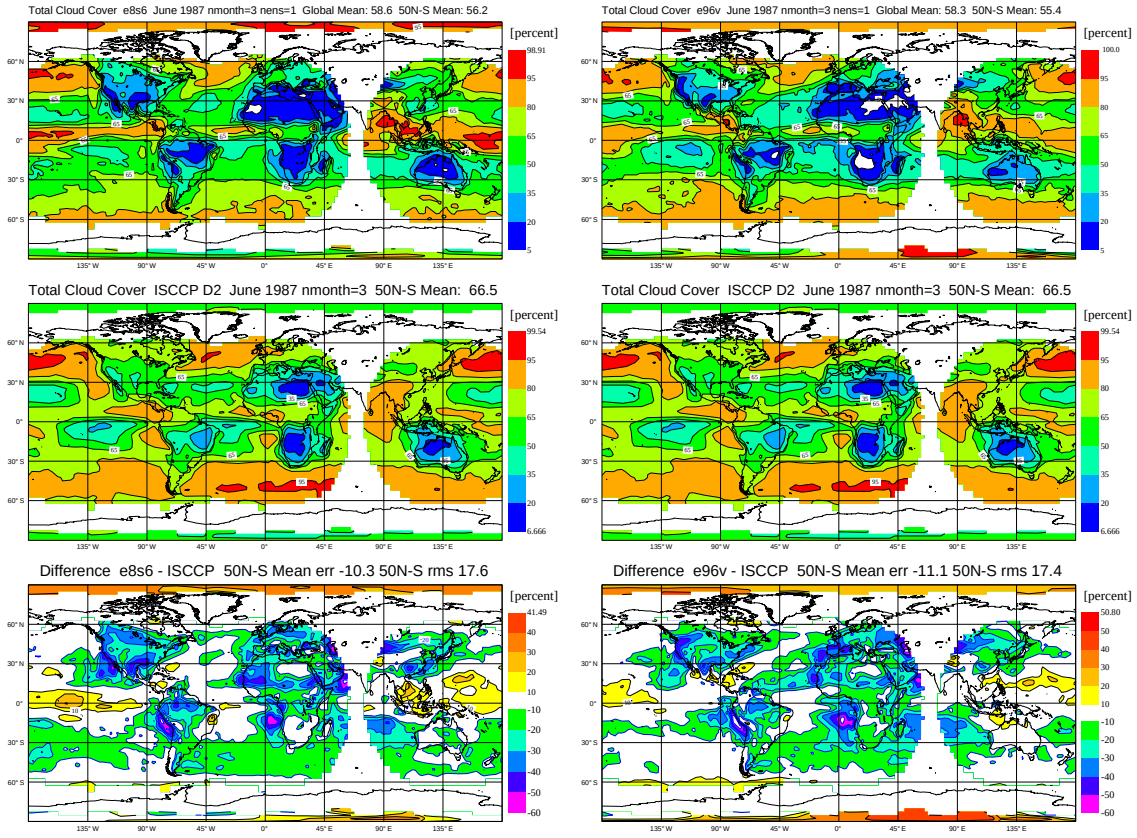

Figure 4.4: Three month average (top) model total cloud cover compared to (middle) ISCCP D2 retrieval and the difference. The left column is for model cycle 25r1 while the right hand column is 25r1 modified by the numerics update

4.4 Future development: Ice microphysics

The future development of the cloud scheme is closely tied to the plans for a parameterization of subgrid-scale fluctuations of total water outlined in section 7. This scheme will be used to parametrize cloud cover, replacing the existing Tiedtke approach of a prognostic cloud cover equation.

However, this section has revealed other weaknesses in the microphysics of the cloud scheme CLD.FC which will be addressed in a parallel development. It is clear that the most significant of these pertain to the representation of the ice microphysics. While knowledge of ice microphysics is currently hampered by a lack of observations, the current use of ice sedimentation rates observed by Heymsfield and Donner (1990) to represent the entirely contrasting autoconversion process of ice crystal aggregation is clearly inadequate. The dependence on the vertical resolution-dependent maximum-random overlap cloud structure is also highly undesirable. Moreover, the current approach of a single cloud variable for ice and liquid water does not allow for the inclusion of super-cooled water droplet and hinders the representation of hetero and homogenous nucleation processes. The current scheme does not permit supersaturation with respect to ice saturation to occur, which is commonly observed in the upper troposphere both in mid latitudes and the tropics (Heymsfield et al., 1998; Gierens et al., 2000; Spichtinger et al., 2003; Gierens et al., 2004), nor does it permit ice clouds to coexist in locally sub-saturated conditions (observed by Strom et al., 2003).

Therefore, in line with the incremental development approach encouraged for the IFS, a multi-stage implemen-

tation of more complex microphysics will be introduced, with a strong collaboration with the UK Met Office envisaged in this process.

4.4.1 Snow autoconversion

In the first stage, a relatively simple formula along the lines of Lin et al. (1983) will be used to represent the ice aggregation process. For compatibility with the existing warm rain processes, this may be implemented using a Sundqvist-type form (see eqn. 4.2) but using (temperature dependent) rate coefficients and critical mixing ratios suitable for the ice process. The sedimentation of ice will subsequently only act as a transport term for ice mixing ratios. As stated above, ice fall speeds frequently breach the CFL stability criterion. This is not a stability issue since an implicit solver is used, but it does imply that the observed fall speeds are not reflected in the model, and that the solution will be timestep dependent. Semi-Lagrangian or time splitting methods will be investigated, although it is noted that neither approach is a panacea for numerical difficulties associated with long timesteps.

4.4.2 Separate prognostic ice equation

The second stage will involve the introduction of a separate ice variable. This will mostly be a technical change, with separate large-scale advection of the new ice equation, and freezing initially constrained to match the current diagnostically imposed ice/liquid division.

4.4.3 Nucleation of ice

With the separate ice variable in place, a framework will be available for the inclusion of homogenous nucleation of ice. With the planned increase in complexity of the representation of aerosols in the model it is even possible that in the long term heterogenous nucleation could be included, along with a separate ice number concentration prognostic variable.

Note that the inclusion of the nucleation process and the presence of supersaturation on the subgrid-scale complicates the implementation of a statistical type cloud scheme based on the parametrization of subgrid total water fluctuations planned in section 7 since these schemes traditionally assume no supersaturation can exist to predict the cloud region (e.g. Mellor, 1977; Sommeria and Deardorff, 1977).

4.5 Conclusions

For cycle 25r4 a significantly effort was made to revamp the cloud scheme. This included both numerics and physics modifications. The numerics changes aimed to treat all cloud physical processes at the same time level without giving priority to any process, while ensuring that the modified scheme adequately conserves total water and moist static energy. An additional benefit of this overhaul is that it enabled the code to be substantially reorganized and modularized to improve its legibility and ease of comprehension, and facilitate future modification.

There were a number of changes to the cloud scheme physics in addition, but it was noted that these were also forced by previous inadequacies in the numerical implementation of the scheme. During the implementation of this new scheme it was ascertained that the numerical scheme adopted to solve the governing equations is just as important as the equations themselves; with changes in cloud water of up to a factor of two obtainable

just from the choice of numerics. A number of tuning parameters thus required readjustment to maintain the quality of the cloud climatology. It was shown that the implementation of the package had some mild benefits for the cloud cover climatology of the model when compared to ISCCP data.

5 Boundary Layer clouds: VDF.FC

5.1 Introduction

Boundary layer (BL) clouds play a major role in the Earth radiation budget and have a strong impact on the energy budget at the surface which is important for the forcing of land and ocean models (e.g. Ma et al., 1996). Because of the strong modulation of the solar radiation by these BL clouds, the perception of the weather is also strongly influenced by them. However, a proper modelling and forecasting of BL clouds still poses a serious problem and has been the subject of a range of model developments by different groups (Lock et al., 2000; Lappen and Randall, 2001; Grenier and Bretherton, 2001; Bretherton et al., 2004).

The IFS has major difficulties with BL clouds as illustrated in sections 2 and 5.4. The main problem is a systematic lack of stratocumulus clouds, but also the cumulus regime shows deficiencies e.g. in the trades and in the diurnal cycle over land (see section 5.5).

A successful treatment of boundary layer clouds relies on realistic large scale conditions as well as sub-grid vertical transports and cloud generation and decay. In the current ECMWF model four separate but interactive parametrizations describe sub-grid physical processes: vertical diffusion, convection, clouds and radiation. Table 4 summarizes these processes and the associated parametrizations in the current system. The dominant components include a vertical diffusion scheme that uses dry conserved variables (dry static energy and specific humidity) and does not consider cloud processes at all. The shallow convection mass flux scheme is designed to simulate cumulus but may also produce stratocumulus cloud if only one vertical layer is covered (thus by definition introducing an undesirable vertical resolution dependence). Finally, single layer stratiform clouds are handled as a special case in the large-scale cloud scheme, based on the boundary layer moisture flux at cloud base. A cloud top entrainment term is also included to ensure a balance between moistening from the surface and drying from the top of the boundary layer.

Table 4: The multiplicity of parametrizations used to describe BL clouds in the current ECMWF model.

	process	**parametrization**
Transport	dry diffusion	vertical diffusion
	moist mass flux	convection
	cloud top entrainment	cloud & vertical diffusion & radiation
Cloud generation	mass flux detrainment	convection
	supersaturation removal	convection & cloud & radiation
Cloud decay	cumulus induced subsidence	convection & cloud
	precipitation	convection & cloud
	cloud erosion	cloud

The main problem with the current configuration of schemes (i.e. dry boundary layer diffusion, cumulus mass flux, cloud and radiation) is that they function almost completely independently, while boundary layer clouds require a high level of coupling between all these processes. Numerical issues are paramount for long time steps, because boundary layer processes are fast, require implicit numerics and in order to have a good balance between processes it is necessary to combine them in a single solver. An additional problem is that the pro-

duction of stratocumulus relies mainly on the detrainment of condensate from the convective mass flux scheme which favors less well-mixed profiles and therefore less liquid water path than common in stratocumulus regions.

To overcome these deficiencies it was decided to formulate a new boundary layer scheme with diffusive mixing and mass flux transport in moist conserved variables (see details in section 5.2). It provides a system in which stratocumulus can be maintained through moist mixing and creates a framework in which future development can take place. The ultimate goal is to unify the treatment of stratocumulus, shallow cumulus and dry turbulent diffusion in the same scheme with the processes solved simultaneously with a single implicit solver.

A general problem in modelling boundary layer clouds is the distinction between shallow cumulus and stratocumulus. From analysis of large eddy simulation (LES) data and from experience with large scale models it is recognized that the mass flux concept is appropriate for the cumulus regime (e.g. Tiedtke, 1989; Siebesma, 1996). Moist diffusion leading towards a well-mixed boundary layer works well in the coupled stratocumulus regime although cloud top entrainment parametrization is still an important issue (e.g. Duynkerke and Hignett, 1993). However, attempting to approach a well-mixed layer with strong diffusion up to cloud top in the cumulus regime would dominate over the less strong mixing from the mass flux scheme and result in a stratiform cloud layer rather than a cumulus layer. The main challenge in a large scale model is to have a parametrization or a set of parametrizations that can handle both regimes. Lock et al. (2000) address this issue by having multiple schemes and switching between them dependent on criteria that rely on the shape of the thermodynamic profiles. The new PBL framework requires a decision algorithm to activate either the existing Tiedtke (1989) shallow convection scheme, or to apply the new moist boundary layer scheme up to cloud top. Section 5.3 investigates four potential decision algorithms and motivates the initial choice of a criterion based on inversion strength (Klein and Hartmann, 1993).

Section 5.4 presents SCM and GCM results from the new scheme and section 5.5 discusses an investigation of modelled shallow convection over land against observations over the ARM SGP site in Oklahoma, USA.

The proposed combined mass flux/diffusion PBL scheme is only the starting point of a more general attempt to unify the schemes for the boundary layer and clouds (see section 5.6). In future, the cumulus transport will be added to the boundary layer scheme, other ways of closure will be explored (e.g. Grant and Brown, 1999), and alternatives to the criterion for cumulus/stratocumulus distinction will be tested (Stevens, 2000).

5.2 New scheme for the dry boundary layer and stratocumulus

5.2.1 Concept

Given the problems with the current scheme in stratocumulus regions it was decided that an entirely new framework was needed. The main ingredients deemed necessary are: (i) moist conserved variables used in the vertical diffusion, (ii) an eventual unification of the BL and shallow convection, and (iii) a mass flux component added to the BL scheme to describe non-local fluxes. Note that for (ii) it is also attractive to have a combined solver for both diffusion and mass flux terms.

The concept behind the combined mass flux/diffusion approach is to describe the strong large-scale organized updraughts with mass fluxes and the remaining small-scale turbulent part with diffusion. The up/down-draughts described by the mass flux term allow for non-local mixing, while the local mixing described by the diffusion term is limited to down gradient transports. Siebesma and Cuijpers (1995) arbitrarily define a strong updraught as a fixed small fractional area a_u containing the strongest upward vertical motions. The horizontal distribution

of a field ϕ can then be described with perturbation terms in both updraught and environment areas separately

$$\phi_u = \phi'_u + \overline{\phi_u}^u, \qquad \text{and} \qquad \phi_e = \phi'_e + \overline{\phi_e}^e, \tag{5.1}$$

where u and e refer to the updraught and environment areas both for the field and the averaging operator. The domain average then becomes

$$\overline{\phi} = a_u \overline{\phi_u}^u + (1 - a_u)\overline{\phi_e}^e. \tag{5.2}$$

After some manipulation the vertical turbulent flux breaks into three terms

$$\overline{w'\phi'} = a_u \overline{w'\phi'_u}^u + (1 - a_u)\overline{w'\phi'_e}^e + M(\phi_u - \phi_e), \tag{5.3}$$

where $M = a_u w_u$ is the mass flux of the strongest updraughts. It is assumed $a_u \ll 1$ while $\overline{w'\phi'_u}^u$ and $\overline{w'\phi'_e}^e$ are of same order of magnitude. This permit the first term on the RHS to be neglected and $\phi_e \simeq \overline{\phi}$. The second term on the RHS can be approximated by diffusion with a coefficient of K_h. Then

$$\overline{w'\phi'} = -K_h \frac{\partial \overline{\phi}}{\partial z} + M(\phi_u - \overline{\phi}). \tag{5.4}$$

Equation (5.4) is the basic equation for vertical transport and will be considered for the moist conserved variables of generalized liquid water static energy s_l and total water mass mixing ratio q_t

$$s_l = gz + c_p T - L_c q_l - L_s q_i \,, \tag{5.5}$$

$$q_t = q_v + q_l + q_i \,. \tag{5.6}$$

Here g is the constant of gravity, c_p is the specific heat at constant pressure, L_c and L_s are the latent heat of condensation and sublimation, and q_v, q_l and q_i are the water vapor, liquid water and ice water mixing ratios.

The details of the mass flux and diffusion components and their combined solver as well as a description of clouds within the boundary layer are described in Appendix A. In short, the mass flux employs a single bulk plume model and is closed near the surface as a fraction of the tail of the vertical velocity distribution. Eddy-diffusion coefficients are the sum of a surface and cloud top driven K-profile, which are overwritten with an explicit BL top entrainment. BL clouds are treated by predicting the variance of total water.

5.3 Cumulus and its distinction from stratocumulus

Fig. 5.1 shows a schematic of the transition from stratocumulus to trade cumulus and deep convection. The new parametrization of stratocumulus, as introduced in the previous section, relies on a diffusion (K) description of the local mixing and a mass flux (M) description of the strongest updraughts. For the stratocumulus regime the original Tiedtke (1989) shallow convection scheme is turned off.

For the shallow or deep convective regimes, the new parametrization uses the cloud base z_{cb}, diagnosed by the BL parcel, as the top of the BL (K). The Tiedtke (1989) convection scheme then adds a mass flux M_2 into the clouds. This updated description of shallow and deep convection is very similar to the old description except that the old scheme used diffusion up to a dry BL top and added a surface based BL top entrainment near cloud base. The new scheme currently excludes the BL mass flux M_1. But we will soon experiment with moving the cloud mass flux M_2 to the BL scheme and adding the dry mass flux M_1.

The challenge then remains to differentiate between the stratocumulus regime, which represents a well-mixed BL up to cloud top, and the cumulus or decoupled BL regime, where the vertical mixing processes do not

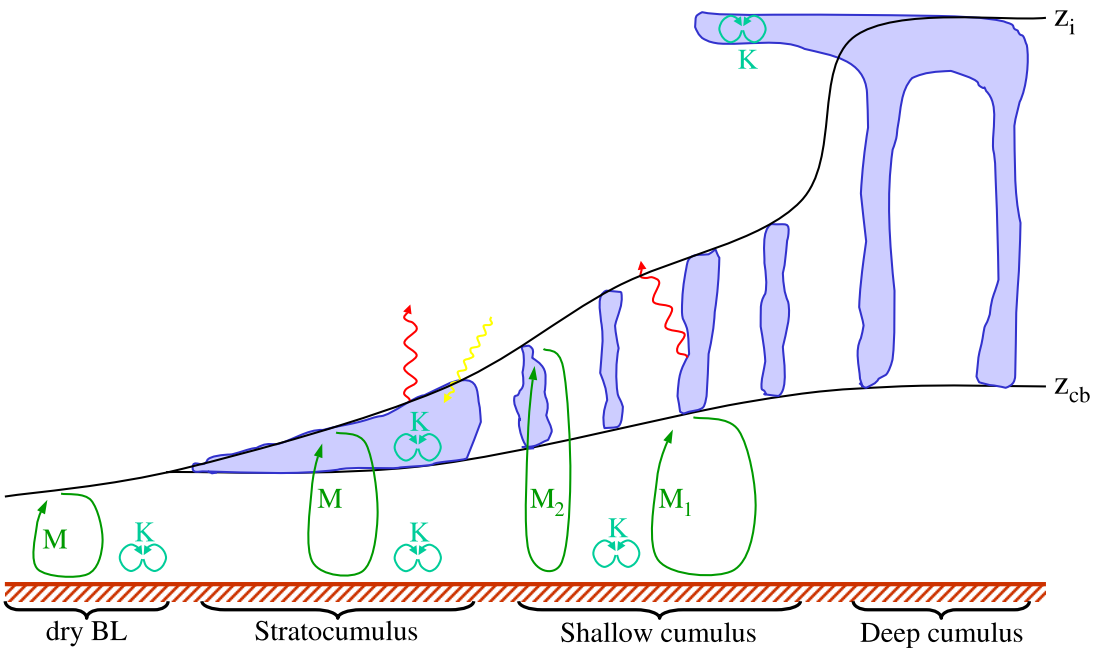

Figure 5.1: Transition of stratocumulus to shallow cumulus and deep convection. The parametrization of the associated convective transports in the new scheme are illustrated in turquoise for the diffusion component and in green for the mass flux component. See text for interpretation.

achieve a single well-mixed layer. The criterion to distinguish between the two regimes will be called *decoupling criteria* in the text below. This distinction is of great importance for GCMs and is a subject of active research (Stevens, 2000). It will therefore be discussed in detail in this section.

Satellite pictures (see Fig. 5.2) of oceanic convection show marked transitions between very high and low cloud cover. Open and closed cell convection, cloud top entrainment instability (explained below), solar heating, drizzle and aerosols have all been mentioned as physical mechanisms involved in this transition.

To illustrate the challenge of distinguishing between stratocumulus and cumulus in the model and test multiple possible decoupling criteria, the potential boundary layer cloud cover and depth is diagnosed by lifting an undiluted parcel until it comes to rest. The idea is that strong BL type mixing in moist conserved variables would result in a cloud cover that is equivalent to this potential cover. It is clear from Fig. 5.3a that such strong mixing would not be realistic because most of the tropical oceans would be covered 100% by cloud.

Even switching off shallow convection has dramatic consequences in the IFS as is illustrated in the Fig. 5.3b. The cloud cover over the oceans goes up to a very unrealistic level. Clearly the shallow convection scheme plays a crucial role in maintaining the thermodynamic structure at the boundary layer top and in drying the boundary layer from above. When this mechanism is switched off, the boundary layer diffusion attempts to mix up to cloud top resulting in very high cloud cover.

From this diagnostic it is clear that the switching between cumulus and well-mixed stratocumulus is a crucial component of the system. For the stratocumulus regime, shallow convection is then turned off, while for the cumulus regime the BL top is set to the cloud base and the BL mass-flux is turned off.

A number of these decoupling criteria are explored.

5.3.1 Decoupling criterion: Cloud thickness

Stratocumulus clouds are typically up to 500m deep and virtually never exceed 1000m depth. Consequently a decoupling criterion of cloud thickness larger than 1000m was tested. One advantage of such a method is its simplicity and numerical robustness; a desirable feature. Fig. 5.4a shows the corresponding decoupling diagnostic. From the potential maximum stratocumulus cover shown in Fig. 5.3a, the fraction shown in Fig. 5.4a is diagnosed as decoupled. This identifies for example the (blue) regions off the coast of California (0% decoupling yet 100% potential cloud) as stratocumulus. Figure 5.4b shows the impact on low cloud cover of using the new PBL parametrization with this cloud height base decoupling criterion compared to the old model. It adds realistic stratocumulus cloud off the West coasts but also increases cloud cover in trade cumulus areas where much lower cloud fractions are observed in nature. Additionally, tropical temperature errors at 850hPa were increased by this implementation because the BL was mixing unrealistically aggressively.

5.3.2 Decoupling criterion: Cloud top entrainment instability

Cloud top entrainment instability (CTEI) was proposed by Randall (1980) and Deardorff (1980) as a mechanism of destabilizing stratocumulus cloud decks. According to Randall (1980), an unsaturated parcel is entrained, cooled and moistened by evaporation and accelerated downward by the buoyancy force. This happens only when the temperature inversion is sufficiently small and the total water inversion is sufficiently large, which for typical conditions, can be described simply by the following criterion:

$$0.4\triangle s_l - 0.3L_c\triangle q_t < 0. \tag{5.7}$$

Fig. 5.4c shows the CTEI decoupling diagnostic on the left and the interactive CTEI climate run on the right. It

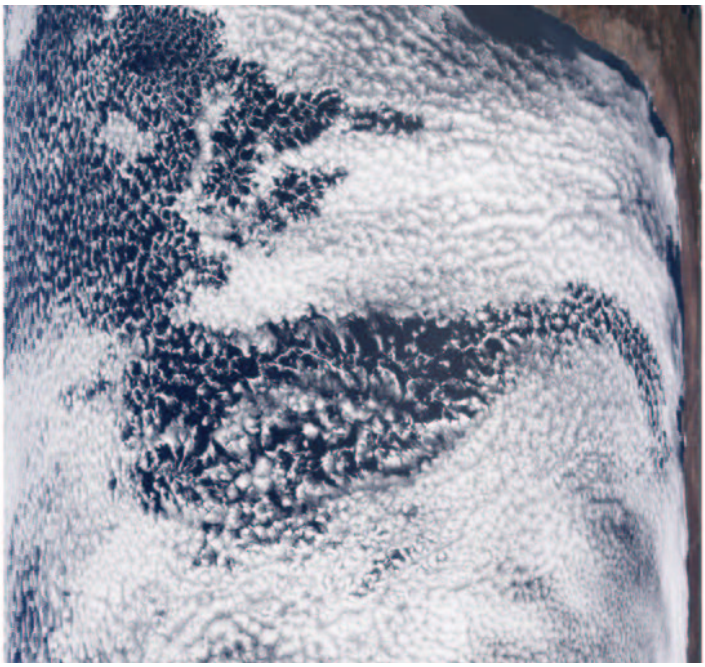

Figure 5.2: Transition of stratocumulus to shallow cumulus from MODIS observation off the coast of Chile during the EPIC stratocumulus field experiment in 2001.

(a) potential cloudiness - diagnostic

(b) LCC for shallow convection off - interactive

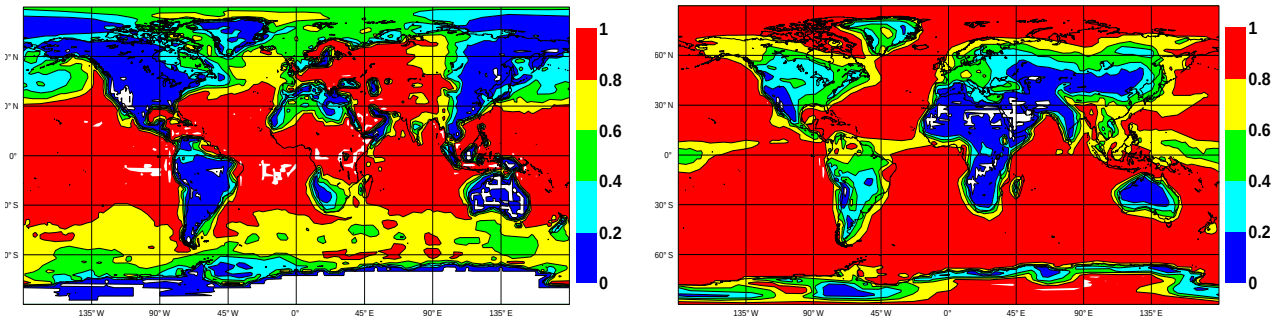

Figure 5.3: The left panel shows the diagnostic potential surface based cloudiness. It is defined as the frequency of condensation below $w_u = 0$ of an undiluted surface parcel. The right panel shows the low cloud cover LCC $(p > 0.8p_{sfc})$ for a simulation where shallow convection was turned off.

is apparent that this criterion decouples the stratocumulus deck unrealistically. The interactive run (Fig. 5.4d) therefore does not add any low cloud cover in the typical stratocumulus regions.

5.3.3 *Decoupling criterion: Static stability*

Klein and Hartmann (1993) showed empirically that the stratus cloud cover increases with the static stability of the atmosphere defined as $\theta_{700hPa} - \theta_{sfc}$. Here it is tested using a threshold of 20K, which corresponds to a seasonally averaged stratocumulus cloud cover of 60% according to their data.

Fig. 5.4ef shows the stability decoupling diagnostic on the left and the corresponding interactive climate run on the right. This criterion provides a very robust diagnostic of the observed stratocumulus regions and subsequently the interactive simulation adds low cloud cover at those locations.

5.3.4 *Decoupling criterion: Buoyancy flux integral ratio*

Turton and Nicholls (1987) suggested a decoupling criterion based on the turbulent kinetic energy (TKE) equation. The buoyancy flux term can either generate or decay TKE within the BL. They postulate that a layer of substantial TKE decay can decouple the BL into two mixed layers. The buoyancy flux integral ratio (*BIR*) is defined as

$$BIR = \frac{\int_{\overline{w'\theta_v'}<0} \overline{w'\theta_v'} dz}{\int_{\overline{w'\theta_v'}>0} \overline{w'\theta_v'} dz} \equiv \frac{N}{P}, \tag{5.8}$$

which is the ratio of the vertical integrals of the negative and positive buoyancy flux regions N and P. Fig. 5.5 illustrates that in a well-mixed layer the most negative buoyancy fluxes are below cloud base. This originates from the fact that the buoyancy flux is a linear combination of the total water flux $\overline{w'q_t'}$ and liquid water potential temperature flux $\overline{w'\theta_l'}$

$$\overline{w'\theta_v'} = \alpha_1 \overline{w'q_t'} + \alpha_2 \overline{w'\theta_l'} \tag{5.9}$$

with different constants α_1 and α_2 in the sub-cloud and cloud layers (sub-cloud: $\alpha_1 = 1$ and $\alpha_2 = 0.61\theta_0$; cloud: $\alpha_1 \cong 0.5$ and $\alpha_2 = \alpha_1 L/c_p - \theta_0$). Turton and Nicholls (1987) originally proposed a threshold of $BIR = 0.4$ for decoupling, while more recently 0.15 (Bretherton and Wyant, 1997) and 0.1 (Stevens, 2000) were suggested based on aircraft and large eddy simulation data. Here the latter threshold of 0.1 is adopted.

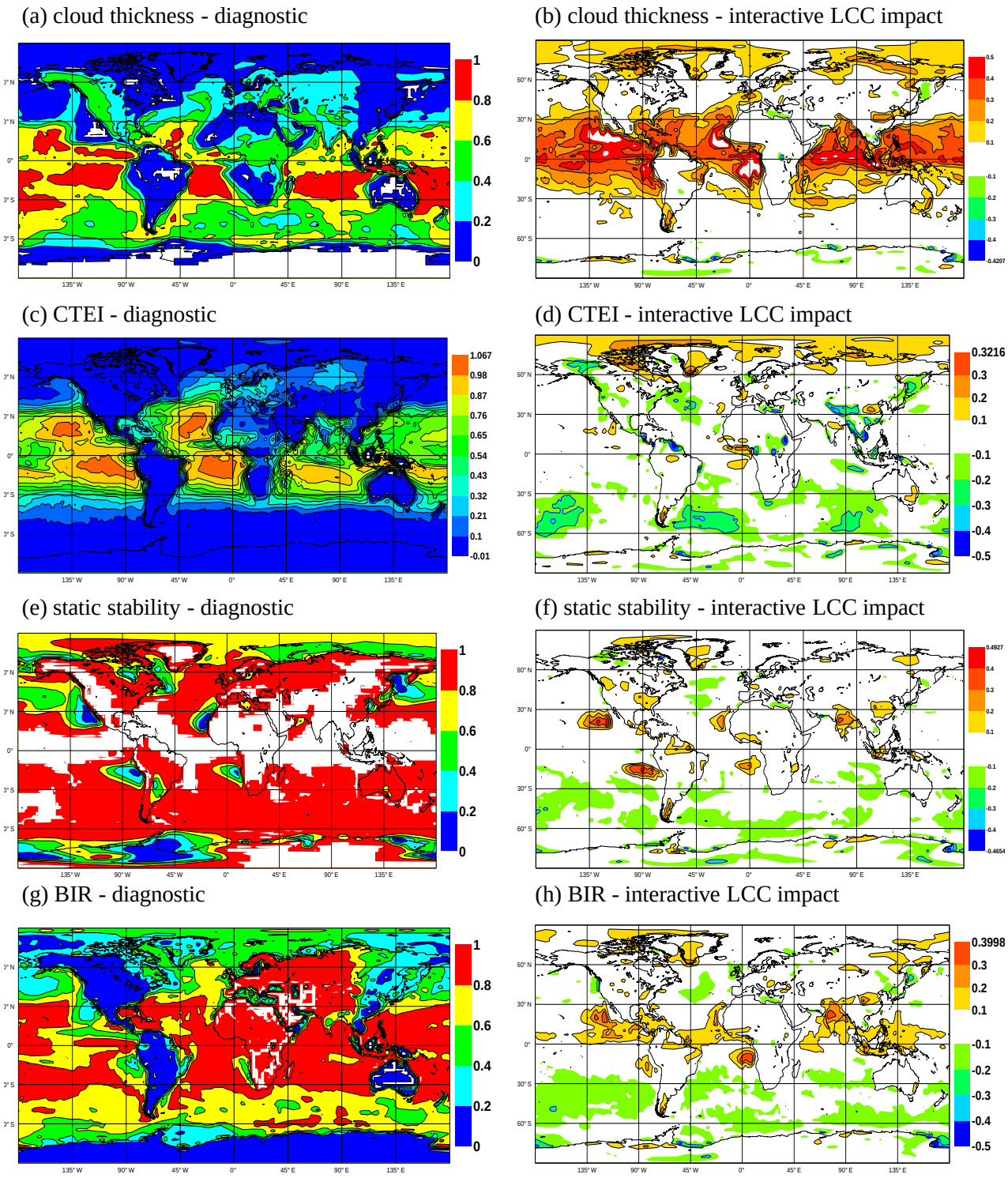

Figure 5.4: The left panels show the frequency of decoupling according to four decoupling criteria using a common reference climate run. They are from top to bottom panel: cloud thickness larger than 1000m, cloud top entrainment instability (CTEI), static stability $\theta_{700hPa} - \theta_{sfc} < 20K$ and buoyancy flux integral ratio $BIR > 0.1$. The right panels show the impact on low cloud cover (LCC) of using the new PBL parametrization with each of these four decoupling criteria as compared to the reference run.

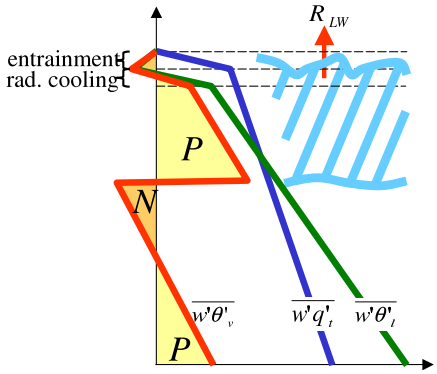

Figure 5.5: Illustration of the buoyancy flux integral ratio criterion (see text). P and N correspond to the positive and negative areas of the buoyancy flux profile (red).

The technical implementation of this BIR decoupling approach is hampered by the fact that the PBL parametrization output - the buoyancy fluxes - are required in the criterion. The technique used assumes a null hypothesis state. The resulting hypothetical fluxes are then used to decide if this state is realistic according to the BIR criterion. This hypothetical state could be (i) a mixed layer, (ii) a decoupled BL or (iii) the state from the last time step. Option (i) would allow the use of a simple diagnostic mixed layer model as a first guess calculation. Option (ii) would require the full calculation of BL and convection processes a priori. Option (iii) relies on the assumption that the large scale condition have not changed much since the last time step[5]. The final solution is sensitive to this choice. Option (i) is chosen and a full calculation of the BL scheme is used for the first guess buoyancy fluxes.

Fig. 5.4gh shows the BIR decoupling diagnostic on the left and the corresponding interactive climate run on the right. This criterion mostly diagnoses the stratocumulus regions successfully but mistakes parts of the ITCZ as well-mixed BLs. Accordingly the impact on low cloud cover is satisfactory in an interactive simulation but not as convincing as that resulting from the use of the temperature based stability criterion. On the other hand this BIR criterion provides a more physically based mechanism of decoupling.

5.3.5 Choice of decoupling criterion

In the light of the its robustness, the stability criterion is selected for the proposed first operational implementation of the new PBL parametrization. More work needs to be carried out on the more physically based BIR criterion before implementation.

5.4 Results with the current and new PBL parametrizations

Fig. 5.6 shows SCM simulations of the DYCOMS II stratocumulus field experiment using the current and the new set of parametrizations. The simulations were run with fixed forcing conditions including the diurnal cycle through the solar radiation. The current model simulation shows a noisy evolution of liquid water mixing ratio (Fig. 5.6a) that originates from two main cloud generation processes occurring at intermittent times: (i) the dry

[5]This is a frequent numerical issue that arises in numerical models requiring decision making. For example, the convection scheme needs to apply rules that govern a test parcel ascent to select whether deep or shallow convection will occur. Opposing final solutions may occur if shallow rather than deep convective entrainment rates are applied to this first guess ascent.

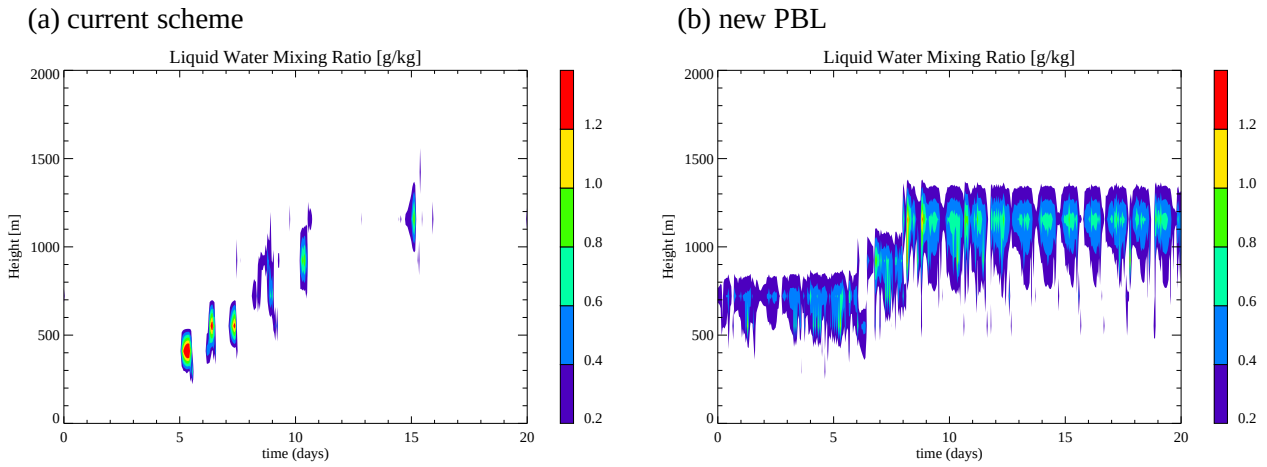

Figure 5.6: Liquid water mixing ratio of SCM simulations of DYCOMS II using the current scheme (CY25r3, left) and the new PBL (right).

BL reaching above cloud base with cloud supersaturation removal creating cloud liquid water; and (ii) shallow convection detraining liquid water.

The new model simulation (Fig. 5.6b) similarly raises cloud base and cloud top after which it experiences a regular and realistic diurnal cycle of liquid water path.

Figure 5.7 (panels a and b) shows annual means of total cloud cover from GCM simulations using the current and new ECMWF model at T95 resolution. The largest errors using the current model of 20 to 40% are associated with the typical stratocumulus cloud regions off the West coasts of America, Africa and Australia (see Fig. 5.7e).

The current scheme's weakness at representing stratocumulus results in part from inherent numerical difficulties. The scheme's inability to establish a well-mixed PBL up to the stratocumulus cloud top and to smoothly handle the transition to a decoupled situation, leads to numerical noise, with the shallow convection scheme intervening periodically in 'bursts' when instability permits.

The new PBL simulation decreases the total cloud cover RMS error compared to ISCCP D2 observations from 13.4% to 11.7% (Fig. 5.7f). The typical stratocumulus regions off California and Peru reduce cloud cover biases from up to 40% to below 10%. It is also encouraging that there is only a small increase in cloud cover in the central and western parts of the oceans.

Figure 5.7, panels e and f, also highlight the persistent underestimate of cloud cover over North America. The following section relates this to a basic difficulty in simulating shallow convection there.

5.5 ARM SGP observations

As part of an ongoing activity to use ARM (Atmospheric Radiation Measurement) data for model validation, observations from the Southern Great Plains (SGP) site have been used to look at the boundary layer structure in the model. The ARM SGP site now deploys an unique set of in-situ, passive and active remote sensing instruments. Routinely retrieved quantities include the surface heat and radiative fluxes, atmospheric profiles (in the boundary layer and in the troposphere), and cloud properties (e.g. base, height, liquid water content, etc). In so far as the SGP site is representative of many aspects of continental meteorology, it is illustrated here

how the available dataset provides several insights into the model behaviour.

Fig. 5.8a shows the diurnal cycle of cloudy hours (defined as hours in which a radar-based retrieval detects at least one cloud) over the SGP, for the July 2003 month. Preliminary tests show that July months for other years exhibit very comparable characteristics. The maxima found in the early morning correspond to the detrainment of ice and liquid water from the convective towers triggered over the Rockies on the previous day, with air masses being advected Eastwards. The afternoon maximum at 800 hPa relates to the frequent occurrence of surface-generated shallow convection, as confirmed by downward short-wave flux measurements, sky imagers, and visible channel plots of the GOES-East satellite. As shown in Fig. 5.8a, the IFS (version 28r1, 18-42 hour forecasts) mostly misses this feature, and over predicts the amount of locally-generated deep convection. More precisely, among the seven days when shallow convection was not perturbed by frontal advection or deep convection, none was diagnosed with fair-weather cumulus in the IFS. This clearly indicates a model deficiency, associated with the under-estimation of the low cloud fraction over continents mentioned above.

Radiosondes - routinely launched every 6 hours at the SGP site Central facility - further help to characterize the

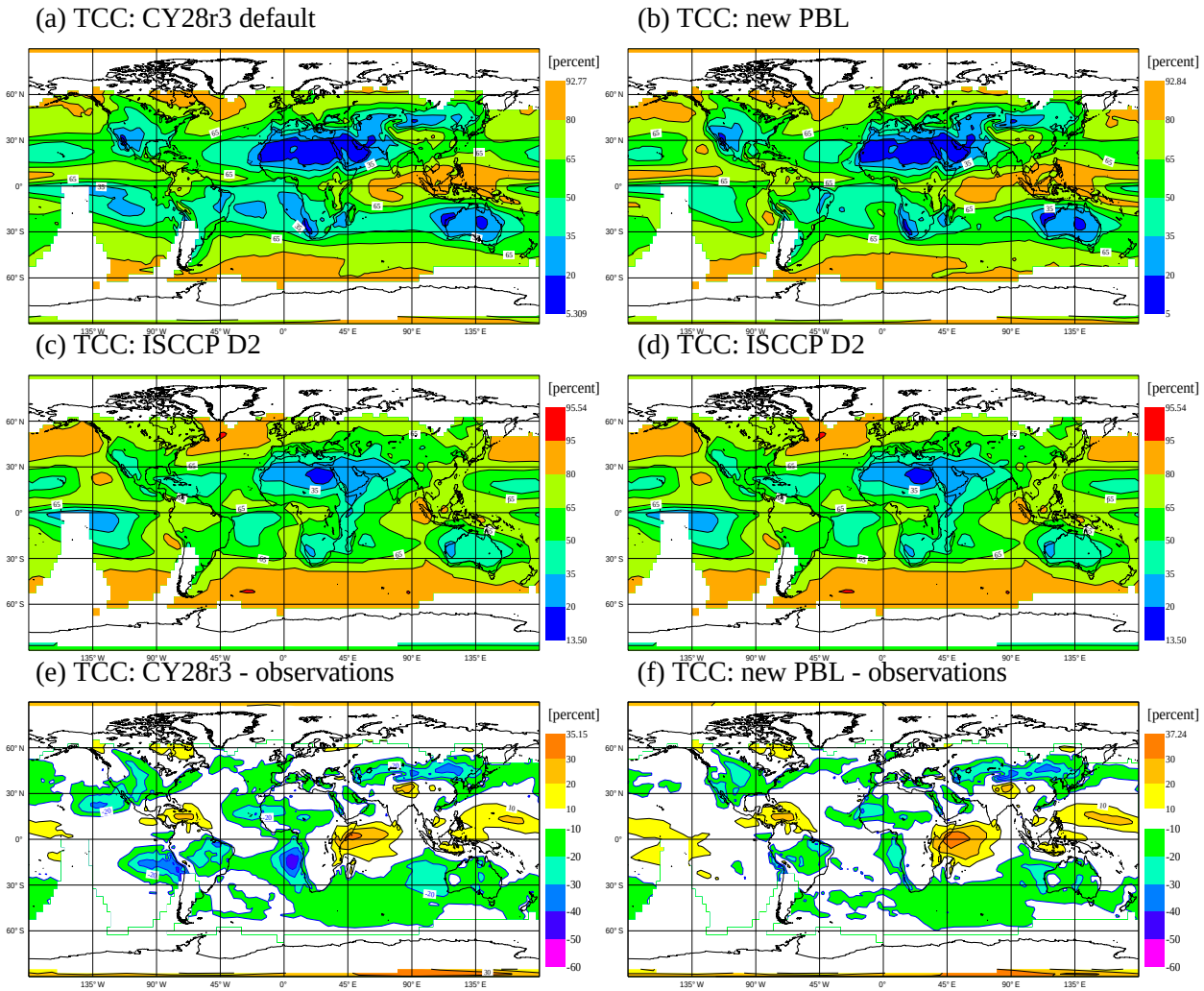

Figure 5.7: Annual mean (Sept. 2000 - Aug. 2001) total cloud cover (TCC) using ECMWF model cycle CY28r3 (a) and the new PBL parametrization (b). The middle panels (cd) are both the corresponding ISCCP D2 observations and the bottom panels (ef) show the errors of each model against observations.

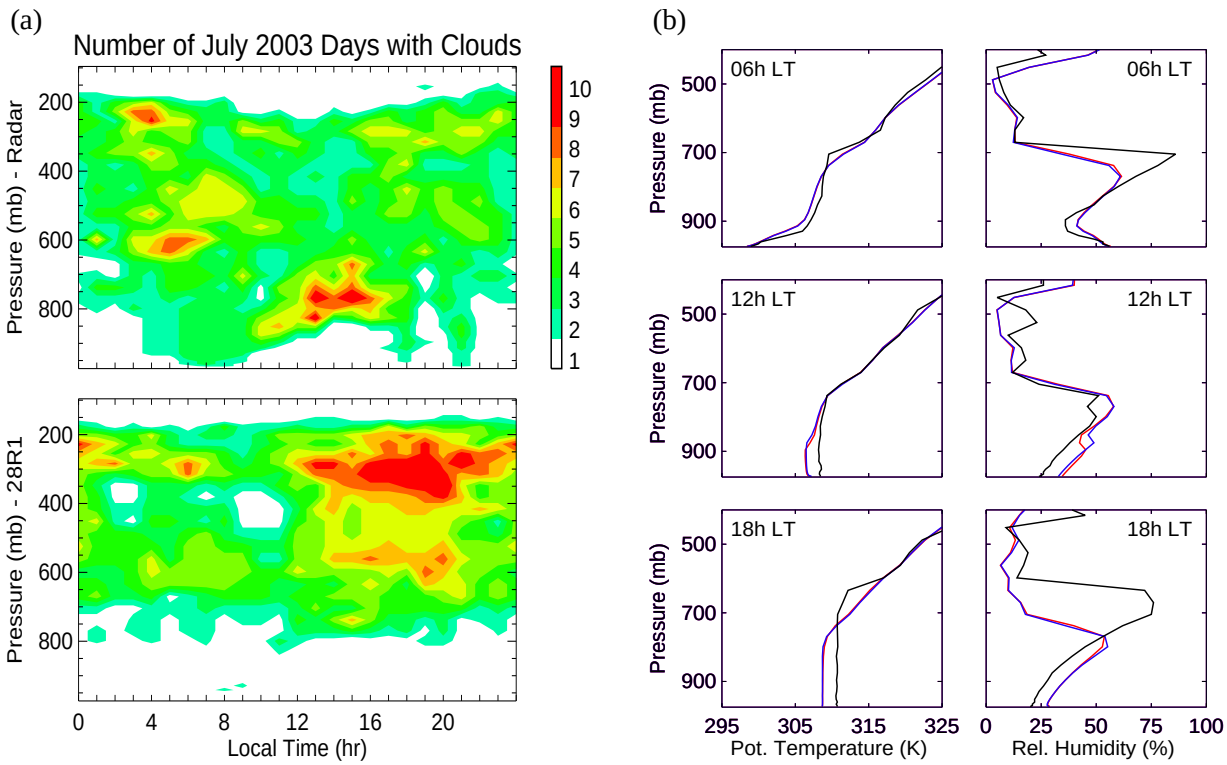

Figure 5.8: Comparisons between IFS 18-41 hours forecasts and observations at the ARM Central Facility in July 2003. (a) Diurnal cycle of cloudy hours, according to radar-based retrieval (top) and to the IFS 28r1 (bottom); (b) Vertical profiles of potential temperature and relative humidity (27 July 2003 at 06h, 12h, 18h Local Time from top to bottom). Radiosondes data are in black, IFS 28r1 in red, IFS 28r1 with new boundary layer scheme in blue.

model behaviour. For clarity, the focus is on one particular date (27 July), chosen as representative of a typical shallow convection day. Fig. 5.8b shows that the predicted morning profiles (temperature, humidity) agree with the observations. Given the well-defined anti-cyclonic situation, locally-driven processes will determine the boundary layer properties during the day. The non-triggering of the early afternoon cloudy convection in the IFS results in the lack of ventilation of the well-mixed layer (too cold and moist) compared to the late afternoon observations. Using the new boundary layer mixing scheme does not alter the results significantly. This was to be expected, because the initial implementation of the new boundary layer scheme addresses the stratocumulus problem only and does not change the model behaviour in cumulus type situations. However, the comparison with ARM data clearly indicates that the diurnal cycle of shallow cumulus over land requires further work. A single column approach will be applied together with the observations to assess the realism of the processes description in the IFS, i.e. to support the evaluation and development of parametrizations. Further work on the inclusion of subgrid heterogeneity in the convective scheme triggering formulation, introduced in section 7.4.3, may also help these efforts.

5.6 Future developments

5.6.1 Unification of the boundary layer and shallow convection

The inclusion of the mass flux component to the BL scheme opens the possibility to unify the BL and shallow convection treatment in one combined scheme. This is desirable, since numerical issues, to which parametrizations often have an uncomfortably large sensitivity, will be greatly simplified. In trade cumulus situations, for example, the BL parameterization acts up to cloud base, while the convection parameterization describes fluxes reaching from the surface to cloud top. Also, the explicitly treated shallow convective mass-fluxes can frequently exceed the maximum allowed by the CFL criterion and are subsequently limited for numerical stability. In the implicit-in-time formulation adopted in the new PBL parametrization this problem is eliminated. Furthermore, the distinction between stratocumulus and shallow convection should be simplified.

To unify the new PBL parameterization described in this section with a treatment of shallow convection would require only small technical changes since it is already designed to unify diffusion and mass flux terms. Four of the key issues involved in the improvement of shallow convective processes are the mass flux closure, the decision criterion to select between stratocumulus, shallow convection and deep convection, the coupling with the cloud scheme and finally the momentum transport. Some options currently available are discussed below.

The planned unification of BL and shallow convection should be viewed as one step towards further unification of the moist processes. This development will greatly benefit from the cooperation of the GCSS and ARM communities.

5.6.2 Mass flux closure

Three available choices for the mass flux closure in shallow convective situations could be easily implemented in a unified scheme: (i) the current sub-cloud layer moist static energy equilibrium closure, (ii) the Grant and Brown (1999) closure, where the mass flux at cloud base $M = 0.03w^*$ is a function of the surface buoyancy flux, or (iii) the Cheinet (2003) closure, which splits the distribution function of surface conditions to generate multiple updraughts. Note that all three shallow convection mass flux closures directly or indirectly rely on the surface fluxes of moisture and heat. This contrasts to most deep convective closure such as the CAPE and quasi-equilibrium closures, which are based on the stability of the atmospheric column and ultimately the free tropospheric and boundary layer forcing.

5.6.3 Decision criteria between stratocumulus, shallow convection and deep convection

Stratocumulus, shallow and deep convection are all representing convection associated with parcels originating near the surface. The new PBL parametrization as described above relies on a static stability criterion to distinguish between stratocumulus and shallow convection. Shallow convection and deep convection are currently distinguished with a height threshold of 200hPa.

It was argued in section 5.3 that stratocumulus and shallow convection are mutually exclusive, which requires a decision criterion. The BIR criterion is considered to be physically more realistic, and therefore this option will be revisited. A unified BL and shallow convection scheme will provide an improved framework to diagnose *BIR*. On the other hand, shallow and deep convection, defined as surface and free-tropospherically driven convection, respectively, are not necessarily mutually exclusive. In nature, they often co-exist within short horizontal distances, yet in the current model shallow and deep convection are not directly coupled (no kernel as in Arakawa and Shubert, 1974). A unified PBL/shallow convection plus a separate deep convection scheme

would allow for such coupling as both shallow and deep convection can operate simultaneously.

5.6.4 Coupling with the cloud scheme

The coupling of the unified PBL/shallow convection to the large-scale cloud scheme depends on the nature of the cloud scheme itself, and specifically the prognostic variables. Currently the variance source and sink terms of the new PBL schemes are converted into the prognostic variables of cloud water and cloud cover. These terms are much more conveniently linked if the cloud scheme instead predicts the higher order moments of the temperature and humidity distributions. Lenderink and Siebesma (2000); Klein et al. (2004) and others have demonstrated how the mass flux component can also be combined to a statistical cloud scheme.

5.6.5 Momentum transport

The new PBL parameterization described above does not directly change the treatment of momentum transport in the BL compared to the old PBL parameterization. In particular, the BL mass flux term doesn't currently transport momentum. The current description of momentum transport by shallow convection proves highly important. Therefore it is paramount, yet uncomplicated, to add the transport of momentum by the mass flux term to the new PBL scheme, and this will be addressed in the near future.

6 Simplified schemes for data assimilation: CNV/CLD.AN

The introduction to this document pointed out that in addition to the nonlinear model used for forecast integrations, the representation of moist processes in the linear physics of the 4D-Var analysis system also plays a critical role for forecast accuracy (Rabier et al., 1998; Janisková et al., 1999; Mahfouf, 1999).

The convection and cloud schemes used with 4D-Var with cycle 23r4 were based on highly simplified versions of the CLD.FC.23r4 and Slingo (1987) schemes (the latter described by Mahfouf and Rabier, 2000; Janisková et al., 2002). Although these were successful in improving the tangent linear approximation to the full nonlinear model and subsequently also forecast skill (e.g. Mahfouf, 1999; Klinker et al., 2000), there were a number of deficiencies in these schemes, including the suppression of convective mass flux perturbations, and the physically independent treatment of rain and cloud processes in the cloud scheme.

In cycle 28r3, these have been addressed by the development and inclusion of two new major parametrizations for convective and cloud processes. The aim of this section is to give an overview of these schemes, and provide examples of their improved characteristics and use in rainfall assimilation scenarios. Since both of these schemes have been documented in detail elsewhere (i.e. Tompkins and Janisková, 2004; Lopez, 2004), only a brief descriptive overview is provided here. The interested reader is referred to these documents for the mathematical detail and technical implementation issues.

6.1 Simplified convection scheme

6.1.1 Description

Previous studies underlined the need for an improvement of the linearized version of the ECMWF simplified convection scheme for a wide range of applications that involve tangent-linear and adjoint calculations. These

applications include 4D-Var assimilation, singular vector computations and 1D-Var retrievals from rain observations (Marécal and Mahfouf, 2000). A new simplified convective scheme (CNV.AN.EXP) based on the mass flux approach has been recently developed with the aim of replacing the current operational scheme (referred to hereafter as CNV.AN.26r3). The new scheme is designed such as to retain some basic similarities with the operational nonlinear convective scheme (CNV.FC.26r3, Tiedtke, 1989) and at the same time to reduce its degree of complexity that can be a source of unwanted strong nonlinearities.

In the new simplified scheme, all types of convection (shallow, mid-level, and deep) are treated in the same way. In particular, the link between the model control variables and the cloud base mass flux (the so-called *closure assumption*) is expressed through a single formulation that depends on the release of convective available potential energy (CAPE). In contrast with CNV.FC.26r3, the equations that describe the vertical evolution of the updraught mass flux, M_u, and of the updraught thermodynamic characteristics, Φ_u (dry static energy and total water), are uncoupled:

$$\frac{\partial M_u}{\partial z} = (\varepsilon_u - \delta_u) M_u \tag{6.1}$$

$$\frac{\partial \Phi_u}{\partial z} = -\varepsilon_u (\Phi_u - \overline{\Phi}) \tag{6.2}$$

where ε_u and δ_u are the fractional entrainment and detrainment rates, respectively. Overbars denote field values in the environment, that is averaged over a model gridbox. The uncoupling allows the removal of the iterative calculations involved in CNV.FC.26r3 for updating the cloud base mass flux thereby leading to a simpler adjoint code. Based on Siebesma and Jakob (personal communication), ε_u is parametrized as $c_\varepsilon/(z - z_{st}) + 10^{-5}$ m^{-1} where c_ε=0.4 and z_{st} is the starting height of the updraught (in m). As for detrainment, δ_u is made smaller than ε_u in the lower part of the updraught and comparable to ε_u further up, in order to match observations (Cohen, 2000). Close to cloud top where updraught buoyancy becomes negative, a constant organized detrainment rate of 2×10^{-4} m^{-1} is added to δ_u.

Convection is assumed to be activated only if the bulk convective updraught vertical velocity remains positive at cloud base. The updraught is assumed to originate from the surface only if its initial vertical velocity is positive, which is calculated from the surface heat fluxes using Holtslag and Moeng (1991). The initial temperature and specific humidity departures of the updraught from the environment are assumed to be proportional to the surface sensible and latent heat fluxes. If convection cannot be initiated from the surface, the convective ascent may originate from higher levels provided relative humidity exceeds 80%, in which case the initial vertical velocity of the updraught is somewhat arbitrarily set to 1 m s^{-1}. Regardless of whether the updraught originates from the surface or from higher up, the vertical evolution of its kinetic energy is computed following Simpson and Wiggert (1969), which involves the buoyancy as well as the entrainment of environmental air into the updraught. The convective ascent is assumed to stop at the level where updraught vertical velocity becomes negative.

Using uncoupled equations similar to Eq. (6.1), a simple parametrization of convective downdraughts that are usually associated with the strong cooling due to the evaporation of precipitation has been implemented.

The updraught mass flux at cloud base is calculated to reduce CAPE with an exponential resolution-dependent timescale ranging from 3600 s from resolutions coarser than T319 to 600 s beyond T511. CNV.AN.EXP also features a simple representation of convective momentum transport. It is based on CNV.FC.26r3 but in contrast with the latter the same entrainment and detrainment rates as for heat and moisture are applied to the two wind components for the sake of simplicity.

Precipitation formation is proportional to the amount of cloud condensate in the updraught as in Tiedtke (1989). That is not the case any longer in CNV.FC.26r3 which uses the formulation of Sundqvist et al. (1989).

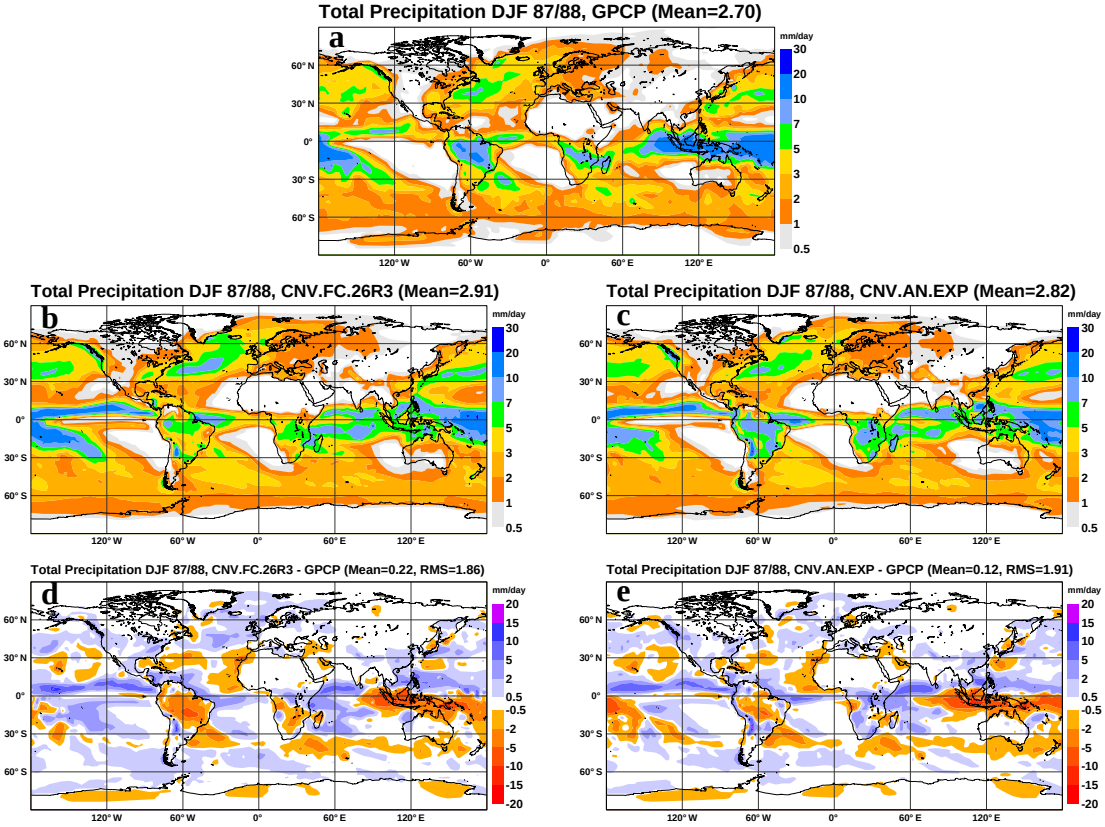

Figure 6.1: Total precipitation over winter 1987-88: (a) GPCP observations, (b) CNV.FC.26r3 and (c) CNV.AN.EXP experiments (see text for more details). Differences CNV.FC.26r3-observations and CNV.AN.EXP-observations are shown in panels (d) and (e) respectively. Mean and root mean square difference (when relevant) are mentioned at the top of each panel. Units are in mm day^{-1}.

The tangent-linear and adjoint versions of CNV.AN.EXP are available and have been tested in different types of experiments, some of which will be presented in section 6.3. Simplifications and modifications that were needed to improve the scheme's linear behaviour will be summarized in the section 6.1.3. It is worth noting that unlike CNV.AN.26r3, CNV.AN.EXP handles perturbations of all convective quantities including mass flux, all updraught characteristics as well as precipitation fluxes. This is expected to be beneficial when combining CNV.AN.EXP with a radiative transfer model sensitive to the presence of cloud condensate and/or hydrometeors.

6.1.2 Validation

Although CNV.AN.EXP was not designed for the purpose of medium or long-range weather forecasting, it was still important to check that its results in a forecast mode do not depart too much from those obtained with CNV.FC.26r3. As an example, four month season-long three member ensemble integrations (using T95L60) are presented for the winter 1987-1988 using either CNV.FC.26r3 or CNV.AN.EXP in cycle 26r3 of the ECMWF forecast model. Three-month averages of the simulated total surface precipitation are shown in Fig. 6.1 and validated against observations from the Global Precipitation Climatology Project (GPCP).

Figure 6.1.(d) and (e) indicate that CNV.FC.26r3 and CNV.AN.EXP exhibit rather similar discrepancies with

respect to the GPCP observations, except over southern Africa. In both experiments, the precipitation simulated in the Inter-Tropical Convergence Zone (ITCZ) tends to be substantially overestimated over the central and eastern Pacific, over the Atlantic and over the Indian Ocean. Local departures reach 15 mm day^{-1} in CNV.FC.26r3 and 8 mm day^{-1} in CNV.AN.EXP slightly east of the dateline. On the other hand, precipitation is clearly underestimated over the Indonesian warm pool by up to 12 mm day^{-1} with both convection schemes. Also note the similar double structure of the ITCZ in the Indian Ocean in Fig. 6.1.(b) and (c), which does not appear in the observations. Overall, the average ratio of convective precipitation (not shown) on the total amount reaches 56% in CNV.FC.26r3 versus 49% in CNV.AN.EXP. The mean departure from the GPCP observations is lower in CNV.AN.EXP (0.12 mm day^{-1}) than in CNV.FC.26r3 (0.22 mm day^{-1}), but the RMS error is slightly higher in CNV.AN.EXP (1.91 versus 1.86 mm day^{-1}).

Figure 6.1 as well as some additional validation of cloud cover and radiative budgets (not shown) demonstrate that, although not designed for the purpose of long simulations, CNV.AN.EXP behaves reasonably well with respect to observations and resembles the full operational convection scheme. The fact that both schemes appear to share common deficiencies (split ITCZ, too much convection over eastern Pacific) could be due to the common basis of the two schemes. On the other hand, it may also be that shortcomings in other components of the model lead to incorrect large-scale fields, to which any reasonable convective scheme is constrained to respond.

6.1.3 Validity of tangent-linear approximation

The linearity of the modified convection scheme CNV.AN.EXP has been assessed through the calculation of nonlinear residuals and compared to the linearity of CNV.FC.26r3. For a given nonlinear operator M and its tangent-linear (TL) version $\mathbf{M}'$, the nonlinear residuals are defined as

$$RES_{NL} = M(\mathbf{x} + \lambda\,\delta\mathbf{x}) - M(\mathbf{x}) - \mathbf{M}'[\mathbf{x}]\lambda\,\delta\mathbf{x} \tag{6.3}$$

where $\mathbf{x}$ denotes the input temperature and specific humidity in the present case[6]. The residuals have been computed for the convective tendencies $\partial T/\partial t$ and $\partial q/\partial t$ that are produced by the convective parametrization M. The calculations of Eq. (6.3) have been repeated for values of the scaling factor λ ranging from 10^{-5} to 1 and from -1 to -10^{-5}. The reference vector of perturbations $\delta\mathbf{x}$ was set equal to typical values of the standard deviation of the background model errors.

Figure 6.2 shows nonlinear residuals, averaged over 100 atmospheric profiles with deep convection, that are obtained when specific humidity perturbations of varying size are applied at the lowest model level (60). Results are shown for this level because input perturbations imposed there usually bring large modifications of convective activity but similar conclusions can be drawn for other levels. The field actually plotted in Fig. 6.2 is $\log_{10}(RES_{NL}/RES_{NL}^{max})$ where RES_{NL}^{max} denotes the maximum value of the residual for a given plot and for both CNV.FC.26r3 and CNV.AN.EXP. This normalization permits the comparison of the residuals obtained with the two parametrizations and the smaller the values of the plotted field, the more valid the linear assumption. Figure 6.2 demonstrates that the nonlinear residuals are almost systematically one order of magnitude smaller with the new scheme than with the operational one. The weak asymmetries about the y-axis result from the fact that large negative moisture perturbations at the surface can turn off convection thereby leading to a less linear behaviour of the scheme.

In earlier Jacobian computations, some sources of excessive sensitivity were isolated and removed by suitable modifications to the code. These code adjustments consisted of

- the removal of the dependence of organized detrainment on the updraught vertical velocity,

[6] In the case of CNV.FC.26r3 for which no TL version exists, a proxy for $\mathbf{M}'$ is computed using finite differences

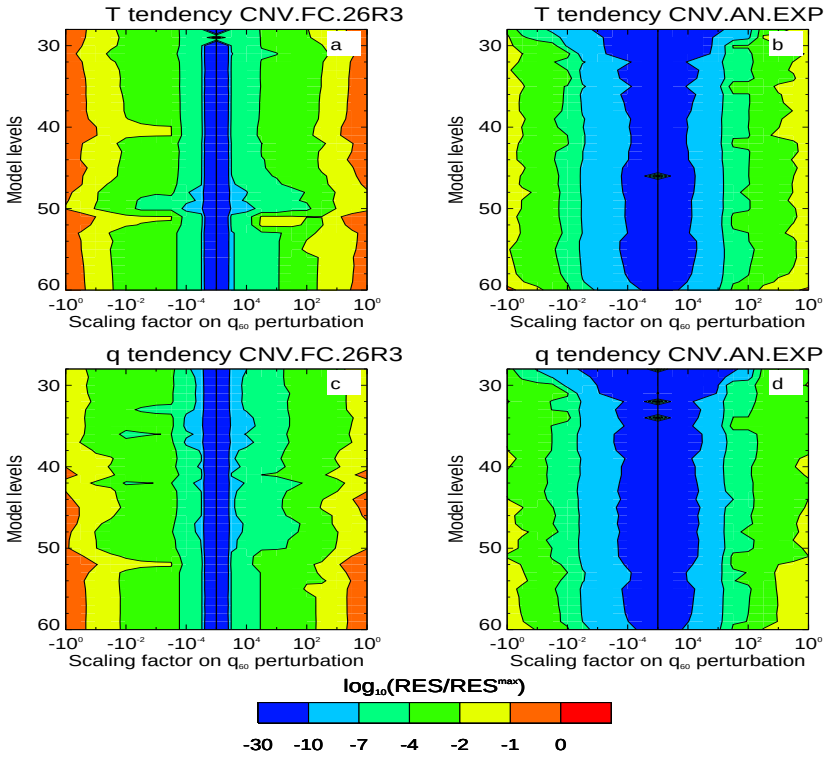

Figure 6.2: Nonlinear residuals of convective temperature and specific humidity tendencies as functions of parameter λ that determines the size of the input specific humidity perturbations imposed on model level 60. The displayed residuals have been averaged over one hundred convective profiles. The field plotted is $\log_{10}(RES_{NL}/RES_{NL}^{max})$ *where* RES_{NL}^{max} *denotes the maximum value of the residual for a given pair of input/output parameters and for both studied convection schemes* (i.e. *for a given row of the figure). Left: CNV.FC.26r3, right: CNV.AN.EXP.*

- the specification of a constant updraught vertical velocity (3 m s^{-1}) in the calculation of precipitation formation whenever the buoyancy becomes negative at levels below 7000 m.

It was also found that the activation of the mass flux limiter that is required to prevent numerical instability triggered by the violation of the Courant-Friedrich-Levy criterion leads to rather unrealistic Jacobians. However, only about 5% of the total number of convective grid points are affected by the mass flux limiter for timesteps smaller than 1800 s and for the current model resolution (T511 L60) and this was thus not considered a major concern.

Furthermore, in some TL evolution experiments run with CNV.AN.EXP a spurious amplification of TL perturbations occurred at a few geographical points after a few hours of integration, which then contaminated the entire Globe. In fact, such problems can arise when the perturbation of a given field becomes as large as the field itself, which was found to be the case for the cloud base mass flux, the buoyancy and the initial vertical velocity of the updraught. To avoid these instabilities, the corresponding perturbations are reduced by a factor of 0.25 for the mass flux and 0.35 for the two other quantities. For the latter field, the limitation is applied only when w_s is lower than 0.5 m s^{-1}. These factors were tuned so as to provide a good compromise between stability and validity of the linear assumption, and are required when running CNV.AN.EXP in all tangent-linear and adjoint calculations involving time integration.

6.2 Simplified cloud scheme

The current linearized diagnostic cloud scheme, which is used in 4D-Var, has recognized weaknesses: the cloud liquid water is proportional to the saturation vapour pressure and can be inconsistent with the cloud cover; the rainfall generation is simply the result of removing super-saturation and is therefore independent of the cloud variables. Rainfall evaporative processes are currently inhibited. A new simplified cloud scheme and its tangent-linear and adjoint versions (Tompkins and Janisková, 2004) have been developed to allow the use of cloud related observations in the 4D-Var system. The attempt was made to develop a scheme which is simple and does not contain discrete transitions, while retaining the central aspects of the Tiedtke (1993) scheme used in the nonlinear forecast model.

6.2.1 Description

The new model diagnoses cloud cover and cloud water (liquid+ice) from the input profiles of the temperature and humidity control variables. From the six broad cloud processes represented by CLD.FC.23r4 listed in section 4.1, it describes the four principal processes, namely:

(i) Detrainment from deep and shallow convection

(ii) Horizontal sub-grid mixing of cloud and environmental air

(iii) Adiabatic or diabatic warming or cooling

(iv) Precipitation processes

As stated earlier, these four terms were shown by Fillion and Mahfouf (2003) to dominate the sensitivity of the CLD.FC.26r1 scheme. It is therefore possible to have confidence that a simplified scheme based on this reduced set of processes can reproduce the sensitivity of the full complex prognostic scheme. A brief overview of the approach for each of these terms is now presented.

(a) Stratiform cloud properties
The scheme is based on statistical ideas assuming a subgrid scale fluctuations of total water and/or temperature. This allows the in-cloud liquid water and cloud cover to be determined by integrating the saturated portion of the grid box. The uniform distribution is used to describe a probability density function (PDF) of subgrid-scale fluctuations for simplicity and for consistency with the full prognostic cloud scheme, which uses the same assumption for the clear sky vapour fluctuations (Tiedtke, 1993). Currently the variance of the distribution is fixed, implying that the cloud cover and liquid water can be reduced to formulations based on relative humidity. In order to account for the asymmetric nature of cloud formulation, the distribution width based on relative humidity is reduced linearly from its maximum value at a critical relative humidity for cloud formation to its minimum value when relative humidity is equal to one.

This relative humidity based form essentially replaces the cloud source/sink terms due to diabatic and adiabatic warming/cooling in CLD.FC.23r4. The simplified approach is necessitated by the diagnostic cloud variables. A future total water control variable would also greatly facilitate the implementation of prognostic cloud water source terms similar to CLD.FC.23r4, but consistent with the assumed PDF for the total water variability.

(b) Convective contribution
One of the most significant sources of cloud in the tropics and mid-latitude summers in the CLD.FC.23r4 cloud scheme is the detrainment from deep convection (e.g. Teixeira, 2001). This information, which the current 4D-Var convection scheme does not provide, will be obtained from the improved convection scheme developed

for data assimilation (CNV.AN.EXP Lopez, 2004, ,described in the previous section). For the cloud cover, the assumption is adopted from CLD.FC.23r4 that convective clouds randomly overlap existing stratiform cloud. Unlike the prognostic Tiedtke scheme, CLD.FC.23r4, no memory exists for cloud water between consecutive timesteps. Therefore the convective source-term is simply handled as a timestep-integrated addition to the basic relative-humidity related cloud cover and cloud water defined above. This simple approach is a first attempt to include deep convective detrainment in the linearized scheme, but is timestep dependent, with the effect of deep convection negated as the timestep approaches zero. An additional assumption made necessary by the lack of memory in the cloud fields is that any convectively detrained cloud water that is not converted to precipitation during the timestep evaporates. This is necessary to prevent convectively active regions from artificially drying during the forward integration.

(c) Precipitation production
As in CLD.FC.23r4, simple auto-conversion terms are used for the generation of rain and snow (based on Sundqvist et al., 1989), which fall out of the model column during one timestep. The Bergeron-Findeisen or collection processes are not included in the new scheme.

A detailed investigation of the tangent-linear approximation for the new scheme revealed that the linearized scheme developed noise during the integration coming from the auto-conversion function which describes the portion of cloud water converted to precipitation. Therefore the linearized version of the function had to be modified by reducing the size of perturbation close to threshold values, which constrain the amount of created precipitation to be between zero and a maximum defined portion.

(d) Rainfall evaporation
Again following the CLD.FC.23r4 scheme, precipitation falls to the surface within one timestep and evaporates during its descent. To retain this important term, the new scheme also bases it on the Newtonian relaxation formulation of Kessler (1969). For simplicity, the diagnostic scheme uses a maximum overlap assumption for the precipitation fraction (the proportion of a grid cell through which precipitation is falling). One novel aspect of the scheme is a new treatment of precipitation evaporation during the descent, which partially accounts for the overlap of precipitation with the subgrid clear sky distribution of humidity fluctuations. This new treatment removes the requirement of artificial and discrete process thresholds used in the full prognostic model, which would impact the feasibility of the tangent linear code.

6.2.2 Validation

(a) 1D tests
The new cloud scheme (CLD.AN.EXP) has been tested by examining physical tendencies of thermodynamical quantities, calculated for a series of input temperature and humidity profiles, to those produced by the complex prognostic scheme (CLD.FC.26r3) used in the forecast model. The performance of CLD.AN.EXP scheme is also compared with the existing operational 4D-Var diagnostic cloud scheme (CLD.AN.26r3). This was conducted over the Atmospheric Radiation Measurement (ARM) program sites located at South Great Plains (SGP) in North America and the two tropics sites based at Nauru and Manus in the Tropical Western Pacific (TWP). This initial test concentrated on the performance of the cloud schemes in a strongly constrained environment where the background thermodynamic fields are not permitted to diverge. In this way serious biases in the underlying cloud scheme physics may be identified.

The mean cloud cover from each scheme is shown in Fig. 6.3 for the different situations at the ARM sites. At the SGP site, the CLD.AN.EXP scheme (Fig. 6.3a) produces a considerable improvement, with upper level cloud cover almost identical to the prognostic scheme. The new scheme is also able to reproduce the cloud fraction structure at the tropical sites (Fig. 6.3b, c), with peaks in the lower and upper cloud fractions due

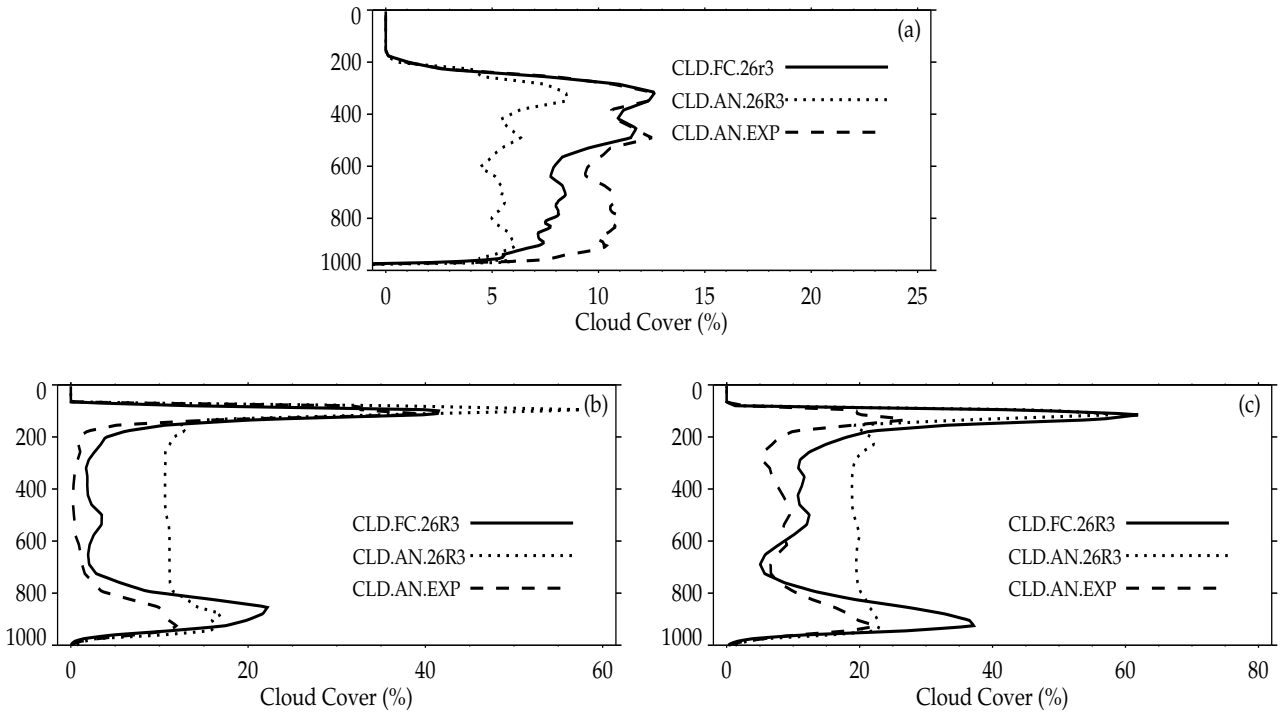

Figure 6.3: Mean cloud fraction over the ARM SGP site during January 2001 (a), the ARM TWP Nauru site during March 2001 (b) and the ARM TWP Manus site during May 2001 (c). Three schemes are used: the operational prognostic scheme (CLD.FC.26r3), 4D-Var operational diagnostic scheme (CLD.AN.26r3) and the new diagnostic scheme (CLD.AN.EXP).

to its direct link to convection through the detrainment term. The CLD.AN.26r3 produces too much cloud throughout the mid troposphere, with a flat featureless profile. A comparison of the liquid water and ice mass mixing ratios (not shown) revealed that the new diagnostic scheme reproduces the ice and liquid water profiles of the prognostic model reasonable well. In comparison to CLD.AN.EXP, the present operational diagnostic scheme is obviously deficient, especially in the Tropics. The new diagnostic scheme is also found to give comparable results to the full forecast model for radiation and cloud observations (not shown).

(b) Global forecasts

As a further test, a series of 12 hour global model integrations was executed, with the full prognostic scheme used in operational forecasts replaced in turn by the nonlinear versions of the current operational assimilation diagnostic cloud scheme, and then by the new scheme described here. Two weeks of forecasts were conducted at T159L60 resolution (120 km horizontal resolution and 60 vertical levels), for the first two weeks of March 2001. The choice of resolution was inspired by the fact that the linearized model with the physical processes, for which the new scheme was developed, is run at T159 in the current inner-loop integration of 4D-Var. Using the default model as a metric, the new scheme improves on the current assimilation cloud scheme for many variables such as cloud cover and ice water content, both in the tropics and mid-latitudes. In particular the new scheme addresses the overriding weakness of the current operational linearized physics package, which produces almost no large-scale precipitation (and associated perturbations of control variables) in the tropics (Fig. 6.4). Instead the new scheme almost perfectly replicated both the pattern and quantity of tropical precipitation. Additional tests also proved that this remains the case at a forecast range of 24 hours, the maximum length assimilation window that is likely to be used in the foreseeable future.

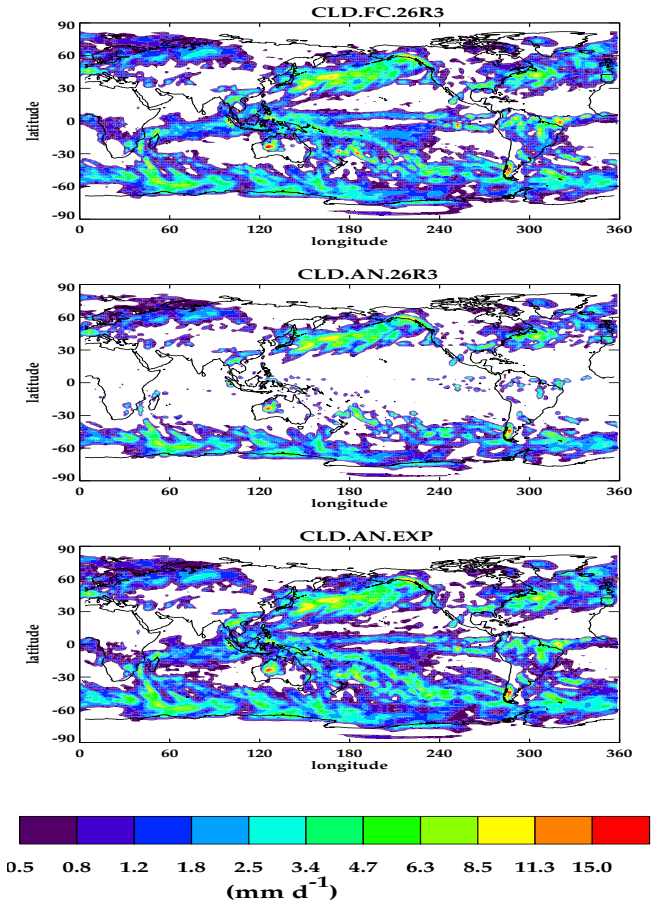

Figure 6.4: 12 hour accumulated large-scale precipitation averaged over 14 forecasts at T159 resolution for the three cloud schemes.

6.2.3 Validity of tangent-linear approximation

The linearized versions (tangent-linear and adjoint) of the cloud scheme described above have been developed. After the standard validation of the tangent-linear and adjoint codes (Taylor formula and adjoint identity), the linear evolution of the model with the new cloud parametrization (CLD.AN.EXP) has been studied in comparison with that of the operational cloud scheme (CLD.AN.26r3). The mean absolute error, E, between a TL run and the corresponding pair of nonlinear integrations is defined as

$$E \quad = \quad \overline{|M(\mathbf{x}^a) - M(\mathbf{x}^b) - \mathbf{M}'(\mathbf{x^a} - \mathbf{x^b})|}. \tag{6.4}$$

Here, $\mathbf{x}^a$ represents the analysis and $\mathbf{x}^b$ the background field. The nonlinear forecasts are conducted with the full nonlinear physical package using the states $\mathbf{x}^a$ and $\mathbf{x}^b$ as different initial conditions. Experiments are performed for three cases to sample the seasonal cycle (15 December 2000, 15 March 2001, 15 June 2001) using the model resolution T159L60 of the ECMWF global spectral model, mimicking an inner-loop integration of the operational 4D-Var system.

Figure 6.5 summarizes the relative impact on E coming from replacing the operational linearized cloud scheme (CLD.AN.26r3) by the new linearized cloud scheme (CLD.AN.EXP). The results are presented for various geographical domains. The new linearized cloud scheme improves globally the fit to the nonlinear model for each evaluated variable. The largest improvement is achieved in the Tropics for temperature and zonal wind and in North20 for specific humidity. A small negative impact is seen for zonal wind in South20. The

ability of the TL model to approximate the finite differences is necessarily dependent on the meteorological situation, but the largest improvements are generally in the Tropics, with the exception of specific humidity for which the improvement is globally uniform. It is probable that evaporation processes, which were neglected in the previous version of the linearized large-scale condensation scheme (Mahfouf, 1999) contribute to an improvement of the tangent-linear approximation of the simplified model to the full nonlinear model (in finite differences) when using the new cloud scheme.

6.3 Applications of the new simplified moist physics

6.3.1 Impact in tangent-linear evolution experiments

In addition to the previous linearity tests performed on the convection and large-scale cloud schemes separately, it is crucial to verify that the inclusion of CNV.AN.EXP in TL integrations can lead to a better approximation of the finite difference of two nonlinear integrations when other processes such as vertical diffusion, large-scale condensation and radiation are also activated and when the perturbations involved are not necessarily limited in size. Indeed, in 4D-Var assimilation for instance, the magnitude of such perturbations may reach several K for temperature, several g kg^{-1} for specific humidity and a several m s^{-1} for wind. Again, the mean absolute error, E, as defined in eqn. 6.4 is used.

In the 2004 version of the 4D-Var system, the model trajectory is calculated using CNV.FC.26r3, while the minimization and the evolution of analysis increments involve the simplified linearized convective parametrization CNV.AN.26r3. Since CNV.AN.EXP is an improved approximation to CNV.FC.26r3, its use in the TL integration should lead to a reduction of the linearity error. It is also important to check how CNV.AN.EXP behaves when combined with the new simplified parametrization of large-scale clouds and precipitation (CLD.AN.EXP Tompkins and Janisková, 2004).

The integrations presented here are run over 12 hours with a spectral resolution of T159 and 60 vertical levels in order to match the current assimilation window and inner-loop horizontal and vertical resolutions of the 4D-Var system. The full simplified physics is activated in all TL integrations but one (adiabatic run).

Figure 6.6 respectively display zonal mean error differences for the temperature field (in K) when the TL model

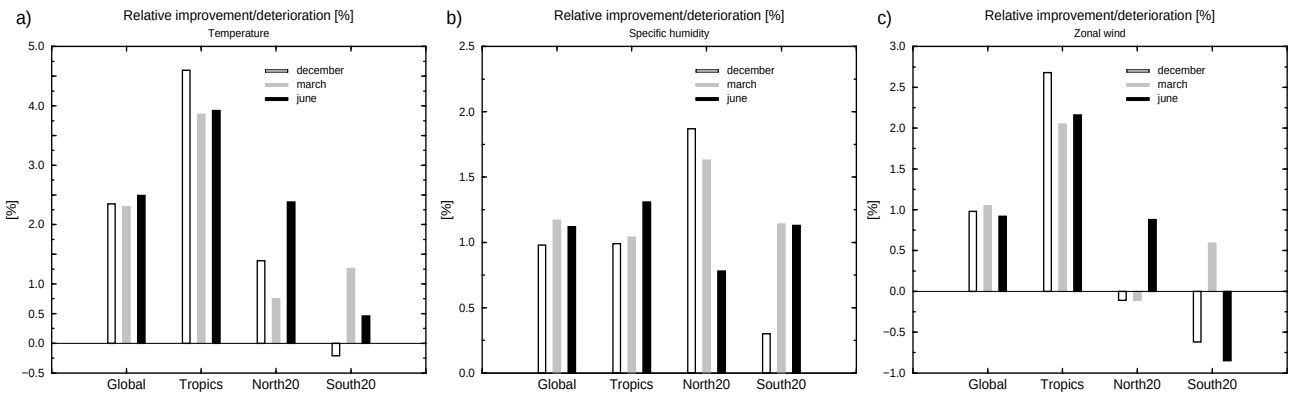

Figure 6.5: Improvement/deterioration (defined as (CLD.AN.26r3-CLD.AN.EXP)/CLD.AN.26r3) of the tangent-linear (TL) model when using the new linearized cloud scheme in place of the current operational diagnostic scheme for the geographical domains of: Tropics: 20N-20S, North20: 20N-90N, South20: 20S-90S and globally. The results are presented as the percentage improvement for (a) temperature, (b) specific humidity and (c) zonal wind. The comparisons are made for 15 December 2000 (white bar), 15 March 2001 (grey bar) and 15 June 2001 (black bar).

is integrated:

(a) with the operational simplified physical package (vertical diffusion, gravity wave drag, deep convection, large-scale moist processes from MA99 and radiation from Janisková et al. (2002), referred to as CONTROL, instead of no simplified physics at all (referred to as ADIAB),

(b) with CNV.AN.EXP as a substitute for CNV.AN.26r3, and

(c) with both CNV.AN.EXP and CLD.AN.EXP instead of standard simplified moist physics.

The global relative change in the linearity error is mentioned at the top of each panel and negative values of the plotted field indicate improvements of the linearity.

First of all, panel (a) shows that the inclusion of the operational simplified physics improves the linearity error by 13.96% for temperature relative to the adiabatic TL run. Statistics computed for panel (b) of Fig. 6.6 indicate that CNV.AN.EXP further reduces the global mean TL error by 0.49%. The strongest reduction of the error occurs between 60°S and 70°N and is confined to model levels 39 to 50. Between the surface and model level 50 the error is slightly increased. Above level 40, error changes remain small and limited to the Tropics. Figure 6.6.(c) shows that the combination of CNV.AN.EXP with CLD.AN.EXP brings an overall reduction of E equal to 2.10% for temperature with respect to the experiment with the current operational simplified moist physics.

6.3.2 1D-Var retrievals in rainy areas

CNV.AN.EXP has been extensively tested in 1D-Var retrievals of temperature and specific humidity profiles from rainfall rates, microwave brightness temperatures (TBs) or precipitation radar reflectivities observed by satellites. An example of results from 1D-Var applied to microwave TBs (1D/TB hereafter) will be presented here. In 1D/TB, vertical profiles of increments of temperature and specific humidity are obtained by minimizing a cost function that measures the fit of the model both to observed and to some background TBs. Error statistics on model and observations need to be properly specified. The new moist physical package (CNV.AN.EXP+CLD.AN.EXP) converts the model state (T,q) into precipitation fields that can be used in turn to simulate microwave TBs using the radiative transfer model of Bauer (2002). The iterative minimization of the cost function involves the adjoint version of the moist physics and of the radiative transfer model. More technical details of 1D-Var retrievals in precipitating areas can be found in Moreau et al. (2004).

Figure 6.7 shows an example of 1D-Var retrieval using TBs observed by the Tropical Rainfall Measuring Mission (TRMM) polar-orbiting satellite for tropical cyclone Ami at 1800 UTC 14 January 2003 in the western Pacific. Note that the surface rainfall rates used as independent validating observations are obtained by applying the retrieval algorithm PATER developed by Bauer et al. (2001). Figure 6.7 demonstrates that 1D/TB is able to produce adjustments of the model's temperature and specific humidity that improve surface rainfall rates with respect to the PATER observations. In the proposed example, 1D/TB has been applied to the 10, 19, 22 and 37 GHz channels in vertical and horizontal polarizations. A rather systematic feature in 1D/TB using CNV.AN.EXP and CLD.AN.EXP is the predominance of specific humidity increments relative to those in temperature (after conversion into equivalent increments of saturation specific humidity). This supports the choice made by (Marécal and Mahfouf, 2003) to define TCWV pseudo-observations that are obtained by vertical integration of the 1D-Var specific humidity increments. These TCWV pseudo-observations can in turn be fed into the 4D-Var assimilation system.

In the near future, CNV.AN.EXP and CLD.AN.EXP will be used operationally in the 1D-Var calculations involved in the '1D-Var + 4D-Var' method proposed by (Marécal and Mahfouf, 2003) to assimilate the 22 GHz channel TBs from the Special Sensor Microwave Imager (SSM/I). Eventually, the new simplified moist physics

will be tested within 4D-Var itself.

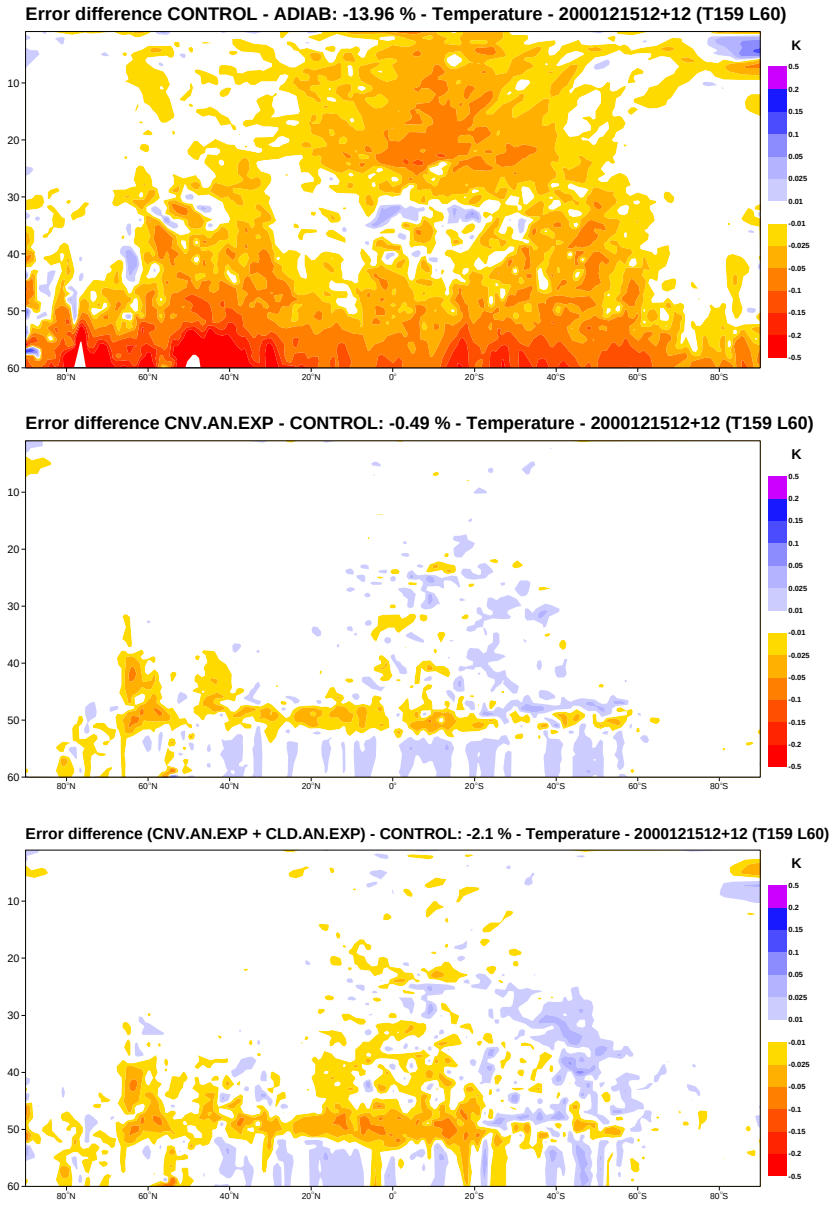

Figure 6.6: Impact of the new moist physics on the tangent-linear approximation error as defined in the text. Panel (a) shows the temperature error difference (in K) when the standard simplified moist physics is used in the tangent-linear calculations instead of no physics at all (adiabatic run). The two other panels show the further changes in the error due to the use (b) of CNV.AN.EXP and (c) of CNV.AN.EXP combined with CLD.AN.EXP. Error changes are displayed as zonal means and model levels are shown on the vertical axis. The global relative error reduction appears at the top of each panel.

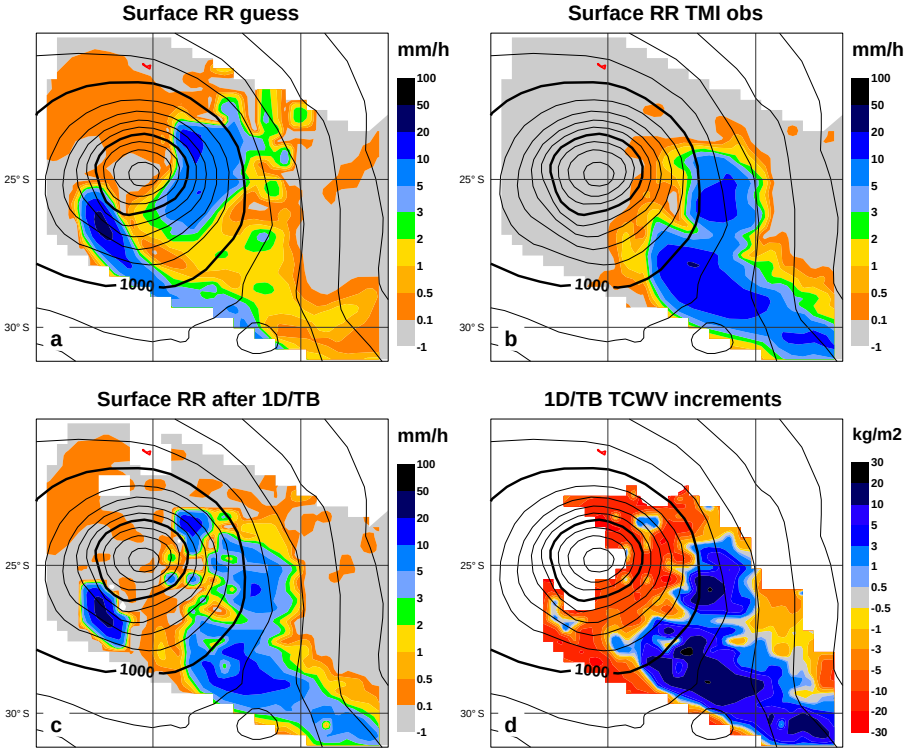

Figure 6.7: 1D-Var experiments using CNV.AN.EXP and CLD.AN.EXP: (a) surface RRs as simulated from the background state of (T,q), (b) as derived from TRMM multi-channel microwave TBs using the PATER algorithm, and (c) as recomputed from the modified model (T,q) profiles after 1D/TB (using the 10, 19, 22 and 37 GHz channels in vertical and horizontal polarizations). 1D-Var Total Column Water Vapour (TCWV) increments from 1D/TB are plotted in panel (d). Background mean-sea-level isobars are drawn every 2 hPa.

6.3.3 1D-Var on ARM observations

To explore the feasibility of assimilation of cloud information from future instruments (e.g. CloudSat or Earth-CARE), assimilation experiments using the new cloud and convection linearized schemes were carried out using cloud radar reflectivity observations taken at the ARM Southern Great Plains site (36.6N–97.5W) during January 2001. The reflectivities were averaged over one hour interval and screened at lower levels to exclude saturated values. The background temperature and specific humidity profiles were taken from the 12-hour forecast from the ECMWF model (T511L60). The profiles represent mean values for the the nearest grid-points around the ARM-SGP site. These profiles of T and q, along with surface pressure, p_s, tendencies, and surface quantities are used in the moist physics routines (simplified convection and cloud schemes described above) to compute cloud properties (cloud cover, ice and liquid-water contents) and precipitation fluxes. A radar observational operator is then applied to the model fields to obtain the equivalent reflectivity. Assimilation experiments were also performed to combine the reflectivity with other observations available at the SGP site such as surface longwave radiation (employing also a radiative-transfer model as observation operator in that case) and total column water vapor.

Results of the assimilation for January 2001 are shown in Figs. 6.8–6.9. Panels (a)-(c) of Figure 6.8 show a comparison of the first guess and the 1D-Var retrieved radar reflectivity versus the Millimeter Cloud Radar (MMCR) observations when only reflectivity is assimilated. The 1D–Var analysis is closer to the observations for most of the profiles. Focusing on the first days of the month, it is possible to see that the 1D–Var showed

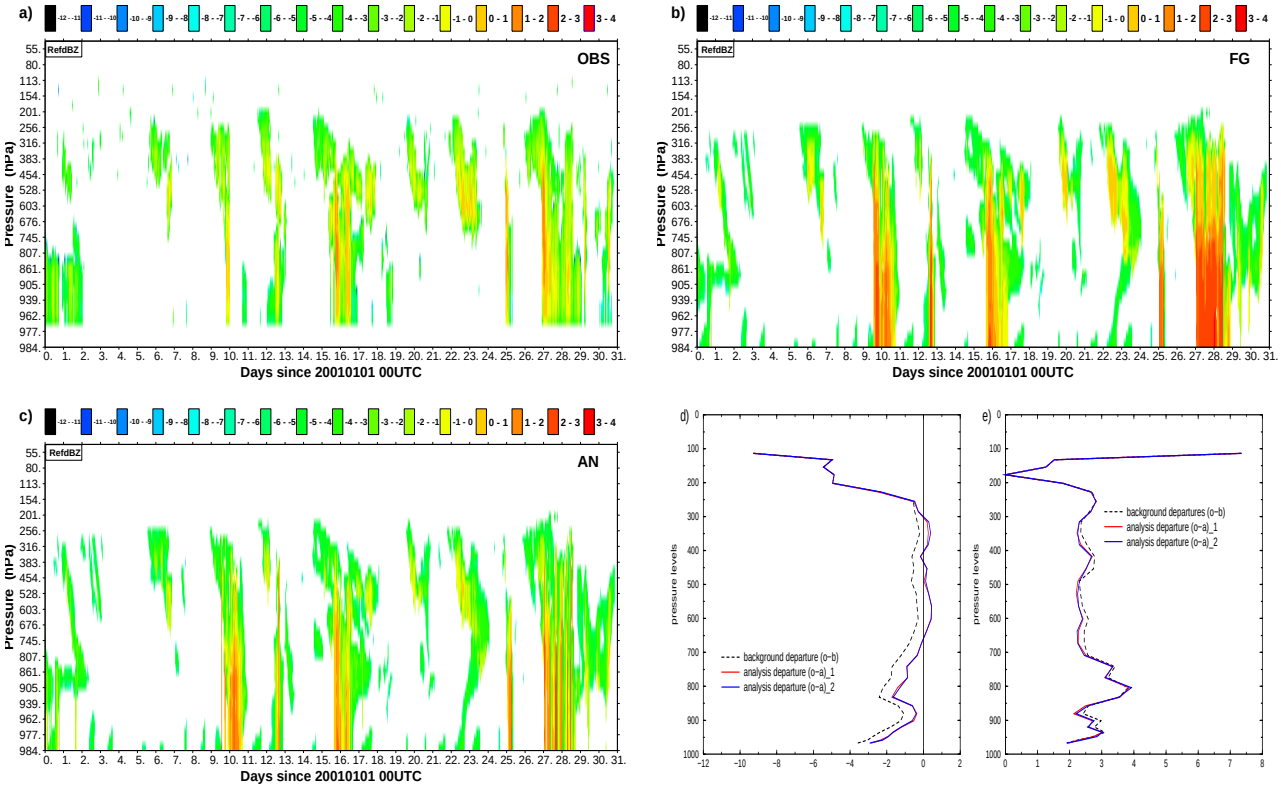

Figure 6.8: SGP site radar reflectivity (dBZ/10) for January 2001: (a) MMCR observations, (b) model first guess, (c) 1D–var retrieval, when assimilating reflectivity only. Panels (d) and (e) show respectively the bias profile averaged over the whole month and the standard deviation: background departures (black line), analysis departures when only the reflectivity profile is assimilated (red line), and analysis departures when the reflectivity is assimilated in conjuction with surface LW flux and TCWV (blue line). See text for explanations.

skills in increasing the reflectivity at lower levels. A reduction in reflectivity consistent with the observations is shown by the analysis at upper levels around January 6-7. Major adjustments from the 1D–Var are also evident toward the end of the month (January 27-28). Figure 6.8d shows the average bias profile (background minus observations and analysis minus observations) over the whole month. The reduction in bias is quite dramatic. When assimilating reflectivity together with surface longwave radiation (LW) flux and total column water vapor (TCWV), the impact on the reflectivity field is almost identical. However, the impact of the extra observations is visible in the comparison with independent radiosonde observations. The profiles of relative humidity bias and standard deviation averaged over a month are shown in Fig. 6.9. The black line represents the background departures (radiosonde observations minus background) while the solid red and blue lines represents respectively the analysis departures (radiosonde observations minus analysis) for the experiment with reflectivity only and the experiment with augmented observations. The analysis produces a relative humidity profile which is closer to the observations (lower bias) and has a smaller standard deviations at most levels in both cases. However, the experiment with extra observations shows a positive signal also at lower levels indicating that the additional constraints imposed by the TCWV and the LW flux act to improve the analysis also at those levels where the reflectivity did not have an impact. This choice of observations was aimed at reproducing an “upside-down” satellite configuration such as that of EarthCARE where the observations from the active sensors will be perfectly co-located with the passive radiation measurements.

Assimilation of radar reflectivities appears to be promising and will be further explored in the near future. The synergy of different cloud observations was proved beneficial toward improving the performance of the cloud

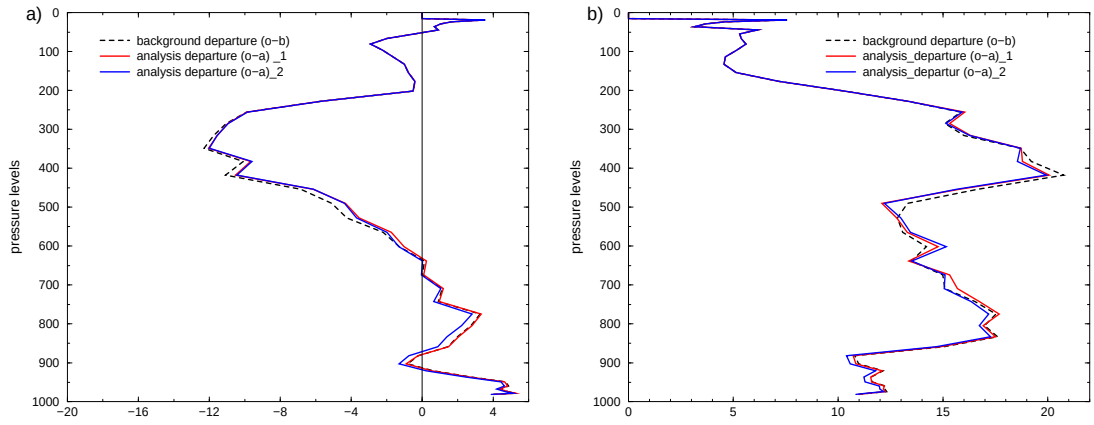

Figure 6.9: Bias and standard deviation with respect to radiosounding observations in relative humidity for background (black line) and 1D-Var retrieved profiles (red and blue lines). See text for explanations.

assimilation system and exploring 4D–Var assimilation of cloud-related measurements. Further improvements in the model will also enable the exploitation of the wealth of satellite observations that should become available in the near future from missions such as CloudSat, CALIPSO and EarthCARE.

6.4 Conclusions

Two new simplified parametrizations for subgrid-scale convective and cloud processes have been developed and tested in the framework of the ECMWF Integrated Forecasting System for the purpose of variational data assimilation, singular vector calculations and adjoint sensitivity experiments.

The convection scheme is based on the full nonlinear scheme that is used in the operational forecasts, but it was demonstrated that a set of simplifications could lead to a substantial improvement of its linear behaviour without significantly degrading its forecasting ability even in seasonal integrations. In contrast with the Mahfouf (1999) simplified convective parametrization, its tangent-linear and adjoint versions account for perturbations of all convective quantities including convective mass flux, updraught characteristics and precipitation fluxes.

The convection scheme has also been successfully combined with a new simplified parametrization of large-scale clouds and precipitation developed by Tompkins and Janisková (2004) and also described here. The cloud scheme is based on a diagnostic statistical concept. The fixed variance form implies that the scheme is currently equivalent to a relative humidity type formulation. However, the framework will facilitate the move to a total water variable and a diagnostic variance scheme in the future. The scheme includes a realistic cloud source term from the new linearized convective scheme and perhaps most importantly binds the precipitation to cloud properties. This latter characteristic of the new scheme greatly improves the performance in the tropics.

The new package has been successfully used in 1D-Var retrievals of TCWV from microwave brightness temperatures in precipitating areas (Moreau et al., 2004). The new schemes are not currently utilized in the operational model 4D-Var system, but the goal would be to activate them in the near future, where their superior representation of the physics, closer approximation of the full nonlinear model and improved linear characteristics are expected to produce substantial gains. Additionally, further investigation into their use for Singular Vector (SV) calculations is underway.

7 Future directions

This document has reviewed the moist physics of the IFS model by outlining the main components, namely, convection, boundary layer, and large-scale cloud parametrisations. This was done in terms of both the complex full non-linear schemes used for the high resolution forecasts and equally importantly the simplified tangent linear and adjoint schemes essential for the data assimilation system.

Each section of this document also provides details on the developments that have occurred in each scheme since the pivotal 23r4 ERA-40 model cycle still used in the system 2 seasonal forecasting. The second section also compared a limited range of statistics illustrating the array of improvements that these modifications have achieved.

Some systematic biases related to moist physics remain in the model climatology, and were identified in table 3 as

(i) Lack of stratocumulus cloud

(ii) Lack of deep convection over tropical continents

(iii) Lack of deep convection over W. Pacific warm pool

(iv) Too little ice in mid latitudes

Although desirable, it is extremely difficult to associate these directly with shortcomings in a specific aspects of parametrization schemes, or indeed a parametrization in general. For example, the lack of stratocumulus would appear to be an obvious instance of a locally forced problem, that could be identified with inadequacies in the vertical diffusion scheme. However, while the revised scheme introduced in section 5 certainly appears to aid this model deficiency, it is not proven that the previous vertical diffusion scheme was entirely at fault. Comparisons of the large scale subsidence fields in section 2 (see Fig. 2.7) indicate that the IFS does not produce sufficient subsidence in the eastern Pacific. The dynamics of the entraining stratocumulus layer are extremely sensitive to the imposed subsidence velocity at the cloud top. The lack of subsidence could arise from the absence of remote forcing from deep convection over the American continent and/or the Western Pacific, and therefore be due to the convection scheme, or alternatively through incorrect cloud/radiation feedbacks providing inaccurate large-scale forcings (thus due to problems in the radiation and/or cloud schemes).

Nevertheless, it is possible to identify the aspects of parametrizations to which (i) there is much sensitivity and (ii) the representation (and possibly also the knowledge) of the physics is known to be poor. For example, the deep convection scheme shows much sensitivity to the trigger function, the entrainment/detrainment profiles, and to the use of moisture convergence in the specification of organized entrainment. The TOA radiative fluxes are sensitive to the ice sedimentation formulation which is identified as a key area of the current cloud scheme earmarked for improvement. Likewise the new boundary scheme was critically dependent on the form of the decoupling criterion that determines the cloud regime. These are all key areas to be focussed upon.

In addition to these parametrization scheme-specific target areas, there is also room for an overarching development strategy for all the moist physics; one that aims to introduce greater coherency between the various model components while at the same time tackling some of the outstanding problems listed above.

7.1 Development strategy

The considerable and in-depth analysis that has been presented in this document repeatedly highlighted the difficulty of unifying the various model components (for example, diffusion and shallow convection in section

5 or shallow and deep convection in section 3). More generally, the array of parametrizations representing the various moist physics outlined here necessarily have to make a number of closure assumptions, that often involve a number of tuning parameters.

Even if theory, modelling or observational undertakings can provide a theoretical or empirical scaling for some of the tuning parameters, their accurate optimization for maximum forecast quality in the medium range is an involved and time consuming task. Efforts will be made to implement tangent linear and adjoint procedures to enable the efficient optimization of these tuning parameters for the convection scheme for example. Nevertheless, model developments that reduce the magnitude of the tuning parameter space are desirable.

Traditionally, parametrizations for moist physical parametrizations have developed as separate modular "units". Linkages, such as the use of convective detrainment as a source term for the cloud scheme, are fairly minimal. An outcome of this approach is that, even if closure assumptions and tuning parameters pertain to a common theme, each scheme makes its own, separate, and sometimes contrasting assumptions.

A good example of this is the representation of subgrid-scale fluctuations. Many model parametrizations involve assumptions concerning subgrid variability of dynamical and thermodynamical parameters. Examples are relative humidity thresholds for cloud formation, corrections to liquid water paths made in the radiation scheme, or fixed thermodynamical and dynamical excesses given to ascending parcels used in the shallow and deep convective schemes. Indeed, many of the model improvements outlined in this document invoked such assumptions, such as the new linear cloud scheme for data assimilation purposes and also the modifications made to convective triggering.

One cause for concern is that each model scheme makes its own assumptions concerning unresolved variability, involving its own set of unknown parameters required for closure. For example, the radiation scheme applies a fixed factor to the cloud liquid content to account for biases arising from the neglect of horizontal variability (Cahalan et al., 1994; Tiedtke, 1996). The Tiedtke (1993) cloud scheme introduces a relative humidity threshold of around 80% throughout much of the troposphere for producing new clouds; an implicit assumption concerning the subgrid nature of humidity fluctuations (which, like the 0.7 cloud water weighting adjustment for the radiation scheme, is unfortunately independent of the local dynamical and thermodynamic situation). The convection scheme applies a 0.2 K temperature excess to updraught parcels.

It is thus clear that if a suitable representation of subgrid thermodynamical and dynamical variability of suitable accuracy were introduced many model components could exploit this without recourse to their own set of assumptions.

This last section introduces part of the development strategy for moist physics, outlines briefly a prototype scheme for subgrid-scale fluctuations, and gives some examples of how this information can be used in many other model components to increase model self-consistency and reduce the number of tuning parameters that require definition.

7.2 Subgrid variability

One simple and implicit way to introduce subgrid variability into the IFS would be to relate the subgrid unresolved variability diagnostically to that resolved by the model on the near grid scale; a methodology employed by Cusack et al. (1999) using a high resolution model to define this relationship. However, the concern with such an approach is whether a model has the ability to represent spatial variability at resolutions close to the grid-scale. The effect of diffusion implies that the "effective" resolution of a model is many times the nominal grid resolution, and variability at the grid-scale can be regarded as numerical 'noise' introduced by column based parametrizations (Lander and Hoskins, 1997).

To test the IFS model's ability to resolve variability at the near grid scale, radiation observations from a high resolution surface network are compared to the model. Within the Atmospheric Radiation Measurement program (ARM), the South Great Plain site (SGP) includes more than 20 stations measuring the components of the surface radiation budget within a 300 x 300 km2 area (Fig. 7.1). Over the month of July 2003, the hourly averages of the downward longwave and downward shortwave radiation derived from 36 hour forecasts started 24 hours apart were compared with hourly averages of the observations. Figure 7.1 compares the timeseries of the normalized standard deviation of the model and observed downward longwave radiation. Over most of the period, the model shows less variability than the observations by roughly 30 percent, even when an attempt is made to include the subgrid information into account available from the cloud cover.

The conclusions that can be drawn are two-fold but not clear-cut. This lack of variability could be linked to the model having a lack of heterogeneity between neighbouring grid cells, in other words, lack of resolution at the near grid-scale. Alternatively, the problem could be the lack of subgrid-scale variability. For example the absence of sub-grid clouds (shallow convective clouds in particular) could cause this difference. In fact, it is likely that the lack of variability in the model is caused by a combination of the above two effects, pointing out the requirement for a parametrisation for subgrid-scale variability and its necessary explicit nature, rather than the approach of Cusack et al. (1999)

7.3 Prototype statistical scheme in the IFS

To show the potential for the implementing a statistical scheme in the IFS, a prototype scheme was tested at model cycle 26r1. The scheme represents the subgrid variability for total water only, and neglects variations in temperature. This can be partially justified by the analysis of observations by Price (2001) and Tompkins (2003). Figure 7.2, taken from the analysis of ARM site aircraft data, indicates that the errors made in the cloud cover when temperature variability is neglected are roughly half those when total water variability is ignored. Furthermore, this relationship appears to hold for a range of horizontal length scales (Tompkins, 2003).

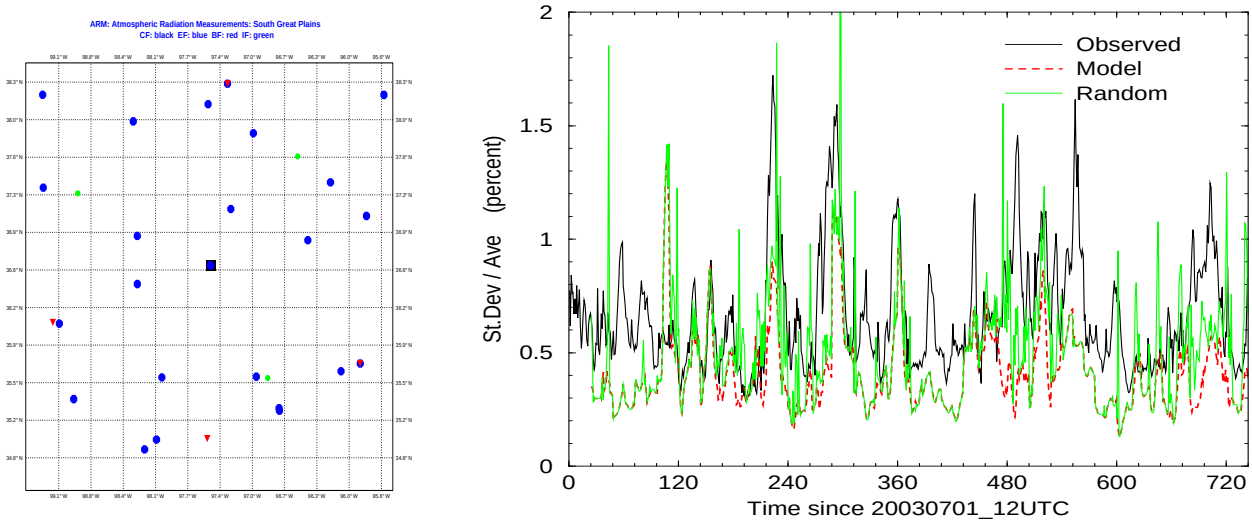

Figure 7.1: Left panel: Location of ARM site observations. Right panel: Observed (black) versus model (red dashed) standard deviation of downward longwave variability. The model result is calculated using grid-mean fluxes. A third calculation (green line) attempts to take the subgrid information into account in the following way. For each time-slot a random number Φ is generated where $0 \leq \Phi \leq 1$. If $0 \leq \Phi \leq TCC$, where TCC is the total cloud cover, the cloud-column radiative flux is used, otherwise the clear sky flux is taken. In this way the subgrid information available from the fractional cloud cover is taken into account.

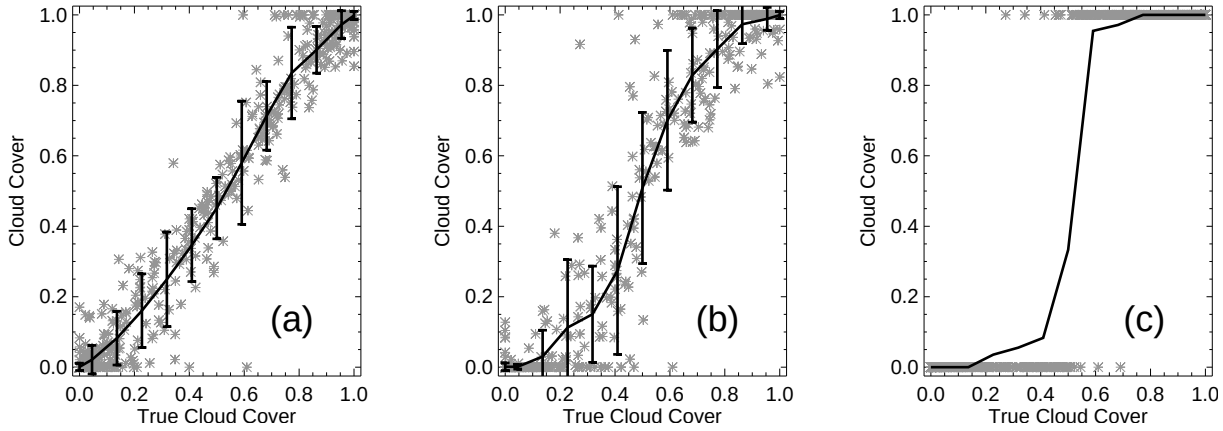

Figure 7.2: Scatter plots of apparent cloud cover versus true cloud cover when (a) temperature, (b) humidity and (c) all variability is neglected. Each point on the scatter plot represents a horizontal aircraft flight segment of 4 km in length. Results for longer or shorter leg length were qualitatively similar.

Eventually, the aim is to move to a scheme that includes a prognostic equation for the variance and skewness of the total water distribution (and possibly also temperature fluctuations). In particular, deriving the source/sink terms for each of the microphysical processes is a difficult task and remains the subject of active research (e.g. Zhang et al., 2002; Klein et al., 2004).

Instead, the simple scheme tested here circumnavigates this problem by simply using the existing prognostic equations to derive the higher order moments of the total water variability and fitting a PDF using this information. One could accomplish this by fitting a 3 moment distribution to the water vapour, cloud water and cloud cover information provided by the operational Tiedtke (1993) scheme. The disadvantage of this approach is that the Tiedtke scheme can produce combinations of these three variables that result in unreasonable or even unphysical PDFs, due to the fact that the sources and sinks of cloud cover and cloud water are not always derived self-consistently with an assumed underlying PDF.

Alternatively, the approach is taken of disabling the prognostic cloud cover, and fitting at each time step a 2-moment distribution to the grid-mean liquid water and water vapour mass mixing ratios. The cloud cover is then obtained by integrating the saturated part of the PDF.

The Beta PDF is used; a bounded, unimodal, 4-moment distribution, with the PDF of total water mixing ratio $G(q_t)$ given by

$$G(q_t) = \frac{1}{B(p,q)} \frac{(q_t - a)^{p-1}(b - q_t)^{q-1}}{(b-a)^{p+q-1}} \tag{7.1}$$

where a and b are the distribution bounds ($a \leq q_t \leq b$) and, $B(p,q)$ represents the Beta function. The distribution is reduced to a 2 parameter distribution by setting the shape parameters to a value of $1+\sqrt{2}$. This imposes the condition of symmetry on the PDF. This is a poor assumption for shallow (Bougeault, 1981; Randall, 1987; Bechtold et al., 1995) or deep (Tompkins, 2002; Klein et al., 2004) convective situations where the updraughts are surrounded by wide subsidence areas, producing positively skewed distributions. However, stratocumulus, stratus and frontal clouds have close to symmetrical distributions (not to mention clear sky regions, although these are not important for a fixed diagnostic scheme such as the one used here), and convective downdraughts can even produce negatively skewed distributions in the boundary layer. Overall, although the prevalence of convection around the global probably implies that skewness has a small positive global mean value, the lack of knowledge of what this value actually is implies that for these first simple tests, a symmetrical distribution is likely to be as adequate as any alternative non-zero skewness assumption.

It should be noted that this scheme is only designed as a simple prototype and many internal inconsistencies remain in some of the source and sink terms. For example, the RH threshold for cloud formation is still in place (although this is necessarily the case until a prognostic variance equation is added for at least clear sky or overcast situations. For further discussion see the implementation details of the hybrid "semi-prognostic" scheme of Tompkins, 2002). The formation and subsequent evaporation of precipitation are also ignorant of the subgrid variability information provided.

Nevertheless, one of the most important cloud source terms, namely the change of cloud water through (a)diabatic cooling/warming, has been modified to be consistent with the subgrid-scale PDF for water vapour. The cloud dissipation/creation via turbulent mixing is also accordingly modified. In addition to these two processes, the convective detrainment source was identified by Fillion and Mahfouf (2003) as being a key term in the Tiedtke (1993) scheme. Now, instead of a direct link, convective detrainment alters (usually increases) cloud cover implicitly through its influence on the cloud water and humidity amounts. It is clear that the scheme serves as an informative and useful first incremental step in the development of a fully prognostic statistical scheme.

The cloud climatology of the simple model is shown in Fig. 7.3. It reveals that all the main features of the cloud climatology have been maintained. However, there is a general reduction in cloud cover relative to the standard Tiedtke scheme, as confirmed by the difference map in the same figure. This reduction is generally detrimental, especially in the SH extra tropics and mid latitude and over the Eurasian summer continent, and is probably

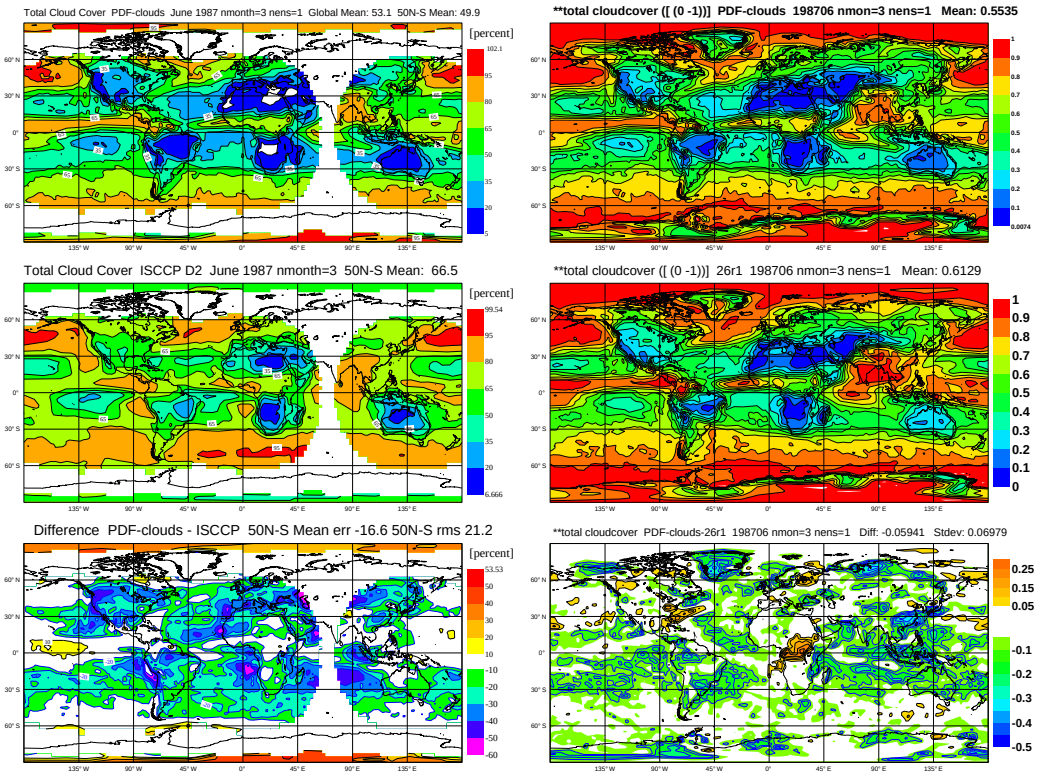

Figure 7.3: Left column: comparison of prototype simple statistical cloud scheme total cloud cover with ISCCP D2 retrievals for the final three months of a single 4 month experiment for summer 1987. Right column: Difference in total cloud cover between the simple statistical cloud scheme (top) and the control 26r1 integration (middle) for the same period.

partially due to the use of a symmetrical distribution which tends to reduce cloud cover in locations where the total water relative humidity (q_t/q_s) is less than unity, which is generally the case. That said, it should again be emphasized that this scheme is extremely simple, discarding the entire complexity of the prognostic cloud cover, and that its implementation here is without further tuning of the model parameters. Bearing this in mind these results are extremely encouraging concerning the benefit that a full statistical cloud scheme may bring.

7.4 Using variability information in other model components

It was stated that one of the main motivations for developing a statistical cloud scheme is to provide subgrid information to other model components in a consistent manner. Thus here consideration is given to how an eventual PDF based scheme might be used to remove biases from, or improve the representation of, microphysical, radiative and convective processes.

Just one example from each of these categories are given for brevity, and naturally these are far from exhaustive. For example, boundary layer turbulent processes are more naturally linked to a statistical parametrisation that provides information concerning higher order moments. Indeed, the description of the new moist turbulent scheme in section 5 includes the derivation of source terms for the total water variance, which are currently converted into equivalent tendencies for the prognostic cloud and humidity variables. This latter step could be discarded once a fully prognostic PDF cloud scheme was in place. Additionally, one of the suggested potential future avenues for the convection scheme development would be a multi-plume approach. Knowledge of the subgrid variability of water vapour would allow convective organisation feedback with water vapour to be represented, with the strongest convective elements developing in the moistest environment.

7.4.1 Microphysics

Results are shown from a preliminary investigation into how taking subgrid variability into account in cloud scheme of the IFS code could affect the cloud evolution. The column model is used with the prognostic cloud scheme replaced by the simple statistical scheme described in section 7.3 above.

The variability described by the variable width symmetrical PDF for total water is taken into account in all processes in the Tiedtke (1993) cloud scheme. Ideally one would perform an analytical solution for each process, integrating across the PDF, such as conducted for autoconversion by Zhang et al. (2002). However, this is an involved procedure, and it is questionable if a efficient solution can be found for all processes concurrently. A numerical solution is instead used, by splitting up the column into a number of sub-columns, where the cloud properties in each column overlap according to the maximum-random overlap assumption used in the radiation scheme. This is similar to the approach of Jakob and Klein (1999), except that here sub-cloud variability is taken into account in addition to the cloud cover mask. In order to resolve the PDF 100 sub-columns are used. This implementation is flexible, but unlike the McICA approach for radiation (see section 7.4.2 and Pincus et al., 2003, which does not increase cost by performing each sub-column calculation once for a different radiative band) it is numerically more expensive. It is affordable in this column model determination of biases, but would be currently infeasible for the full GCM.

The integration of the column model using the 100 sub-columns is compared to a control experiment where the microphysical processes operate on the mean in-cloud water content as usual. The integration simulates a 6 day period during the TOGA-COARE campaign in the tropical Western Pacific, during which prevalent deep convection occurs in the model.

Figure 7.4 gives the timeseries of vertically integrated liquid water path (LWP) and ice water path (IWP) for the two integrations. It is immediately clear that the two experiments differ substantially. The integration that

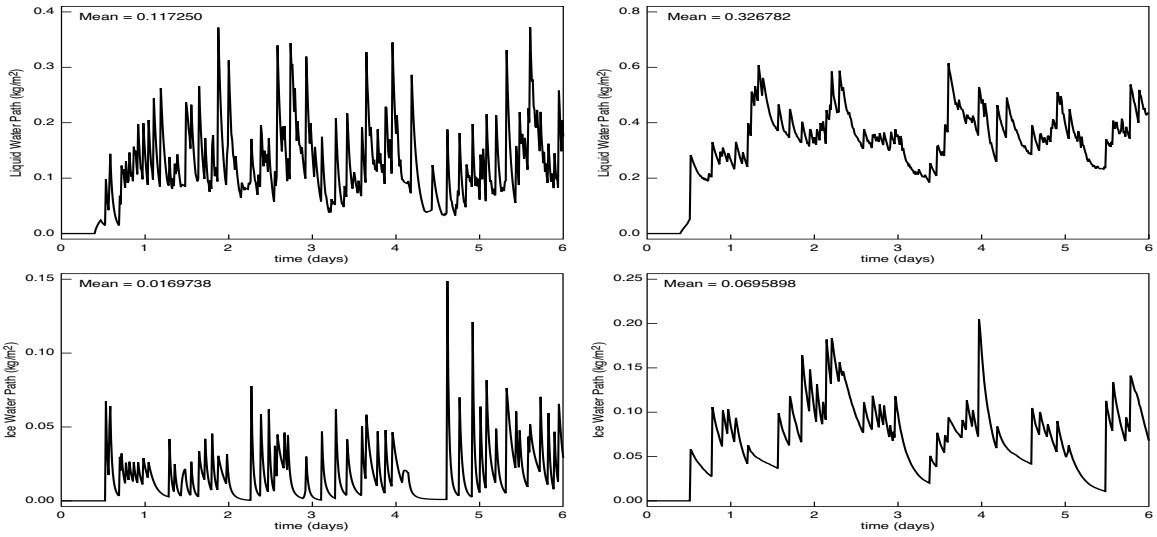

Figure 7.4: Right panels: timeseries of LWP and IWP when subgrid variability is taken into account using 100 sub-columns. Left panels: timeseries of LWP and IWP when subgrid variability is neglected.

takes subgrid variability into account increases IWP and LWP by over a factor of 3, and reduces the temporal variability of the clouds. This is also apparent if the cloud cover is examined (not shown).

Are these changes as expected? In fact, the opposite effect is usually anticipated from the nonlinearity of the warm rain autoconversion process (although the Sundqvist formulation is virtually linear for appreciable cloud water contents). The answer lies with the ice autoconversion to snow. This is currently parametrized as a side-effect of the ice-sedimentation process, giving an effective autoconversion rate from ice to snow that is proportional to $q_i^{0.16}$, where q_i is the ice mass mixing ratio. This is quite a weak nonlinearity. However, it is found to dominate the response of the model in deep convective situations. The reason is related to the significant non-diagonal Jacobian sensitivity documented by Fillion and Mahfouf (2003). The precipitation flux generated at higher levels in the model is able to strongly influence the autconversion rates in warm and mixed phase clouds through the adjustments made to account for accretion processes. Thus the nonlinearity of this ice-phase process accumulates throughout the column and produces larger cloud water amounts when variability is accounted for. While the relationship for ice fall speeds has been observationally determined, it is clear that it does not represent the physics of the snow generation process. Indeed, many models such as Lin et al. (1983) represent snow generation with an exponent greater than or close to unity, and thus the sensitivity would be zero or even of the opposite sign. This study thus underlines the importance of gaining a more accurate understanding of complex ice microphysics, which becomes more crucial when sub-cloud variability is accounted for.

7.4.2 Radiation

At the moment the subgrid unresolved variability is crudely accounted for with a adjustment by a factor of 0.7 to the cloud water as introduced by Tiedtke (1996). With a statistical cloud scheme in place it is possible to replace this with a bias correction based on the unresolved variability, as accomplished by Bäuml (2002) using the information provided by the statistical scheme in the ECHAM climate model.

As a first step towards taking cloud water fluctuations into account, it is possible to introduce a framework to improve the handling of the cloud mask. Recently, Barker et al. (2003) and Pincus et al. (2003) introduced

a new method for computing broadband radiative fluxes in GCMs yielding unbiased radiative fluxes over an ensemble average of one-dimensional RT simulations. It is referred to as the Monte-Carlo Independent Column Approximation (McICA). The most attractive features of McICA are two-fold: first, it extricates the description of the sub-grid scale cloud structure from the radiative transfer algorithm through a cloud generator that provides the cloud parameters for the radiation schemes by sampling the cloud information randomly from the cloud fraction and water profiles provided by the GCM; second, its radiative fluxes, unbiased with respect to ICA, are consistent with assumptions made about the unresolved structure in other parts of the model. In practice, this sub-grid scale cloud structure is related either to the overlapping of the cloud layers in the vertical and/or to the horizontal variability of the cloud characteristics. Whether on the vertical or on the horizontal, the cloud characteristics here referred to correspond to input parameters in a traditional radiation transfer scheme, namely the distribution of condensed water in various phases, that of the particle effective dimension, which together with the distribution of intervening gases should define the radiation exchange on the vertical within a grid of the GCM.

The McICA versions of $RRTM_{LW}$ and $RRTM_{SW}$ differ from the operational versions in two respects: Clouds when present occupy the full horizontal extent of the layer, and the vertical distribution of such clouds (of 0 or 1 cloud cover) is defined independently for each of the 140 (224) essentially monochromatic calculations of the longwave (shortwave) scheme by the cloud generator.

Preliminary results with a 1D model of the McICA radiation schemes are presented over a two-month period (April-May 1999) at the ARM-South Great Plains site, using the vertical profiles of temperature, humidity, and cloud parameters, and other boundary conditions produced by 24-hour forecasts with the ECMWF model. To check that both the generators and the McICA-modified radiation schemes are performing correctly, the cloud generator of Pincus et al. (2003) is used to provide, for each of the 1464 one-hour time slots, 100 independent draws of 224 profiles of cloud cover information. An average of the radiation fields computed by the McICA radiation schemes over these 100 draws should perfectly reproduce the radiation fields obtained with the ICA approach. Assuming that the cloud overlap treatment within the standard radiation schemes describes properly the radiative interactions between cloud layers, results from the standard radiation schemes should also be equivalent to the ICA results.

Figure 7.5 presents the TOA upwards fluxes (i.e., the outgoing longwave radiation (OLR) and reflected shortwave radiation (TUSW) and downward fluxes at the surface, SDLW and SDSW, for the two-month period. For such a large number of draws (N=100), the McICA and ICA computations are quasi-identical in terms of results. However the McICA calculation is far more computationally efficient.

With the implementation of a parametrisation for the subgrid-scale variability of total water fluctuations it is clear that the McICA approach could be taken a step further. In addition to handling the cloud overlap, each column used for a radiative calculation could also taken sub-cloud variability into account. This would allow the Tiedtke (1996) fixed adjustment to be abandoned in favour of a a scheme that consistently takes sub-grid fluctuations into account in a consistent way.

7.4.3 Convection

The final example concerns the convection scheme. In section 2 it was shown that the IFS currently has insufficient convection over the tropical continents of Africa and South America, in additional to the Asian Maritime continent, evidenced by the observations of surface precipitation, cloud climatology and outgoing longwave radiative fluxes.

One obvious question to pose is exactly how the surface conditions impact the updraught conditions in nature and in the model. One obvious difference pertains to the subgrid-scale variability issue once again. Land sur-

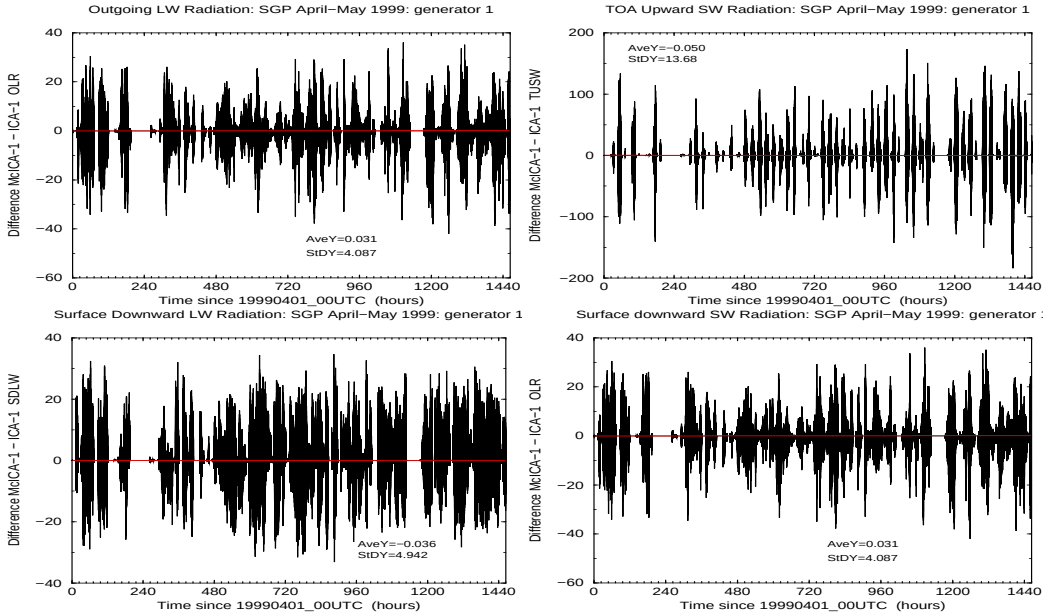

Figure 7.5: The range of values taken by the differences in outgoing longwave radiation (top left), upward shortwave radiation at the top of the atmosphere (top right), surface downward longwave radiation (bottom left) and surface downward shortwave radiation (bottom right) between 100 McICA draws and the average of a 100 sub-column ICA computations. ICA and McICA radiative computations are done independently for each hour during the March-April May period over the ARM-South Great Plains site, based on a series of 24-hour forecasts with the ECMWF forecast model. For each field, the mean and standard deviation is computed over the 100 x 1464 computations. All values are in W m^{-2}. The cloud generator is the one originally used in Pincus et al. (2003)

faces are marked by their horizontal heterogeneity. This can be in terms of the orography, soil type, land use or subgrid-scale water surfaces, to cite a few possibilities. It can even occur in the form of feedbacks occurring between soil moisture and convection (e.g. Taylor and Lebel, 1998; Taylor et al., 2003). Thus for a given buoyancy flux in a convective boundary layer, a land surface is likely to be subject to much greater variance in local temperature, humidity and velocity excesses than a homogeneous oceanic region. The buoyancy and ability of these most energetic parcels to spawn shallow or deep convection is tested at each grid point without taking surface type into account. While shallow convection uses parcel excesses based on the surface fluxes of heat and moisture, the ascent for deep convection is initiated with a fixed excess of 0.2 K in temperature, 0.1 g kg^{-1} in humidity and 1 m s^{-1} in vertical velocity.

In a test for the sensitivity to this effect, a study was carried out in which these excesses are multiplied by a fixed ratio based on the land-sea mask φ. A simple ad hoc linear relationship is used given by $1+2\varphi$. In order to prevent the strong mixing in the boundary layer diluting these contrasting characteristics, the parcel mixing is similarly reduced, reflecting the inverse relationship between entrainment and updraught velocity advocated and used by Siebesma (1998); Neggers et al. (2002) and Cheinet (2003).

The resulting change in precipitation compared to the default model is given in Fig. 7.6, along with the comparison to the GPCP dataset. The plot shows the desired effect over the African and American continents, with the surface precipitation in the sensitivity study very similar to the observations. Additionally, the strong biases in TOA longwave radiation in these regions are almost eradicated when comparison to CERES data is made, which the maps show is associated with a strong increase in high cloud cover in these regions.

The modifications also increase the convective activity over the land areas of the maritime continent, but do so

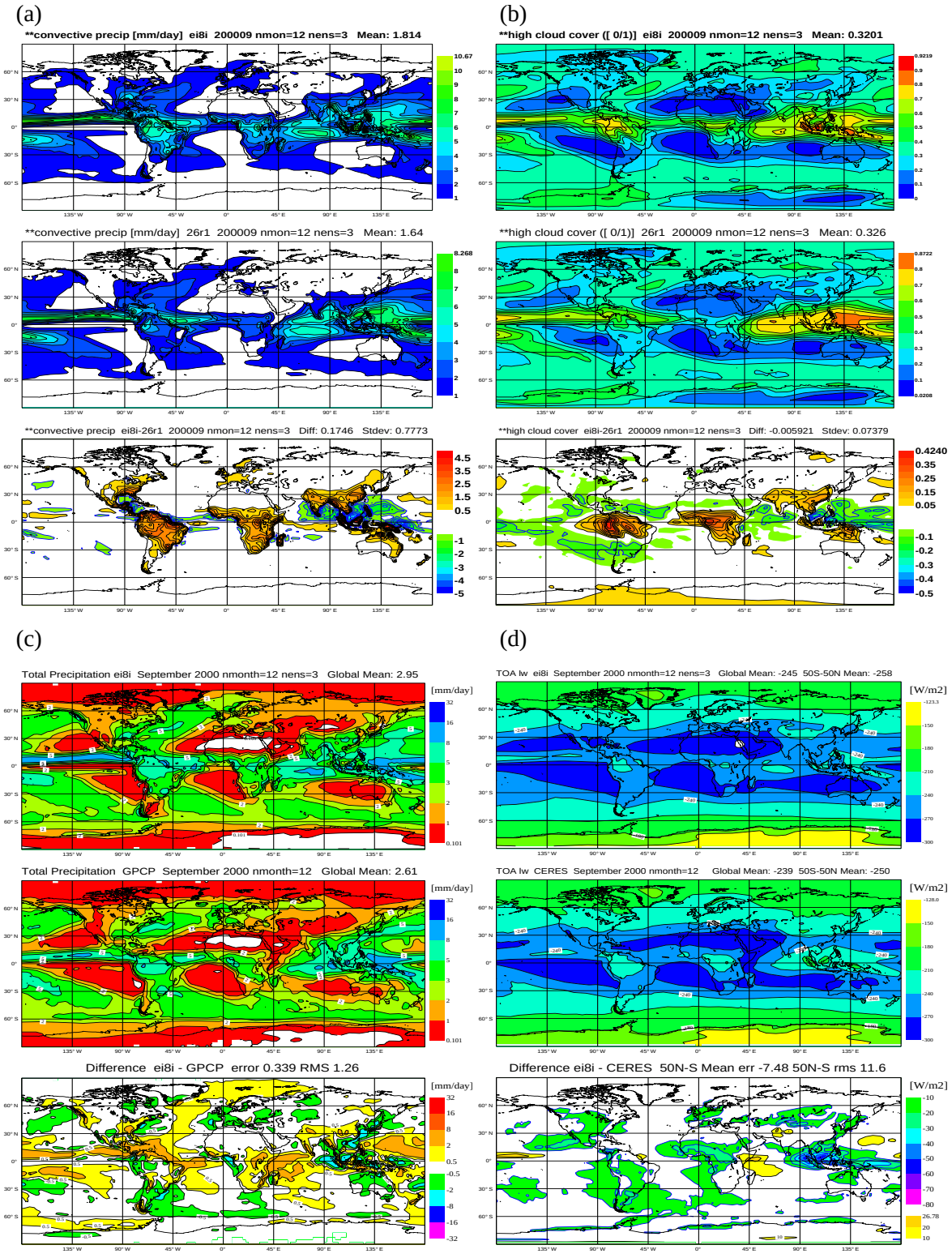

Figure 7.6: (a) comparison of annual mean convective precipitation between cycle 28r1 and the revised trigger function. (b) comparison of high cloud cover. (c) comparison of revised trigger function experiment total surface precipitation to GPCP. (d) Comparison of TOA longwave radiation to CERES data.

at the detriment of the surrounding oceanic regions, which are further suppressed. The model already suffers from a lack of convection in this location. As pointed out in section 2 this is likely to be associated with the low wind speeds in this area, and further investigations into the parametrization of mesoscale gustiness will aim to target this problem.

This example again shows the potential for including subgrid information in a consistent way into the IFS model physics components. Rather than the crude and static function used here, with a future implementation of a prognostic parametrization for subgrid-variability, the triggering of convection would be based on an estimate of thermodynamical and perhaps also dynamical variability that is a function of the air parcel's history and would be entirely consistent with that used in the other model components.

7.5 Conclusions

The developments that have occurred in the IFS moist physics over the recent period spanning model cycles 23r4 to 28r3 have been outlined, along with the associated benefits to the medium range forecasts quality and the longer term model climatology.

The opportunity was also taken to outline the development strategy for the IFS moist physics, both in the short and medium term future. Many of these promise further enhancements to model skill.

Moreover, the target of the medium term moist physics evolution is a greater *coherency* between model components. Increased model complexity tends to introduce further requirements for closure parameters, which in turn impedes future model development, since the difficultly of their re-optimization when new parametrizations are introduced grows exponentially with their number.

By viewing the moist physics as a unified system, with each process accessing a central *core* for closure information, the number of parameters can be substantially reduced. The obvious example is the provision of information concerning subgrid variability upon which so many model components depend. By reducing the size of the tunable parameter space, it is possible to have increased confidence that any eventual gains in forecast skill are not simply due to the addition of adjustable parameters, but rather results from a fundamental and tangible advance in the representation of moist physical processes.

Diagnostics and verification will remain a crucial ingredient for model development. Apart from verification with operational data, it is essential to have access to good research-type observations. This will be achieved through collaboration with outside partners (e.g. through CloudNet, ARM, Cloudsat, GEWEX, Earthcare). The planned data assimilation of precipitation and clouds will also provide valuable information about model deficiencies. For the development of parametrizations and for the understanding of processes and their interactions, fine scale models will become increasingly important. Therefore good contacts will be maintained with outside partners (e.g. European institutes, the new Multi Modelling Framework Science and Technology Centre at Colorado State University). The GEWEX Cloud System Studies (GCSS) working groups are an obvious platform for such a collaboration.

A Appendix: Details of the new combined mass flux/diffusion PBL parametrization

A.1 Mass flux component and plume model

An air parcel is traced through its updraught to find cloud base, cloud/PBL top and the updraught properties. This is done with an entraining/detraining bulk plume model for the variables $\phi = \{s_l, q_t\}$ (e.g. Betts, 1973) and updraught kinetic energy $\frac{1}{2}w_u^2$ (Simpson and Wiggert, 1969)

$$\frac{\partial \phi_u}{\partial z} = -\varepsilon\left(\phi_u - \overline{\phi}\right), \tag{A.1}$$

$$\frac{1}{2}\frac{\partial w_u^2}{\partial z} = -\varepsilon\left(w_u^2 - \overline{w_e}^2\right) + g\frac{\theta_{v,u} - \overline{\theta_v}}{\overline{\theta_v}}, \tag{A.2}$$

where ε is the fractional entrainment rate. The last term represents the buoyancy acceleration. The environmental kinetic energy $\frac{1}{2}\overline{w_e}^2$ can be neglected. The top of the boundary layer z_i (inversion height) is found when the vertical velocity drops to zero. z_i is interpolated between model levels. If condensation occurs, a cloud base height z_{cb} is defined.

The parcel is initialised by taking mean fields at the lowest model level z_1 and adding an excess that scales with the surface fluxes (Troen and Mahrt, 1986), i.e. for variables $\phi = \{s_l, q_t\}$

$$\phi_u(z_1) = \overline{\phi(z_1)} + b\frac{\overline{w'\phi'}^s}{\sigma_w(z_1)}, \tag{A.3}$$

where s refers to the surface mean and b is a parameter estimated as 1.0 based on LES experiments (Siebesma and Teixeira, 2000). For the standard deviation of vertical velocity σ_w an empirical expression based on atmospheric data, tank measurements and LES data is used (Holtslag and Moeng, 1991)

$$\sigma_w \simeq 1.2\left(u_*^3 + 1.5\kappa w_*^3\frac{z}{z_i}\right)^{1/3}\left(1-\frac{z}{z_i}\right)^{1/2} = 1.2\left(u_*^3 + 1.5\kappa\frac{g}{\overline{\theta_v}^s}\overline{w'\theta_v'}^s z\right)^{1/3}\left(1-\frac{z}{z_i}\right)^{1/2}, \tag{A.4}$$

where $\kappa = 0.4$ is the van Karman constant, $u_* \equiv (\overline{u'w'}^{s2} + \overline{u'w'}^{s2})^{1/4}$ is the friction velocity, and $w_* \equiv (z_i\frac{g}{\overline{\theta_v}^s}\overline{w'\theta_v'}^s)^{1/3}$ is the free convective velocity scale. Because z_i is not known yet when the updraught properties are computed and since σ_w at the lowest model level is not very sensitive to z_i, the last term $(1-\frac{z}{z_i})^{1/2}$ in equation (A.4) in neglected.

The parcel entrainment ε is written as

$$\varepsilon = \frac{1}{w\tau_\varepsilon} + c_\varepsilon\frac{1}{z}. \tag{A.5}$$

For the first term a mixing time scale τ_ε of 500 s has been selected (Siebesma, 1998; Cheinet, 2003, 2004). The second term represents the limiting of the length scale by the proximity of the surface and is inspired by the LES simulations by Siebesma and Teixeira (2000). They found that in the convective boundary layer ε scales with $1/z$ near the surface with a factor c_ε equal to 0.55. Sensitivity experiments have shown that the second term is rather crucial as it has a big impact on the resulting boundary layer depths.

With the different height scales defined and the updraught properties known, it is still necessary to define the profiles of mass flux and diffusion coefficients. The mass flux M is directly calculated from the entrainment ε and the detrainment δ

$$\frac{\partial M}{\partial z} = \left(\varepsilon - \delta\right)M. \tag{A.6}$$

M is initialised at the lowest level as $a_u\overline{w_u}$, where a_u represents the updraught fraction in the surface layer. This is a free parameter in the parametrization that can be set to any fraction of the vertical velocity spectrum that one intends to parametrise with the mass flux. Here $a_u = 0.05$. Assuming a Gaussian distribution of vertical velocities, the mean of the upper 5% tail of the distribution corresponds to a

$$\overline{w_u}(a_u, \sigma_w) = b\sigma_w \tag{A.7}$$

with $b = 2.05$. This $\overline{w_u}(a_u, \sigma_w)$ is also used to initialize the parcel. For simplicity, the temperature and moisture perturbations are assumed to be correlated with the vertical velocity perturbations. Therefore, the parameter b is also used in equation A.3.

For detrainment, two choices were tested: (i) Zero detrainment within the BL and all detrainment at the top of the BL. This corresponds to a single entraining plume model, which assumes that the mass flux term only describes the biggest eddies. (ii) Detrainment as $3 \cdot 10^{-4} m^{-1}$ above cloud base and zero below. This corresponds to a bulk plume model. Option (ii) was adopted for better compatibility with the shallow convective plume model in the current ECMWF model, although the sensitivity to this was limited.

A.2 Diffusion component

For the surface driven diffusion a simple K-profile is specified, similar to the current dry scheme (Troen and Mahrt, 1986; Holtslag, 1998)

$$K_h^{sfc} = \kappa u_* \phi_{h0}^{-1} \left(1 - \frac{z}{z_i}\right)^2, \tag{A.8}$$

where ϕ_{h0} is a stability function given by

$$\phi_{h0} = \left(1 - 39\frac{z}{L}\right)^{-1/3}, \tag{A.9}$$

and $L = -u_*^3(\kappa\overline{w'\theta_v'}g/\theta_v)^{-1}$ is the Obukhov length. Cloud top driven diffusion is described after Lock et al. (2000) as

$$K_h^{top} = 0.85\kappa v_{cld} \frac{z - z_{mb}}{z_i - z_{mb}} \left(1 - \frac{z - z_{mb}}{z_i - z_{mb}}\right)^{1/2}, \tag{A.10}$$

where z_i is the inversion height or cloud top and z_{mb} is the level below cloud base to which the top driven mixing extends. A value of $z_{mb} = 0$ is assumed, implying a strong coupling between the cloud layer and the sub-cloud layer. Parameter v_{cld} represents a top entrainment velocity scale encompassing a radiative cooling and a buoyancy reversal term

$$v_{cld}^3 = v_{rad}^3 + v_{br}^3. \tag{A.11}$$

The buoyancy reversal term is neglected, giving

$$v_{rad}^3 = \frac{g}{\theta_0} z_i \Delta R/(\rho c_p) \tag{A.12}$$

after Lock (1998), where ΔR is the radiative flux jump at cloud top.

Boundary layer top entrainment is explicitely specified from surface and cloud top driven components

$$\overline{w'\theta_v'}^{entr} = -0.2\overline{w'\theta_v'}^s - 0.2\triangle R/(\rho c_p) = -K_h^e \frac{\partial \theta_v}{\partial z} \approx -K_h^e \frac{\Delta\theta_v}{\Delta z} \equiv w_e \Delta\theta_v. \tag{A.13}$$

Within the PBL the total diffusion coefficient for s_l and q_t is specified as

$$K_h = K_h^{sfc} + K_h^{top} \tag{A.14}$$

while at the top of the PBL

$$K_h = max(K_h^{sfc} + K_h^{top}, K_h^e) \tag{A.15}$$

is used.

A.3 Cloud

In order to provide coupling of the boundary layer scheme to the cloud scheme, the variance of total water is computed from the following equation (Deardorff, 1974)

$$\frac{\partial \sigma_{qt}^2}{\partial t} = -2\overline{w' q_t'}\frac{\partial q_t}{\partial z} - \frac{\partial \left(\overline{w' \sigma_{qt}^{2'}}\right)}{\partial z} - \frac{\sigma_{qt}^2}{\tau_{\sigma qt}}. \tag{A.16}$$

The first term is the generation term in the presence of a vertical q_t gradient, the second term represents transport which is neglected and the third term is the decay term. The associated decay time scale is written as

$$\tau_{\sigma qt} = \frac{z_i}{\overline{w_u}^{PBL}}\,, \tag{A.17}$$

where the updraught velocity $\overline{w_u}^{PBL}$ is averaged over the height of the boundary layer z_i.

In future, the variance of total water will be a prognostic variable in a statistical cloud scheme (see section 7), with the boundary layer sources and sinks described by equation A.16 included. The distribution function assumptions of the cloud scheme will provide cloud cover and cloud water/ice. Until these are available, these terms currently need to be transformed into the Tiedtke (1993) cloud scheme's prognostic variables of cloud water and cloud cover. At the beginning of the boundary layer parametrization time step, the model variables, q_v, q_l, q_i, T, and f_c (cloud cover), are converted to q_t, q_l, and $\sigma_{qt}(q_v, q_l + q_i, q_{sat}(T))$, assuming a Beta distribution as used by Tompkins (2002) and described in section 7. The variance of the total water σ_{qt} is diagnosed that gives the specified liquid water and cloud cover. Then, equation A.16 is integrated for one time step and the total water distribution function is used to diagnose the equivalent change in cloud cover and cloud water/ice (see Tompkins, 2002; Bushell et al., 2003; Larson, 2004, for more details of this approach). The differences between cloud variables before and after the time step are then used as a tendency (from boundary layer processes) for the cloud scheme.

A.4 Numerical aspects

The combined mass flux and diffusion equation for moist conserved variables ($\phi = s_l$ and q_t)

$$\frac{\partial}{\partial t}\overline{\phi} = -\frac{\partial}{\partial z}\left(-K\frac{\partial \overline{\phi}}{\partial z} + M(\phi_u - \overline{\phi})\right) \tag{A.18}$$

is solved with a centered finite difference scheme in the vertical and an implicit time integration scheme for stability.

The updraught equation is integrated from the surface to the top using backward finite differences. All finite difference equations are written in conservative form.

References

Ackerman, T. P. and G. M. Stokes, 2003: The Atmospheric Radiation Measurement program. *Phys. Today*, **56**, 38–44.

Arakawa, A. and W. H. Shubert, 1974: Interaction of a cumulus ensemble with the large- scale environment. Part 1. *J. Atmos. Sci.*, **31**, 674–701.

Arking, A. and P. P. Xie, 1994: The global precipitation climatology project: First algorithm intercomparison project. *Bull. Amer. Meteor. Soc.*, **75**, 401–419.

Barker, H. W., R. Pincus, and J.-J. Morcrette, 2003: The Monte-Carlo Independent Column Approximation: Application within large-scale models. In: *Proc. GCSS/ARM Workshop on the Representation of Cloud Systems in Large-Scale Models*, p. 10pp. GCSS/ARM, Kananaskis, Al, Canada. Available at: http://www.met.utah.edu/skrueger/gcss-2002/Extended-Abstracts.pdf.

Barkstrom, B. R., 1984: The Earth radiation budget experiment (ERBE). *Bull. Am. Meteor. Soc.*, **64**, 1170–1185.

Bauer, P., 2002: Microwave radiative transfer modelling in clouds and precipitation. Part I: Model description. Technical report, European Centre for Medium-Range Weather Forecasts, available at http://www.ecmwf.int/publications/. Satellite Application Facility for Numerical Weather Prediction, NWPSAF-EC-TR-005, version 1.0.

Bauer, P., P. Amayenc, C. D. Kummerow, and E. A. Smith, 2001: Over-ocean rainfall retrieval from multisensor data of the Tropical Rainfall Measuring Mission (TRMM). Part II: Algorithm implementation. *J. Atmos. Ocean. Tech.*, **18**, 1838–1855.

Bäuml, G., 2002: *Influence of Sub-Grid Scale Variability of Clouds on the Solar Radiative Transfer Computations in the ECHAM5 Climate Model*. Ph.D. thesis, University of Hamburg. Available from: Max Planck Institute for Meteorology, Bundesstr 55, 20146 Hamburg, Germany. pp. 108.

Bechtold, P., J.-P. Chaboureau, A. Beljaars, A. K. Betts, M. Köhler, M. Miller, and J.-L. Redelsperger, 2004: The simulation of the diurnal cycle of convective precipitation over land in a global model. *Q. J. R. Meteorol. Soc.*, **130**, in press.

Bechtold, P., J. W. M. Cuijpers, P. Mascart, and P. Trouilhet, 1995: Modeling of trade-wind cumuli with a low-order turbulence model - toward a unified description of Cu and Sc clouds in meteorological models. *J. Atmos. Sci.*, **52**, 455–463.

Betts, A. K., 1973: Non-precipitating cumulus convection and its parameterization. *Q. J. R. Meteorol. Soc.*, **99**, 178–196.

Betts, A. K. and C. Jakob, 2002: Evaluation of the diurnal cycle of precipitation, surface thermodynamics and surface fluxes in the ECMWF model using LBA data. *J. Geophys. Res.*, **107**(D20), 8045, doi:10.1029/2001JD000427.

Bougeault, P., 1981: Modeling the trade-wind cumulus boundary-layer. Part I: Testing the ensemble cloud relations against numerical data. *J. Atmos. Sci.*, **38**, 2414–2428.

Bretherton, C. S., J. R. McCaa, and H. Grenier, 2004: A new parameterization for shallow cumulus convection and its application to marine subtropical cloud-topped boundary layers. Part I: Description and 1D results. *Mon. Wea. Rev.*, **132**, 864–882.

Bretherton, C. S. and M. C. Wyant, 1997: Moisture transport, lower tropospheric stability, and decoupling of cloud-topped boundary layers. *J. Atmos. Sci.*, **54**, 148–167.

Bushell, A. C., D. R. Wilson, and D. Gregory, 2003: A description of cloud production by non-uniformly distributed processes. *Q. J. R. Meteorol. Soc.*, **129**, 1435–1455.

Cahalan, R. F., W. Ridgway, W. J. Wiscombe, T. L. Bell, and J. B. Snider, 1994: The albedo of fractal stratocumulus clouds. *J. Atmos. Sci.*, **51**, 2434–2455.

Cheinet, S., 2003: A multiple mass-flux parameterization for the surface generated convection. Part 1: Dry plumes. *J. Atmos. Sci.*, **60**, 2313–2327.

Cheinet, S., 2004: A multiple mass-flux parameterization for the surface generated convection. part 2: Cloudy cores. *J. Atmos. Sci.*, **61**, 1093–1113.

Cohen, C., 2000: A quantitative investigation of entrainment and detrainment in numerically simulated cumulonimbus clouds. *J. Atmos. Sci.*, **57**, 1657–1674.

Craig, G. C. and B. G. Cohen, 2004: Fluctuations in an equilibrium convective ensemble. Part I: Theoretical formulation. *J. Atmos. Sci.*, **61**, submitted.

Cusack, S., J. M. Edwards, and R. Kershaw, 1999: Estimating the subgrid variance of saturation, and its parametrization for use in a GCM cloud scheme. *Q. J. R. Meteorol. Soc.*, **125**, 3057–3076.

da Silva, A., C. C. Young, and S. Levitus, 1994: Atlas of surface marine data 1994. Vol 1: Algorithms and procedures. Technical Report NOAA Atlas NESDIS 6, US Department of Commerce, Washinton DC. pp83.

Deardorff, J. W., 1974: Three dimensional numerical study of a heated planetary boundary layer. *Bound.-Layer Meteor.*, **7**, 81–106.

Deardorff, J. W., 1980: Cloud top entrainment instability. *J. Atmos. Sci.*, **37**, 131–147.

Derbyshire, S. H., I. Beau, P. Bechtold, J.-Y. Grandpeix, J.-M. Piriou, J.-L. Redelsperger, and P. M. M. Soares, 2004: Sensitivity of moist convection to environmental humidity. *Q. J. R. Meteorol. Soc.*, **130**, in press.

Dubal, M., N. Wood, and A. Staniforth, 2004: Analaysis of parallel versus sequential splittings for time-stepping physical parameterizations. *Mon. Wea. Rev.*, **132**, 121–132.

Duynkerke, P. and P. Hignett, 1993: Simulation of diurnal validation in a stratiform-capped marine boundary layer during FIR. *Mon. Wea. Rev.*, **121**, 3291–3300.

Emanuel, K. A., 1991: A scheme for representing cumulus convection in large-scale models. *J. Atmos. Sci.*, **48**, 2313–2335.

Esbensen, S., 1978: Bulk thermodynamic effects and properties of small tropical cumuli. *J. Atmos. Sci.*, **35**, 826–831.

Fillion, L. and J.-F. Mahfouf, 2003: Jacobians of an operational prognostic cloud scheme. *Mon. Wea. Rev.*, **131**, 2838–2856.

Fournier, A., 2002: Atmospheric energetics in the wavelet domain. part i: Governing equations and interpretation for idealized flow. *J. Atmos. Sci.*, **59**, 1182–1179.

Gierens, K., R. Kohlhepp, P. Spichtinger, and M. Schrödter-Homscheidt, 2004: Ice supersaturation as seen from TOVS. *Atmos. Chem. Phys.*, **4**, 539–547.

Gierens, K., U. Schumann, M. Helten, H. Smit, and P. H. Wang, 2000: Ice-supersaturated regions and subvisible cirrus in the northern midlatitude upper troposphere. *J. Geophys. Res.*, **105**, 22743–22753.

Grabowski, W. W., 2003: MJO-like coherent structures: Sensitivity simulations using the cloud-resolving convection parameterization (CRCP). *J. Atmos. Sci.*, **60**, 847–864.

Grant, A. L. M. and A. R. Brown, 1999: A similarity hypothesis for shallow-cumulus transports. *Quart. J. Roy. Meteor. Soc.*, **125**, 1913–1936.

Gregory, D., J.-J. Morcrette, C. Jakob, A. C. M. Beljaars, and T. Stockdale, 2000: Revision of convection, radiation and cloud schemes in the ECMWF Integrated Forecasting System. *Q. J. R. Meteorol. Soc.*, **126**, 1685–1710.

Grenier, H. and C. S. Bretherton, 2001: A moist PBL parametrization for large-scale models and its application to subtropical cloud-topped marine boundary layers. *Month. Weath. Rev.*, **129**, 357–377.

Guan, H., S. G. Cober, G. A. Isaac, A. Tremblay, and A. Methot, 2002: Comparison of three cloud forecast schemes with in situ aircraft measurements. *Wea. and Forecasting*, **17**, 1226–1235.

Heymsfield, A. J. and L. J. Donner, 1990: A scheme for parameterizing ice-cloud water content in general circulation models. *J. Atmos. Sci.*, **47**, 1865–1877.

Heymsfield, A. J., L. M. Miloshevich, C. Twohy, G. Sachse, and S. Oltmans, 1998: Upper-tropospheric relative humidity observations and implications for cirrus ice nucleation. *Geophys. Res. lett.*, **25**, 1343–1346.

Holtslag, A. A. M., 1998: Modelling of atmospheric boundary layers. In: A. A. M. Holtslag and P. G. Duynkerke, eds., *Clear and cloudy boundary layers*, pp. 85–110. Royal Netherlands Academy of Arts and Sciences.

Holtslag, A. A. M. and C.-H. Moeng, 1991: Eddy diffusivity and countergradient transport in the convective atmospheric boundary layer. *J. Atmos. Sci.*, **48**, 1690–1698.

Hsieh, W. H. and B. Tang, 1998: Applying neural network models to prediction and data analysis in meteorology and oceanography. *Bull. Amer. Meteor. Soc.*, **79**, 1855–1870.

Huffman, G. J., R. F. Adler, P. Arkin, A. Chang, R. Ferraro, A. Gruber, J. Janowiak, A. McNab, B. Rudolf, and U. Schneider, 1997: The Global Precipitation Climatology Project (GPCP) Combined Precipitation Dataset. *Bull. Amer. Meteor. Soc.*, **78**, 5–20.

Iguchi, T., T. Kozu, R. Meneghini, J. Awaka, and K. Okamoto, 2000: Rain profiling algorithm for TRMM Precipitation Radar data. *J. Appl. Meteor.*, **39**, 2038–2052.

Jakob, C., 2002: Ice clouds in numerical weather prediction models: Progress, problems and prospects. In: D. K. Lynch, K. Sassen, D. Starr, and G. Stephens, eds., *Cirrus*, pp. 327–345. Oxford University Press.

Jakob, C. and S. A. Klein, 1999: The role of vertically varying cloud fraction in the parametrization of microphysical processes in the ECMWF model. *Q. J. R. Meteorol. Soc.*, **125**, 941–965.

Jakob, C. and A. P. Siebesma, 2003: A new subcloud model for mass-flux convection schemes. influence on triggering, updraught properties and model climate. *Mon. Wea. Rev.*, **131**, 2765–2778.

Janisková, M., J.-F. Mahfouf, J.-J. Morcrette, and F. Chevallier, 2002: Linearized radiation and cloud schemes in the ECMWF model: Development and evaluation. *Q. J. R. Meteorol. Soc.*, **128**, 1505–1527.

Janisková, M., J.-N. Thepaut, and J.-F. Geleyn, 1999: Simplified and regular physical parameterizations for incremental four-dimensional variational assimilation. *Mon. Wea. Rev.*, **127**, 26–45.

Johnson, R. H., 1978: Cumulus transports in a tropical wave composite for phase-III of GATE. *J. Atmos. Sci.*, **35**, 484–494.

Jung, T. and A. M. Tompkins, 2003: Systematic errors in the ECMWF forecasting system. Technical Report 422, European Centre for Medium-Range Weather Forecasts, available at http://www.ecmwf.int/publications/. pp72.

Kessler, E., 1969: *On the distribution and continuity of water substance in atmospheric circulation, Meteorological Monography, 10*. American Meteorological Society.

King, M. D., W. P. Menzel, P. S. Grant, J. S. Myers, G. T. Arnold, S. Platnick, L. E. Gumley, S. C. Tsay, C. C. Moeller, M. Fitzgerald, K. S. Brown, and F. G. Osterwisch, 1996: Airborne Scanning Spectrometer for Remote Sensing of Cloud, Aerosol, Water Vapor, and Surface Properties. *J. Atmos. Oceanic Technol.*, **13**, 777–794.

Klein, S. A. and D. L. Hartmann, 1993: The seasonal cycle of low stratiform cloud. *J. Climate*, **6**, 1587–1606.

Klein, S. A., R. Pincus, C. Hannay, and K.-M. Xu, 2004: Coupling a statistical scheme to a mass flux scheme. *J. Geophys. Res.*, p. submitted.

Klinker, E., F. Rabier, G. Kelly, and J.-F. Mahfouf, 2000: The ECMWF operational implementation of four-dimensional variational assimilation. I: Experimental results with improved physics. *Q. J. R. Meteorol. Soc.*, **126**, 1171–1190.

Lander, J. and B. J. Hoskins, 1997: Believable scales and parameterizations in a spectral transform model. *Mon. Wea. Rev.*, **125**, 292–303.

Lappen, C.-L. and D. A. Randall, 2001: Toward a unified parameterization of the boundary layer and moist convection. Part I: A new type of mass-flux model. *J. Atmos. Sci.*, **58**, 2021–2036.

Larson, V. E., 2004: Prognostic equations for cloud fraction and liquid water, and their relation to filtered density functions. *J. Atmos. Sci.*, **61**, 338–351.

Lenderink, G. and A. P. Siebesma, 2000: Combining the massflux approach with a statistical cloud scheme. In: *Proc. 14th Symp. on Boundary Layers and Turbulence*, pp. 66–69. Amer. Meteor. Soc., Aspen, CO, USA.

Liebmann, B. and C. A. Smith, 1996: Description of a complete (interpolated) outgoing longwave radiation dataset. *Bull. Amer. Meteor. Soc.*, **77**, 1275–1277.

Lin, Y. L., R. D. Farley, and H. D. Orville, 1983: Bulk parameterization of the snow field in a cloud model. *J. Climate Appl. Meteor.*, **22**, 1065–1092.

Lock, A. P., 1998: The parameterization of entrainment in cloudy boundary layers. *Q. J. R. Meteorol. Soc.*, **124**, 2729–2753.

Lock, A. P., A. R. Brown, M. R. Bush, G. M. Martin, and R. N. B. Smith, 2000: A new boundary layer mixing scheme. Part I: Scheme description and single-column model tests. *Mon. Wea. Rev.*, **128**, 3187–3199.

Lohmann, U. and E. Roeckner, 1996: Design and performance of a new cloud microphysics scheme developed for the ECHAM general circulation model. *Clim. Dyn.*, **12**, 557–572.

Lopez, P., 2004: A convection scheme for data assimiliation purposes: Description and initial tests. *Q. J. R. Meteorol. Soc.*. Submitted.

Ma, C.-C., C. R. Mechoso, A. W. Robertson, and A. Arakawa, 1996: Peruvian stratus clouds and the tropical pacific circulation: A coupled ocean-atmosphere gcm study. *J. Climate*, **9**, 1635–1645.

Madden, R. A. and P. R. Julian, 1971: Detection of a 40-50 day oscillation in the zonal wind in the tropical pacific. *J. Atmos. Sci.*, **5**, 702–708.

Mahfouf, J.-F., 1999: Influence of physical processes on the tangent-linear approximation. *Tellus*, **51**, 147–166.

Mahfouf, J.-F. and F. Rabier, 2000: The ECMWF operational implementation of four-dimensional variational assimilation. II: Experimental results with improved physics. *Q. J. R. Meteorol. Soc.*, **126**, 1171–1190.

Marécal, V. and J.-F. Mahfouf, 2000: Variational retrieval of temperature and humidity profiles from TRMM precipitation data. *Mon. Wea. Rev.*, **128**, 3853–3866.

Marécal, V. and J.-F. Mahfouf, 2003: Experiments on 4D-Var assimilation of rainfall data using an incremental formulation. *Q. J. R. Meteorol. Soc.*, **129**, 3137–3160.

McFarquhar, G. M. and A. J. Heymsfield, 1997: Parameterization of Tropical Cirrus Ice Crystal Size Distributions and Implications for Radiative Transfer: Results from CEPEX. *J. Atmos. Sci.*, **54**, 2187–2200.

Mellor, G. L., 1977: Gaussian cloud model relations. *J. Atmos. Sci.*, **34**, 356–358.

Miller, M. J., A. C. M. Beljaars, and T. N. Palmer, 1992: The sensitivity of the ECMWF model to the parameterization of evaporation from the tropical oceans. *J. Climate*, **5**, 418–434.

Moreau, E., P. Lopez, P. Bauer, A. M. Tompkins, M. Janisková, and F. Chevallier, 2004: Rainfall versus microwave brightness temperature assimilation: A comparison of 1D-Var results using TMI and SSM/I observations. *Q. J. R. Meteorol. Soc.*, **130**, 827–852.

Neggers, R., P. Siebesma, and H. Jonker, 2002: A multiparcel model for shallow cumulus convection. *J. Atmos. Sci.*, **59**, 1655–1668.

Nicholls, S. and M. A. Lemone, 1980: The fair weather boundary-layer in GATE - The relationship of sub-cloud fluxes and structure to the distribution and enhancement of cumulus clouds. *J. Atmos. Sci.*, **37**, 2051–2067.

Pincus, R., H. W. Barker, and J. J. Morcrette, 2003: A fast, flexible, approximate technique for computing radiative transfer in inhomogeneous cloud fields. *J. Geophy. Res.*, **108**, 10.1029/2002JD003322.

Price, J. D., 2001: A study on boundary layer humidity distributions and errors in parameterised cloud fraction. *Q. J. R. Meteorol. Soc.*, **127**, 739–759.

Rabier, F., J.-N. Thepaut, and P. Courtier, 1998: Extended assimilation and forecast experiments with a four-dimensional variational assimilation system. *Q. J. R. Meteorol. Soc.*, **124**, 1861–1887.

Rädel, G., C. J. Stubenrauch, R. Holz, and D. L. Mitchell, 2003: Retrieval of effective ice crystal size in the infrared: Sensitivity study and global measurements from TIROS-N Operational Vertical Sounder. *J. Geophy. Res.*, **108**, 10.1029/2002JD002801.

Randall, D. A., 1980: Conditional instability of the first kind upside-down. *J. Atmos. Sci.*, **37**, 125–130.

Randall, D. A., 1987: Turbulent fluxes of liquid water and buoyancy in partly cloudy layer. *J. Atmos. Sci.*, **44**, 850–858.

Randall, D. A., M. Khairoutdinov, A. Arakawa, and W. Grabowski, 2003: Breaking the cloud parameterization deadlock. *Bull. Amer. Meteor. Soc.*, **84**, 1547–1564.

Redelsperger, J. L., F. Guichard, and S. Mondon, 2000: A parameterization of mesoscale enhancement of surface fluxes for large-scale models. *J. Climate*, **13**, 402–421.

Rossow, W. B. and R. A. Schiffer, 1991: ISCCP cloud data products. *Bull. Amer. Meteor. Soc.*, **72**, 2–20.

Schneider, K. N., K.-R. Kevlahan, and M. Farge, 1997: Comparison of an adaptive wavelet method and nonlinearly filtered pseudospectral methods for two-dimensional turbulence. *Theor. Comput. Fluid Dyn.*, **9**, 191–206.

Shin, D.-B., L. S. Chiu, and M. Kafatos, 2001: Comparison of the monthly precipitation derived from the TRMM satellite. *Geophys. Res. Lett.*, **28**, 795–798.

Siebesma, P., 1996: On the mass flux approach for atmospheric convection. In: *Workshop on new insights and approaches to convective parametrization*. ECMWF, Shinfield Park, Reading RG2 9AX, U.K.

Siebesma, P., 1998: Shallow cumulus convection. In: E. J. Plate et al., ed., *Buoyant convection in geophysical flows*, pp. 441–486. Kluwer Academic.

Siebesma, P. and J. W. M. Cuijpers, 1995: Evaluation of parametric assumptions for shallow cumulus convection. *J. Atmos. Sci.*, **52**, 650–666.

Siebesma, P. and J. Teixeira, 2000: An advection-diffusion scheme for the convective boundary layer: description and 1D-results. In: *Proc. 14th symposium on boundary layers and turbulence*. Amer. Meteor. Soc.

Simpson, J. and V. Wiggert, 1969: Models of precipitating cumulus towers. *Mon. Wea. Rev.*, **97**, 471–489.

Slingo, J. M., 1987: The development and verification of a cloud prediction scheme for the ECMWF model. *Q. J. R. Meteorol. Soc.*, **113**, 899–927.

Slingo, J. M., K. R. Sperber, J. J. Morcrette, and G. L. Potter, 1992: Analysis of the temporal behavior of convection in the tropics of the european centre for medium-range weather forecast model. *J. Geophys. Res.*, **97**, 18119–18135.

Sommeria, G. and J. W. Deardorff, 1977: Subgrid-scale condensation in models of nonprecipitating clouds. *J. Atmos. Sci.*, **34**, 344–355.

Spichtinger, P., K. Gierens, and W. Read, 2003: The global distribution of ice-supersaturated regions as seen by the Microwave Limb Sounder. *Q. J. R. Meteorol. Soc.*, **129**, 3391–3410.

Stevens, B., 2000: Cloud transitions and decoupling in shear-free stratocumulus-topped boundary layers. *Geophys. Res. Lett.*, **27**, 2557–2560.

Strom, J., M. Seifert, B. Kärcher, J. Ovarlez, A. Minikin, J.-F. Gayet, R. Krejci, A. Petzold, F. Auriol, W. Haag, R. Busen, U. Schumann, and H. C. Hansson, 2003: Cirrus cloud occurrence as function of ambient relative humidity: a comparison of observations obtained during the INCA experiment. *Atmos. Chem. Phys.*, **3**, 1807–1816.

Sundqvist, H., E. Berge, and J. E. Kristjansson, 1989: Condensation and cloud parameterization studies with a mesoscale numerical weather prediction model. *Mon. Wea. Rev.*, **117**, 1641–1657.

Taylor, C. M., R. J. Ellis, D. J. Parker, R. R. Burton, and C. D. Thorncroft, 2003: Linking boundary-layer variability with convection: A case-study from JET2000. *Q. J. R. Meteorol. Soc.*, **129**, 2233–2253.

Taylor, C. M. and T. Lebel, 1998: Observational evidence of persistent convective-scale rainfall patterns. *Mon. Wea. Rev.*, **126**, 1597–1607.

Teixeira, J., 2001: Cloud fraction and relative humidity in a prognostic cloud fraction scheme. *Mon. Wea. Rev.*, **126**, 1750–1753.

Tiedtke, M., 1989: A comprehensive mass flux scheme for cumulus parameterization in large-scale models. *Mon. Wea. Rev.*, **117**, 1779–1800.

Tiedtke, M., 1993: Representation of clouds in large-scale models. *Mon. Wea. Rev.*, **121**, 3040–3061.

Tiedtke, M., 1996: An extension of cloud-radiation parameterization in the ECMWF model: The representation of subgrid-scale variations of optical depth. *Mon. Wea. Rev.*, **124**, 745–750.

Tisler, P. and H. Savijarvi, 2002: On the parameterization of precipitation in warm clouds. *Atmos. Res.*, **63**, 163–176.

Tompkins, A. M., 2002: A prognostic parameterization for the subgrid-scale variability of water vapor and clouds in large-scale models and its use to diagnose cloud cover. *J. Atmos. Sci.*, **59**, 1917–1942.

Tompkins, A. M., 2003: Impact of temperature and total water variability on cloud cover assessed using aircraft data. *Q. J. R. Meteorol. Soc.*, **129**, 2151–2170.

Tompkins, A. M. and M. Janisková, 2004: A cloud scheme for data assimiliation: Description and initial tests. *Q. J. R. Meteorol. Soc.*, **130**, 2495–2518.

Troen, I. and L. Mahrt, 1986: A simple model of the atmospheric boundary layer; Sensitivity to surface evaporation. *Bound.-Layer Meteor.*, **37**, 129–148.

Tung, W.-W. and M. Yanai, 2002a: Convective momentum transport observed during the TOGA COARE IOP. Part I: General features. *J. Atmos. Sci.*, **59**, 1857–1871.

Tung, W.-W. and M. Yanai, 2002b: Convective momentum transport observed during the TOGA COARE IOP. Part II: Case studies. *J. Atmos. Sci.*, **59**, 2535–2549.

Turton, J. D. and L. Nicholls, 1987: A study of the dirunal variation of stratocumulus using a multiple mixed layer model. *Q. J. R. Meteorol. Soc.*, **113**, 969–1009.

Webster, P. J. and R. Lukas, 1992: The coupled ocean-atmosphere response experiment. *Bull. Amer. Meteor. Soc.*, **73**, 1377–1416.

Wentz, F. J., 1997: A well-calibrated ocean algorithm for SSM/I. *J. Geophy. Res.*, **102**, 8703–8718.

Wielicki, B. A., B. R. Barkstrom, E. F. Harrison, R. B. Lee, G. L. Smith, and J. E. Cooper, 1996: Clouds and the earth's radiant energy system (CERES): An earth observing system experiment. *Bull. Amer. Meteor. Soc.*, **77**, 853–868.

Yang, G.-Y. and J. Slingo, 2001: The diurnal cycle in the tropics. *Mon. Wea. Rev.*, **129**, 784–801.

Yano, J.-I., P. Bechtold, J.-L. Redelsperger, and F. Guichard, 2004: Wavelet-compressed representation of deep moist convection. *Mon. Wea. Rev.*, **132**, 1472–1486.

Zhang, J., U. Lohmann, and B. Lin, 2002: A new statistically based autoconversion rate parameterization for use in large-scale models. *J. Geophys. Res.*, **107**, doi:10.1029/2001JD001484.